

Biological Functions of Ribonuclease 1 and Angiogenin

by

Emily R. Garnett

B.S. Biochemistry, Cell, and Molecular Biology, B.A. Chemistry
Drake University, 2012

Submitted to the Department of Chemistry
in Partial Fulfillment of the Requirements for the Degree of

DOCTOR OF PHILOSOPHY
IN BIOLOGICAL CHEMISTRY

at the

Massachusetts Institute of Technology

June 2018

© 2018 Massachusetts Institute of Technology. All rights reserved.

Signature redacted

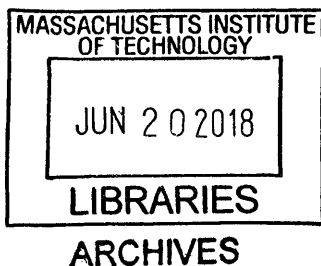
Signature of Author: _____
Department of Chemistry
May 18, 2018

Signature redacted

Certified by: _____
Firmenich Professor of Chemistry
Thesis Supervisor
Ronald Raines

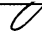
Signature redacted

Accepted by: _____
Robert W. Field
Haslam and Dewey Professor of Chemistry
Chairman, Departmental Committee on Graduate Students

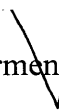


This doctoral thesis has been examined by a committee of professors
from the Department of Chemistry as follows:

Signature redacted

 Elizabeth Nolan
Associate Professor of Chemistry
Thesis Committee Chair

Signature redacted

 Ronald Raines
Firmenich Professor of Chemistry
Thesis Supervisor

Signature redacted

David Bartel
Professor of Biology
Thesis Committee Member

Biological Functions of Ribonuclease 1 and Angiogenin

by

Emily R. Garnett

Submitted to the Department of Chemistry on
May 18, 2018 in Partial Fulfillment of the Requirements
for the Degree of Doctor of Philosophy in
Biological Chemistry

Abstract

Pancreatic-type ribonucleases (ptRNases) are a large family of vertebrate-specific secretory endoribonucleases. They catalyze degradation of many RNA substrates, mediating a variety of biological functions. The homology shared by ptRNases has enabled extensive biochemical characterization and evolutionary study of these enzymes, yet understanding of their biological roles is still incomplete. The goal of this thesis is to identify novel physiological functions for two ptRNases, RNase 1 and angiogenin, through characterization of murine model systems.

In Chapter 1, I introduce the ptRNase superfamily and highlight evidence of biological function for RNase 1 and angiogenin that has motivated and informed our study of these enzymes.

Extracellular RNA drives blood coagulation, which is preventable by administration of RNase A. In Chapter 2, I demonstrate that loss of RNase 1, a nonspecific and extracellular ptRNase similar to RNase A, results in the potentiation of blood coagulation by activation of coagulation factors in mice.

Angiogenin is a ptRNase with unique angiogenic activity and suggested biological function in cancer and amyotrophic lateral sclerosis, as well as in cellular growth and quiescence. My studies demonstrate a fundamental role for angiogenin. In Chapter 3, I find that this enzyme is essential for the development of mice, with heterozygosity for angiogenin resulting in impaired vascularization of the placenta and reduced survival of offspring.

Biological study of ptRNases is hampered by the high degree of conservation of the family, which engenders antibody nonspecificity. In Chapter 4, I describe efforts to generate novel specific anti-ptRNase antibodies by producing tagged ptRNases for use in an antibody phage–display workflow. Finally, Chapter 5 outlines future directions for the study of RNase 1 and angiogenin.

Taken together, this thesis reveals a more complete picture of the physiological niches of these two enzymes, confirming some previously suspected roles, ascribing new ones, and providing groundwork for future characterization of the biology of these and other ptRNases.

Thesis Supervisor: Ronald T. Raines
Title: Firmenich Professor of Chemistry

Acknowledgments

Many, many people have encouraged me and supported me on my journey through graduate school.

First and foremost, I have to thank my parents for always providing opportunities for me to learn, and for unconditional love and support. They instilled in me a love of learning and exploration, and have always pushed me to be independent and to go further – which is what drove me to pursue graduate education in the first place. I also have to thank my entire family for their constant encouragement and infectious attitude – I have truly been lucky to grow up surrounded by support, positivity, and a sense of delight in what the world has to offer.

I have to thank my undergraduate advisors, Julia Moffitt and Marc Busch, as well as Amanda Jepson, for being excellent coaches as I was first learning to do research. It was under their guidance that I really learned how “science” is done in academic laboratories, and the experience was invaluable in orienting myself once I began working independently. I also have to thank Mark Vitha and Vib Petersen for pushing my boundaries, driving me to think critically, and encouraging me to see myself as a scientist.

I have to thank the people who got me on my feet as a student of Molecular and Cellular Pharmacology (MCP) at the University of Wisconsin. Patty Keely and Vincent Cryns got me through the initial hurdles of “how to be a graduate student,” and the students of the MCP program (dozens over the five years I spent at UW) gave me a sense of community and a sounding board. I also have to thank Jon Audhya and Kristin Cooper for all their support as administrators of the MCP program, and the program as a whole for funding me through NIH T32 GM008688.

I have to thank my graduate advisor, Ron Raines, who has given me complete freedom to pursue my research in directions totally unfamiliar to our group, and the support I needed to do so. In forging ahead into biological spheres unknown, I was able to develop an independence and confidence in my work that has served me extremely well so far, and will be a valuable asset as I move forward. I also have to thank Ron for making sure our research was never wanting for funding – my work was supported by NIH R01 CA073808.

I have to thank the Raines lab as a whole for creating such a great environment to grow personally and professionally. Even though my research was outside of the general repertoire of our group, I never felt alone, and I loved the enthusiasm and the thoughtful feedback that came from all of you. I especially have to thank Kristen Andersen, Joelle Lomax, Chelcie Eller, and Trish Hoang for their guidance as I got started, and for being amazing role models as women scientists.

I have to thank my undergraduate assistants, Conner Feldman and Katharine Tippins, for being such skilled and dedicated managers of our mouse colony. Moving a mouse project forward without their assistance would have been impossible, and I am proud to have been able to watch their growth as scientists. I also have to thank the animal care staff, veterinarians, and

administrators who helped keep our mice safe and healthy, and taught me how to navigate the regulations associated with performing government-funded research.

I have to thank my collaborator, John Sheehan, for excellent advice and encouragement about my lab work and my career, as well as for teaching me the intricacies of the blood coagulation cascade from an expert (and physician's) perspective. I owe much of what I understand about this subject to him. I also have to thank Deane Mosher, Pam Westmark, and the Molecular Hematology group at the University of Wisconsin for their instruction and feedback.

I have to thank my former thesis committee members at the University of Wisconsin, Emery Bresnick, Beth Weaver, and Lara Collier, for their excellent advice and their support of me as I pursued fellowships, grants, and postdoctoral appointments.

I have to thank the people who supported me in the move to the Massachusetts Institute of Technology: The Kiessling lab students and postdocs, who moved from Wisconsin to Massachusetts with us, have become friends and commiserators, the Women in Chemistry and the Buchwald lab made me feel especially welcome, Brian Pretti has been superhuman in helping reassemble our lab, and Jennifer Weisman has been instrumental in getting me oriented as a Chemistry student. I am particularly grateful to Liz Nolan and David Bartel for being such attentive and thoughtful readers of my thesis and acting as my new thesis committee at MIT.

I have to thank a number of people who supported me in my journey towards a fellowship in Clinical Chemistry. Sarah Hackenmueller introduced me to the field and ultimately helped me edit my postdoctoral applications, and I received encouragement about my career choice by many clinical chemists and fellows-in-training who took the time to chat with me over the last few years. I especially have to thank Sridevi Devaraj and the Clinical Chemistry program at Texas Children's Hospital for giving me the opportunity to continue my training after my time at MIT is finished.

I have to thank Lauren Zasadil and Val Ressler for being incredible friends and roommates during the last few years of graduate school – you inspired me with your drive, thoughtfulness, generosity, and creativity. I also have to thank Chris Evans for the support, encouragement, and for bringing many new adventures into my life. I have to thank all of these people also for the very specific type of support that comes from knowing what it's like to wrap up a dissertation while far away from loved ones.

Finally, I have to thank the contributors to the freefood and vultures mailing lists, the Graduate Student Council, and the Chemistry Education office for always keeping me apprised of opportunities to find food on campus. I have never eaten so well for so cheaply.

Table of Contents:

Abstract	3
Acknowledgments	4
List of figures	9
List of tables	10
List of equations	10
Abbreviations	11
Chapter 1	14
Emerging biological functions of pancreatic-type ribonucleases	14
1.1: Introduction	15
1.2: The pancreatic-type ribonuclease superfamily	15
1.2.1: Characteristic biochemical features of ptRNases	16
1.2.2: Known biological functions of the ptRNase superfamily	18
1.3: Ribonuclease 1	19
1.3.1: Early studies of the biology of RNase 1	20
1.3.2: Extracellular RNA – key to the function of an extracellular RNase	21
1.3.3: New biological roles for RNase 1	22
1.4 Angiogenin	26
1.4.1 A ptRNase with unique structural and signaling properties	26
1.4.2 Angiogenin-mediated cell growth	28
1.4.3 Angiogenin-mediated protection from cell stress	30
1.5 Connections to vertebrate physiology	32
1.6 Prospectus	35
Chapter 2	36
Loss of ribonuclease 1 produces a hypercoagulable phenotype	36
2.1: Abstract	37
2.2: Introduction	38
2.3: Experimental procedures	39
2.3.1: Materials	39
2.3.2: Generation of Rnase 1 knockout mice	40
2.3.3: Quantitative PCR	42
2.3.4: Gross phenotypic analysis	43
2.3.5: Preparation of plasma samples	43
2.3.6: Quantitation of RNA in plasma	43
2.3.7: Ribonucleolytic activity assay	44
2.3.8: Ribonuclease zymogram assay	44
2.3.9: Kinetic coagulation assay	45
2.3.10: ELISA and immunoblotting	46
2.3.11: Thrombin–antithrombin complex formation assay	47
2.3.12: Tail-vein bleeding time assay	47
2.3.13: Saphenous vein hemostasis assay	47
2.3.14: FeCl ₃ -induced thrombosis assay	48
2.3.15: Factor activity assay	48
2.3.16: Statistical analyses	49
2.4: Results	50
2.4.1: Generation of <i>Rnase1</i> ^{-/-} mice by Cre–LoxP recombination	50
2.4.2: <i>Rnase1</i> ^{-/-} mice express neither Rnase1 mRNA nor RNase 1 protein	50

2.4.3: <i>RnaseI</i> ^{-/-} mice are viable and appear physically normal	54
2.4.4: Loss of RnaseI results in increased plasma RNA.....	55
2.4.5: <i>RnaseI</i> ^{-/-} plasma clots more quickly than does <i>RnaseI</i> ^{+/+} plasma	57
2.4.6: <i>RnaseI</i> ^{-/-} mice do not exhibit coagulation abnormalities in vivo	59
2.4.7: <i>RnaseI</i> ^{-/-} plasma exhibits elevated FXII and FXI activity	59
2.5: Discussion	61
2.6: Supplementary information.....	65
Chapter 3	67
Angiogenin is necessary for embryonic development in mice.....	67
3.1 Abstract	68
3.2 Introduction	69
3.3 Experimental procedures.....	70
3.3.1: Materials.....	70
3.3.2: Expansion of <i>AngI</i> ^{+/-} mice and genotyping	70
3.3.4: Gross phenotyping analysis.....	71
3.3.5: Developmental viability studies.....	71
3.3.6: Quantitative PCR	72
3.3.7: Ribonuclease zymogram assay	73
3.3.8: Immunoblotting	73
3.3.9: Statistical analyses	74
3.4 Results.....	74
3.4.1: <i>AngI</i> ⁺ mice have reduced <i>AngI</i> gene expression.....	74
3.4.2: <i>AngI</i> ^{+/-} plasma exhibits reduced angiogenin expression and activity.....	76
3.4.3: <i>AngI</i> ^{-/-} mice are not produced from <i>AngI</i> ^{+/-} intercrosses	76
3.4.4: <i>AngI</i> ^{+/-} mice experience partial litter loss	77
3.4.5: <i>AngI</i> ^{+/-} dams exhibit impaired uterine vascularization and elevated incidence of embryonic loss during pregnancy	77
3.5 Discussion	79
3.6: Supplemental information	83
Chapter 4	85
Towards novel anti-secreted ribonuclease antibodies using phage display.....	85
4.1 Abstract	86
4.2 Introduction	87
4.3 Experimental procedures.....	89
4.3.1: Materials.....	89
4.3.2: Design of tagged ribonuclease constructs	89
4.3.3: Cloning of tagged ribonucleases.....	90
4.3.4: Production of tagged ribonucleases	91
4.3.5: Biotinylation of tagged ribonucleases	91
4.3.6: Ribonucleolytic activity assays.....	92
4.3.7: TEV protease cleavage assays	92
4.3.8: Acetylation of RNase	93
4.3.9: Statistical analyses	93
4.4 Results.....	93
4.4.1: Evolutionarily divergent residues in ptRNases are not present near the amino acid termini ..	93
4.4.2: Tagged ptRNases express in E. coli, are of expected molecular weight, and retain ribonuclease activity	94
4.4.3: Tagged ptRNases are successfully biotinylated, and the tag successfully cleaved.....	98

4.4.4: mRNase 1 is successfully acetylated.....	99
4.5 Discussion	100
Chapter 5	103
Conclusions and future directions	103
5.1 Conclusions	104
5.2: Future directions	106
5.2.1: Roles for RNase 1 in growth	106
5.2.2: Roles for RNase 1 in cancer	107
5.2.3: Roles for RNase 1 in inflammation.....	108
5.2.4: Fundamental roles for nonspecific, extracellular ribonucleolytic activity	109
5.2.5: Mechanisms of impaired fertility and embryonic development in <i>Ang1^{+/-}</i> mice.....	110
5.2.6: Characterization of anti-ptRNase antibodies	111
Appendix 1.....	113
Evaluation of metabolic and inflammatory phenotypes in <i>Rnase1^{-/-}</i> mice.....	113
6.1 Abstract	114
6.2 Introduction	115
6.3 Experimental procedures	116
6.3.1: Materials.....	116
6.3.2: Body weight and length measurements.....	116
6.3.3: Food and water consumption studies	117
6.3.4: Urinary protein and glucose excretion studies.....	117
6.3.5: Fecal lipid content studies	117
6.3.6: Plasma cholesterol measurement	118
6.3.7: Visceral adipose tissue measurement.....	118
6.3.8: Quantitative PCR	119
6.3.9: Statistical analyses	120
6.4 Results.....	120
6.4.1: <i>Rnase1^{-/-}</i> mice are heavier and larger than <i>Rnase1^{+/+}</i> mice.....	120
6.4.2: <i>Rnase1^{-/-}</i> mice are metabolically similar to <i>Rnase1^{+/+}</i> mice.....	120
6.4.3: <i>Rnase1^{-/-}</i> mice do not exhibit elevated plasma cholesterol or increased body fat.....	123
6.4.4: <i>Rnase1^{-/-}</i> mice do not have altered inflammatory factor expression relative to <i>Rnase1^{+/+}</i> mice	124
6.5 Discussion	126

List of figures

1.1: Structures of RNase 1 and RI.....	16
1.2: Putative mechanism for the transphosphorylation and hydrolysis of RNA catalyzed by ptRNases.....	17
1.3: Ribbon diagram of the structure of RNase 1	20
1.4: Schematic of RNase 1 and angiogenin activities and substrates	25
1.5: Ribbon diagrams of the structure of angiogenin.....	27
1.6: Phylogenetic tree of species by ptRNase homology	33
2.1: Generation of <i>Rnase1</i> knockout mice.....	51
2.2: Verification of the loss of RNase 1 in <i>Rnase1</i> ^{-/-} mice	52
2.3: General phenotyping and longevity studies of <i>Rnase1</i> ^{-/-} mice.....	54
2.4: Effect of <i>Rnase1</i> on coagulation <i>in vitro</i>	56
2.5: Effect of <i>Rnase1</i> on coagulation <i>in vivo</i>	58
2.6: Effect of <i>Rnase1</i> on the levels of FXII and FXI	60
S2.1: Generation of <i>Rnase1</i> knockout mice: strategy and results.....	65
S2.2: Bar graph showing the tissue-specific expression of relevant genes in <i>Rnase1</i> ^{-/-} mice relative to that in <i>Rnase1</i> ^{+/+} littermates as measured by qPCR.....	66
3.1: Verification of the reduction of Ang in <i>Ang1</i> ^{+/-} mice	75
3.2: Effect of <i>Ang1</i> heterozygosity on litter size and survival.....	76
3.3: Embryonic development and effect of <i>Ang1</i> heterozygosity on uterine vascularization	78
S3.1: Genotyping for the <i>Ang1</i> allele.....	83
S3.2: Effect of <i>Ang1</i> heterozygosity on expression of other angiogenin genes	84
4.1: PyMOL renderings of ptRNases, with evolutionary conservedness mapped by residue	95
4.2: Design schematic for tagged ribonuclease constructs.....	96
4.3: Tagged ribonucleases are readily purified and retain activity	97
4.4: Gel showing purity of biotinylated ribonucleases.....	98
4.5: TEV protease cleaves the c-terminal peptide tag of ribonucleases.....	99
4.6: Mass spectrum of mRNase 1 acetylation.....	100
4.7: Reactivity of an anti-RNase 1 antibody across species	102
6.1: Effect of <i>Rnase1</i> on mouse body weight and length.....	121
6.2: Effect of <i>Rnase1</i> on consumption and metabolism.....	122
6.3: Effect of <i>Rnase1</i> on plasma lipids and body fat.....	123
6.4: Effect of <i>Rnase1</i> on gene expression of inflammatory markers	125

List of tables

2.1: Primers used for qPCR	42
3.1: Primers used for qPCR	72
4.1: Sequence and structure identity and similarity between ptRNases.....	94
4.2: Molecular weights of tagged ribonucleases.....	97
6.1: Primers used for qPCR.....	119

List of equations

2.1: Calculation of ribonuclease concentration from activity.....	44
2.2: Calculation of coagulation factor activity from a standard curve.....	49
4.1: Calculation of ribonucleolytic activity from concentration.....	92
6.1: Gompertz function for modeling growth curves of mice	117

Abbreviations

ALS	Amyotrophic lateral sclerosis
Ang	Angiogenin
ApoE	Apolipoprotein E
aPTT	Activated partial thromboplastin time
APAF1	Apoptotic peptidase activating factor 1
bp	Base pair
<i>C. albicans</i>	<i>Candida albicans</i>
Cas9	CRISPR-associated system 9
Ccl2	Chemokine C-C motif ligand 2/Monocyte chemoattractant protein 1
CD34	Cluster of differentiation protein 34
cDNA	Complementary deoxyribonucleic acid
CHO	Chinese hamster ovary
CMV	Cytomegalovirus
CNS	Central nervous system
CpA	Cytidylyl(3'→5')adenosine
CRAMP	Cathelin-related antimicrobial peptide
CRISPR	Clustered regularly interspaced short palindromic repeats
C _T	Cycle threshold
DEXA	Dual-energy x-ray absorptiometry
DNA	Deoxyribonucleic acid
DNase	Deoxyribonuclease
dsRNA	Double-stranded ribonucleic acid
<i>E. coli</i>	<i>Escherichia coli</i>
ELISA	Enzyme-linked immunosorbent assay
eRNA	Extracellular RNA
ES	Embryonic stem
FAM	Fluorescein
FPLC	Fast protein liquid chromatography
FSL	Factor sensitive and lupus
FIX	Coagulation factor IX
FXI	Coagulation factor XI
FXIa	Activated coagulation factor XI
FXII	Coagulation factor XII
FXIIa	Activated coagulation factor XII
<i>Gapdh</i>	Glyceraldehyde 3-phosphate dehydrogenase gene
hAng	Human angiogenin
HCC	Hepatocellular carcinoma
HEPES	4-(2-Hydroxyethyl)-1-piperazineethanesulfonic acid
HIV	Human immunodeficiency virus
HPSC	Hematopoetic progenitor/stem cells
<i>Hprt1</i>	Hypoxanthine phosphoribosyltransferase 1 gene
hRNase	Human ribonuclease
Icam-1	Intracellular adhesion molecule 1
IFNg	Interferon gamma

IgG	Immunoglobulin G
IL-1beta	Interleukin 1 beta
IL-6	Interleukin 6
IL-8	Interleukin 8
IL-10	Interleukin 10
IL-12	Interleukin 12
iNOS	Inducible nitric oxide synthase
K_D	Equilibrium dissociation constant
kDa	Kilodaltons
LC-MS	Liquid chromatography-mass spectrometry
lncRNA	Long noncoding ribonucleic acid
LPS	Lipopolysaccharide
MALDI	Matrix-assisted laser desorption-ionization
mAng	Mouse angiogenin
MBP	Maltose binding protein
mRNA	Messenger ribonucleic acid
mRNase	Mouse ribonuclease
miRNA	Micro-ribonucleic acid
NFkB	Nuclear factor kappa-light-chain enhancer of activated B cells
NKT	Natural killer T
NLS	Nuclear localization signal
nt	Nucleotide(s)
PC:PS:C	Phosphatidylcholine:phosphatidylserine:cholesterol
PCR	Polymerase chain reaction
piwiRNA	Piwi-interacting ribonucleic acid
PNGase F	Peptide- <i>N</i> -glycosidase F
Poly(A)	Poly(adenylic acid)
Poly(C)	Poly(cytidylic acid)
Poly(I)	Poly(inosinic acid)
Poly(U)	Poly(uridylic acid)
pRNA	NoRC associated RNA
ptRNase	Pancreatic-type ribonuclease
qPCR	Quantitative polymerase chain reaction
SDS-PAGE	Sodium dodecylsulfate polyacrylamide gel electrophoresis
SEM	Standard error of the mean
sTF	Soluble tissue factor
ssRNA	Single-stranded ribonucleic acid
rDNA	Ribosomal deoxyribonucleic acid
RI	Ribonuclease inhibitor
RNA	Ribonucleic acid
RNase	Ribonuclease
<i>Rpl13a</i>	60S ribosomal protein L13a gene
rRNA	Ribosomal ribonucleic acid
SEM	Standard error of the mean
SLE	Systemic lupus erythematosus
sncRNA	Small noncoding ribonucleic acid

<i>S. pneumoniae</i>	<i>Streptococcus pneumoniae</i>
TACE	Tumor necrosis factor alpha converting enzyme
TAMRA	5-Carboxytetramethylrhodamine
TAT	Thrombin–antithrombin
TBST	Tris-buffered saline with Tween
TEV	Tobacco etch virus
tiRNA	Transfer RNA halves
TLR7	Toll-like receptor 7
TM	Template modeling
TNFalpha	Tumor necrosis factor alpha
TNFR1	Tumor necrosis factor alpha receptor 1
TNFR2	Tumor necrosis factor alpha receptor 2
TOF	Time of flight
tRNA	Transfer ribonucleic acid
Vcam-1	Vascular cell adhesion protein 1
VE-cadherin	Vascular endothelial cadherin
VEGF	Vascular endothelial growth factor

Chapter 1

Emerging biological functions of pancreatic-type ribonucleases

1.1: Introduction

Ribonucleases (RNases) are omnipresent enzymes, fulfilling a variety of functions that are essential for the proper processing of RNA. These RNAs act in many biological niches: RNA primers that promote the replication of DNA are ultimately removed by RNase H, tRNAs for the ribosomal translation of proteins are matured by RNase P, and miRNAs that modulate expression of other RNA transcripts are processed by Dicer and Drosha. All of these functions are highly conserved in eukaryotes and are essential (1-4). Vertebrates express a unique RNase superfamily, termed the vertebrate secreted or pancreatic-type ribonucleases (ptRNases). ptRNases are secreted enzymes, and in contrast to the well-defined function of most intracellular RNases, our understanding of the biological function of ptRNases is still evolving. In recent years, we have begun to appreciate that RNAs in the extracellular space exert biological function as inflammatory mediators and enzyme activators. We have also learned more about the evolution and expression of the ptRNase family tree – which, taken together, have enabled new conclusions to be drawn about the biological roles of ptRNases.

1.2: The pancreatic-type ribonuclease superfamily

Pancreatic-type ribonucleases are perhaps the most well-studied enzyme family of the past century. This familiarity with ptRNases is owed to extensive studies of the prototypical member of this enzyme family, Ribonuclease A (RNase A), which was first isolated from pancreatic tissue of pigs and cows in the early 20th century, and was favored as a model protein during the “golden age of biochemistry.” During this time, studies of RNase A were used to pioneer many areas of biochemical research – it was the first enzyme for which an amino acid sequence was

determined (5), the first enzyme for which a mechanism of catalysis was identified (6), the third enzyme for which a crystal structure was determined (7), and was the subject of three Nobel-prize-winning studies on protein folding (8), protein chemical structure (9), and protein solid-phase synthesis (10). In addition to their contributions to biochemistry as a field, these studies informed the biochemical properties of other ptRNases that were discovered in the years that followed.

1.2.1: Characteristic biochemical features of ptRNases

ptRNases are small enzymes. RNase A is composed of 124 amino acid residues, with a molecular mass of 13.7 kDa, which is similar to that of other family members (11). Each ptRNase contains a signal peptide that directs secretion of the protein (12). Despite the low sequence identity between ptRNase genes (11), the protein structure of their encoded enzymes is

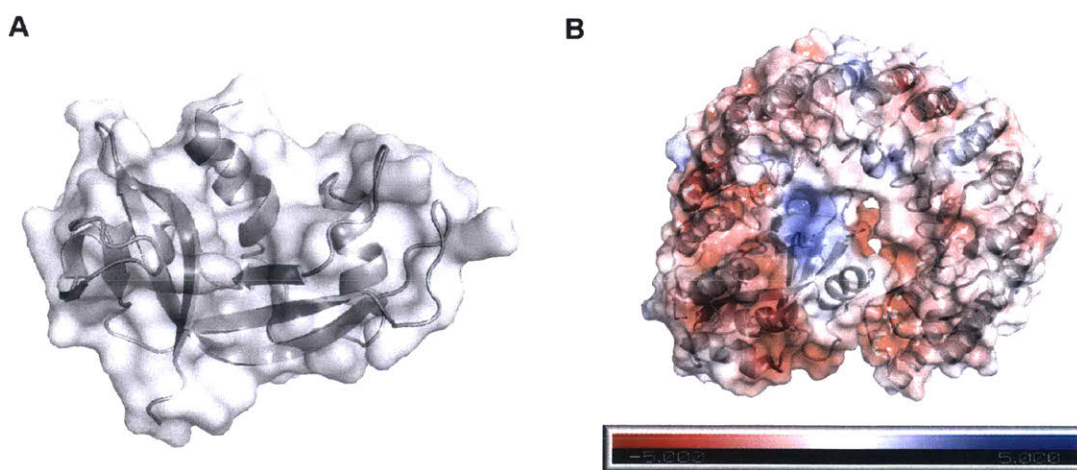


FIGURE 1.1. **Structures of RNase 1 and RI.** PyMOL renderings are based on PDB entry 1z7x. *A*, Ribbon diagram of RNase 1, with surface shown. This structure is conserved among ptRNases. *B*, Complex of RNase 1 with RI. Surface charges of the protein complex are shown on a scale from highly anionic (red) to highly cationic (blue), using the APBS plugin for PyMOL (13).

highly conserved (Figure 1.1, panel A). An invariant catalytic triad (His12, Lys41, and His119) endows ptRNases with nonspecific endonucleolytic activity, cleaving and hydrolyzing the P-O^{5'} bond on the 3' side of pyrimidine residues, with a general preference for cytidine over uridine (14,15) (Figure 1.2). ptRNases are cationic in character, and are also highly thermostable, owing to the presence of four intramolecular disulfide bonds (Figure 1.3) (16).

Additionally, all ptRNases interact with – and have their ribonucleolytic activity blocked by – ribonuclease inhibitor (RI), a 50-kDa protein that is likewise conserved in vertebrates (17) and is ubiquitously and abundantly expressed in the cytosol of cells (18). RI is comprised of leucine-

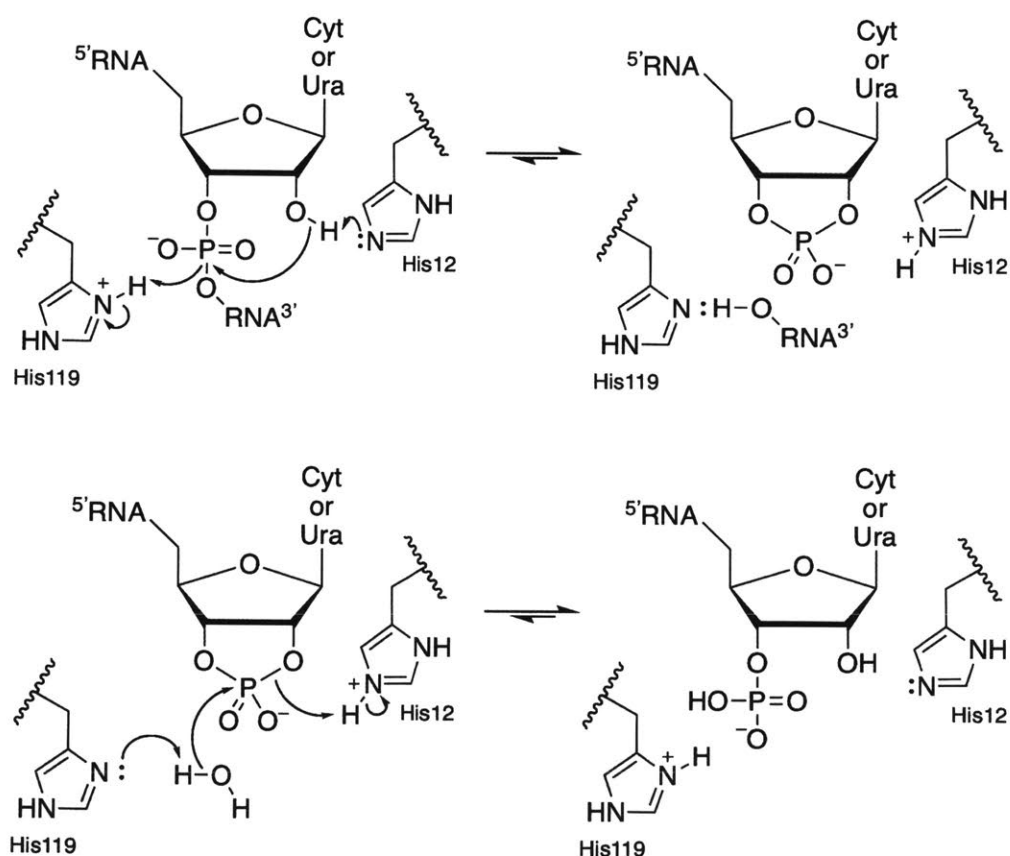


FIGURE 1.2. **Putative mechanism for the transphosphorylation and hydrolysis of RNA catalyzed by ptRNases.** Figure is adapted from reference (14).

rich repeats (19) and is anionic, facilitating coulombic interactions with ptRNases (20). The two proteins form a 1•1 complex with a K_D value on the order of 10^{-15} M, forming one of the tightest known protein-protein interactions (21). This interaction blocks the activity of ptRNases (22,23). (Figure 1.1, panel B). Consequently, RI is capable of protecting the cell from the action of free ptRNases, which would otherwise degrade cellular RNAs and drive cell death (24).

Based on these characteristics, ptRNases have been identified in all vertebrate species evaluated to date. Humans express 13 such enzymes, clustered near one another on chromosome 14 (12), with eight classified as “canonical” ptRNases (25). The remaining five exhibit more unusual features, such as the lack of one or more catalytic residues and lack of cationic character (11). Other species also express multiple ptRNases, with gene duplication resulting in larger numbers of enzymes in some species – mice express about 20 ptRNases, owing to duplication of the ribonuclease 2 and 3 and ribonuclease 5 (angiogenin) subfamilies (11).

1.2.2: Known biological functions of the ptRNase superfamily

Understanding of the biological roles of ptRNases has increased substantially since the first report on the function of RNase A in 1969, which claimed that the enzyme participated in ruminant digestion but was vestigial in non-ruminants (26). Now, we appreciate that ptRNases have other roles, with many family members exhibiting functions in innate immunity.

Antimicrobial activity has been described for a cluster of closely related ptRNases, including ribonucleases 2 and 3, as well as 6, 7, and 8 (25), which are expressed in eosinophil granules, placenta, and skin and exhibit relatively broad-spectrum cytotoxicity (27-31). Angiogenins derive their name from their well-documented angiogenic activity, but some subfamily members also been described to exhibit immunomodulatory activity. Ribonucleases 9 and 10, non-

canonical members of the ptRNase superfamily, play roles in the maturation of sperm (32,33). For other members of the ptRNase superfamily, however, biological functions are still emerging. Recent research on two family members in particular, RNase 1 and angiogenin (RNase 5), has revealed numerous new functions for these enzymes in various biological niches, ranging from control of vascular homeostasis and inflammation to cellular growth and quiescence. Here, we survey these newly identified biological roles.

1.3: Ribonuclease 1

Ribonuclease 1 is the most catalytically-active member of the ptRNase superfamily in humans. Its activity against ssRNA is the highest among ptRNases, and it is uniquely nonspecific in its substrate preference, showing the ability to degrade poly(C), poly(U), and poly(A) as well as dsRNA and RNA:DNA hybrids where other ptRNases degrade only a subset of these species (15). In contrast to the restricted expression of other ptRNases, RNase 1 is also very widely-expressed, with *Rnase1* mRNA being detectable in all tissue types (34). RNase 1 circulates in serum at a concentration of 250 ng/mL in healthy individuals (35), and this RNase 1 is produced predominantly by vascular endothelial cells (36,37). RNase 1 is secreted constitutively, but also accumulates in Weibel-Palade bodies in endothelial cells (38). Additionally, RNase 1 can be *N*-glycosylated at Asn34, Asn76, and Asn88 (39), a phenomenon that appears to vary with the tissue of origin (40,41) but has as-of-yet unknown biological implications (Figure 1.3). RNase 1 also interacts with multiple cell-surface glycans with micromolar affinity (42), exhibiting an especially specific interaction with Globo H (43).

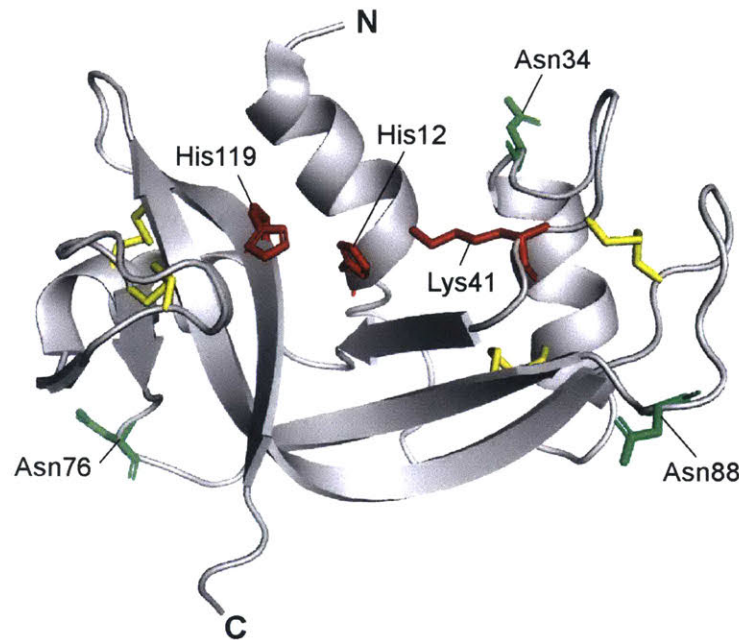


FIGURE 1.3. **Ribbon diagram of the structure of RNase 1.** PyMOL rendering is based on PDB entry 1z7x. Important side chains are shown as sticks. Active-site residues His12, Lys41, and His119 are shown in red. The three *N*-glycosylation sites at Asn34, Asn76, Asn88 are shown in green. The four intramolecular disulfide bonds are highlighted in yellow.

1.3.1: Early studies of the biology of RNase 1

The first studies of RNase 1 in humans to draw widespread attention identified its upregulation in the plasma of patients with pancreatic cancer (44), which spurred excitement about the use of RNase 1 as a biomarker. Later studies showed that RNase 1 expression was elevated not only in pancreatic cancer, but in other malignant states (35,45,46). The idea of RNase 1 as a biomarker was ultimately abandoned, as it is nonspecific – RNase 1 is upregulated in a wide variety of disease states, including bacterial and viral infection (47), smoking (48), burn injury (49), surgery (50), myocardial infarction (51), ageing (52), Alzheimer’s disease (53), malnutrition (54), and arthritis (55).

Yet, RNase 1 returned to the forefront of cancer research with the identification of a homolog in the northern leopard frog (*Rana pipiens*) that exhibited toxicity against cancer cells (56). This cytotoxicity was attributed to its ability to enter the cytosol and degrade cellular RNA, while being insensitive to binding by human RI (57). Variants of RNase 1 were endowed with the ability to evade association with RI, and showed promise as anti-cancer cytotoxic agents (58), using the same mechanism outlined for the amphibian enzyme, without immunotoxicity (42,58,59). Clinical trials are underway to bring ptRNase therapy to the clinic based on this mechanism of action (60,61).

During these studies, the function of endogenous RNase 1 remained elusive. It was only with the appreciation that RNA exists in the extracellular space – where RNase 1 is free to act without inhibition by RI – that new ideas began to emerge as to biological roles for RNase 1.

1.3.2: Extracellular RNA – key to the function of an extracellular RNase

RNA was long thought to be unstable outside of the cellular environment – ptRNases had been known to exist in the extracellular space for many years, and were thought to immediately degrade any extracellular RNA (eRNA) species (62). More recent studies showed that RNA can indeed persist in serum long enough to permit analysis – EBER1 RNAs from Epstein–Barr virus, as well as tyrosinase mRNA from melanoma cells, were successfully isolated from serum and plasma (63,64). Characterization of eRNAs has revealed that almost every known class of RNA exists outside the cell. Whereas the bulk of eRNA are miRNAs, mRNA, and tRNA, other types of RNA, such as rRNA, piwiRNA, lncRNA, and sncRNA have also been detected in varying

proportions (65-67). These eRNAs are carried in a variety of ways, including in membrane vesicles such as microvesicles and apoptotic bodies (68), ribonucleoprotein complexes (69), and high-density lipoproteins (70).

We now appreciate that eRNA can be actively released from cells (71), with cancer cells releasing RNA at a significantly higher rate than noncancerous cells (72,73). This eRNA has been reported to act as a messenger between cells, driving changes in gene expression in paracrine via delivery of mRNA or miRNA (74,75). eRNA does not need to be coding RNA to exert biological function, as it has been demonstrated to act as a potent inflammatory mediator. eRNA stimulates lymphocyte adhesion to smooth muscle by upregulating expression of adhesion molecules such as Vcam-1, Icam-1, P-selectin, and Ccl2 in smooth muscle cells (76), and drives macrophage polarization to an M1 (proinflammatory) phenotype, increasing expression of inflammatory markers such as TNF α , IL-1 β , IL-6, IL-12, and iNOS (77). eRNA also potentiates blood coagulation by acting as an anionic scaffold for the activation of intrinsic coagulation proteases FXI, FXII, and plasma prekallikrein (78,79). At least for its procoagulant activities, the size and secondary structure of eRNA appears to be just as important as its sequence, with coagulation protease activity only potentiated with RNAs greater than 100 nt in size, and more strongly potentiated with RNAs forming a stable hairpin structure (80). Poly(G) and poly(I) RNAs have been reported to be the best activators of intrinsic proteases *in vitro* (81).

1.3.3: New biological roles for RNase 1

In light of these discoveries, studies on RNase 1 highlighted new roles for the enzyme that were mediated through degradation of these eRNAs rather than cell internalization. Interestingly, in

parallel with other studies demonstrating the anti-cancer properties of modified RNase 1, wild-type RNase A was capable of reducing tumor growth in mice when administered exogenously (73). Rather than direct cytotoxicity, the slowing of tumor growth was due to the prevention of pro-inflammatory activity of eRNA. eRNA was found to drive TNF α expression via activation of TNF α -converting enzyme (TACE) in macrophages (76), thereby producing an inflammatory environment conducive to tumor growth.

Other studies have shown similar effects of RNase 1 on inflammation in other contexts. In a mouse model of atherosclerosis, eRNA accumulated in atherosclerotic plaques and was able to recruit macrophages to these plaques (77). Elevated plasma eRNA was also associated with the incidence of ischemia-reperfusion injury in patients undergoing heart surgery (82), and with edema and tissue death in a mouse model of myocardial infarction (83). These negative effects of eRNA were blocked by administration of exogenous RNase 1, although notably, RNase 1 therapy was reported to be most effective when given prophylactically, as changes engendered by eRNA exposure were irreversible by RNase—after injury occurred (84). Additionally, a TLR7-overexpression mouse model of systemic lupus erythematosus suffered fewer inflammatory symptoms when RNase A was knocked-in (85), resulting in extended lifespan, reduced myeloid cell number, and reduced inflammatory deposits in the kidneys and liver of mice. Pre-treatment of an ischemic murine stroke model with RNase A also resulted in less edema, smaller brain lesions, and reduced vascular permeability in treated animals than controls (86,87). Treatment of rats undergoing heart transplantation surgery with RNase 1 also resulted in reduced edema, reduced thrombus formation, and improved graft survival (88).

RNase 1 has been shown to be beneficial in a mouse model of arterial thrombosis, with treatment resulting in clearance of eRNA from the thrombus, delay of vascular occlusion, and reduction in thrombus size (79). Studies in our laboratory have also demonstrated that loss of RNase 1 results in a procoagulant phenotype, with absence of the enzyme causing accumulation of eRNA in the plasma and activation of intrinsic coagulation factors. The mechanism of action of eRNA in blood clotting is activation of intrinsic coagulation factors FXII and FXI, as well as the upstream protease plasma kallikrein (79,81). This process is closely linked to inflammation, as plasma kallikrein is a protein that, when cleaving plasma kininogen, releases bradykinin, a potent vasodilator and vascular permeabilizing agent. Interestingly, eRNA alone spurs vascular permeabilization in a manner mediated through VEGF and nitric oxide synthase, leading to disintegration of tight junctions in cells (87).

Given the myriad pro-inflammatory functions ascribed to eRNA and the studies conducted to date on RNase 1, the biological function of this enzyme appears to be more complex and multifaceted than appreciated previously. Early studies demonstrating the upregulation of RNase 1 in many disease-states likely point to a general role for RNase 1 as a regulator of inflammatory processes, particularly in the cardiovascular system (Figure 1.4). A role for RNase 1 in this niche reflects its high compatibility with the pH of the vascular environment (42), and its colocalization in endothelial cells with other vascular regulators, such as von Willebrand factor and P-selectin (38). RNase 1 could modulate the effects of RNA accumulating in the extracellular space secondary to tissue damage, malignancy, or death, and thus prevent excess activation of macrophage activity, blood coagulation, and vascular permeabilization. Future

studies of RNase 1 are likely to uncover not only the functions of the enzyme, but the biological roles of many poorly characterized RNA substrates on which this nonspecific enzyme acts.

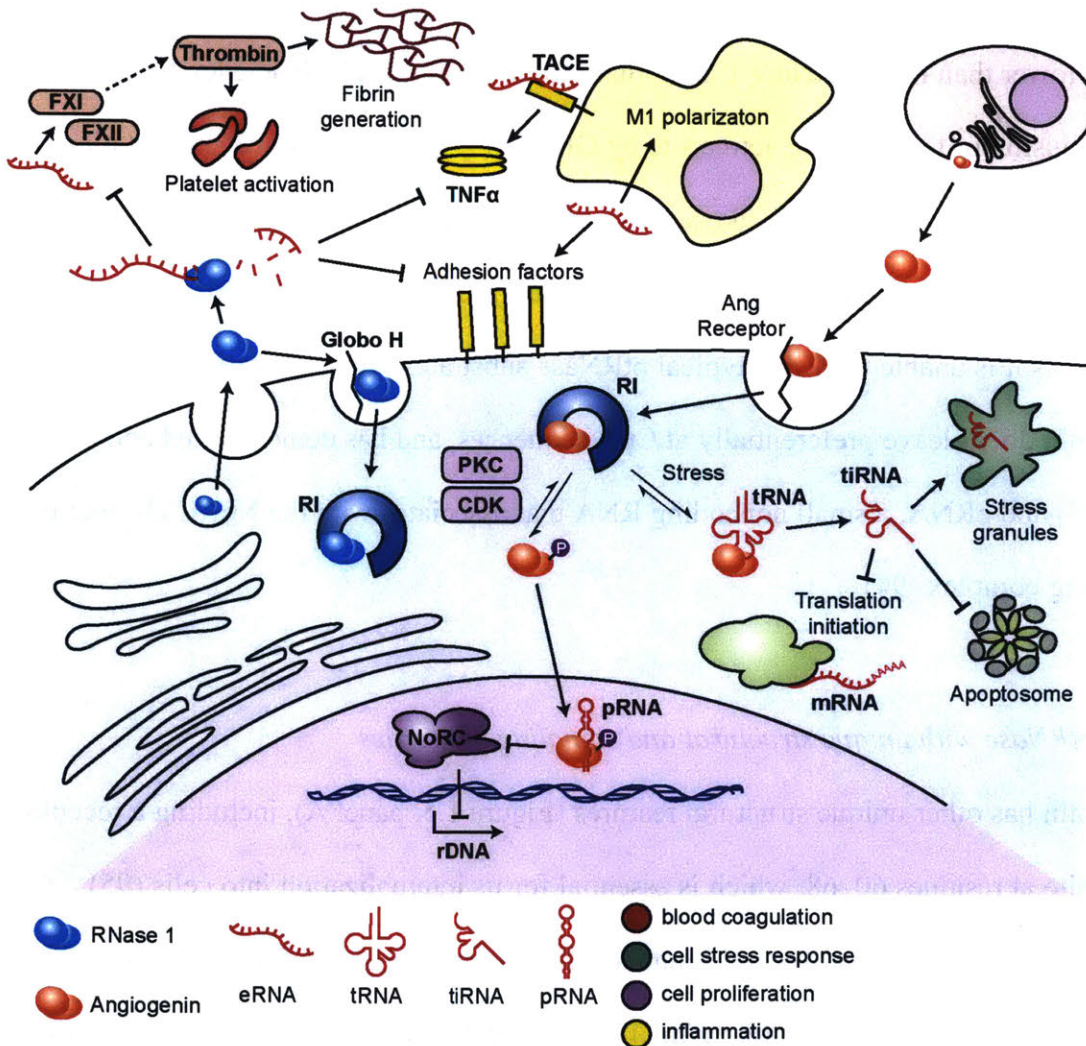


FIGURE 1.4. Schematic of RNase 1 and angiogenin activities and substrates. RNase 1 acts primarily on targets outside of the cell, where it degrades extracellular RNAs (eRNA). These eRNA would otherwise act as activators of coagulation and inflammatory pathways. Angiogenin, in contrast, mediates its effects intracellularly, driving both cellular proliferation via pRNA degradation and cellular quiescence in response to stress via tRNA degradation.

1.4 Angiogenin

Angiogenin is named for its ability (unique among ptRNases) to stimulate blood-vessel growth (89). This activity coincides with other unusual features. For example, angiogenin has activity 10^4 -fold lower than that of RNase 1 and other ptRNases (90). This deficiency has been attributed to the occlusion of the enzymic active site by Gln117 (91). Notably, however, mutation of this residue does not restore RNase 1-like activity to angiogenin, suggesting that other conformational differences exist (92). The substrates preferred by angiogenin are also somewhat restricted, as it is unable to cleave typical ptRNase substrates such as poly(C) and poly(U). Angiogenin does cleave preferentially at CpA sequences, and has demonstrated activity against tRNA (93) and pRNA, a small noncoding RNA that associates with the NoRC chromatin remodeling complex (94).

1.4.1 A ptRNase with unique structural and signaling properties

Angiogenin has other unique structural features (Figure 1.5, panel A), including a receptor-binding site at residues 60–68, which is essential for its internalization into cells (95).

Angiogenin was determined to act through a cell-surface receptor, as the circulating concentration of the enzyme (~400 ng/mL) is much higher than the concentration required to stimulate its angiogenic activity (96) – yet, this activity occurs in normal cells in a density-dependent manner (97). Several different proteins have been identified as receptors that mediate angiogenin activity, including Syndecan-4 in astrocytes (98) and Plexin B2 in multiple cell types

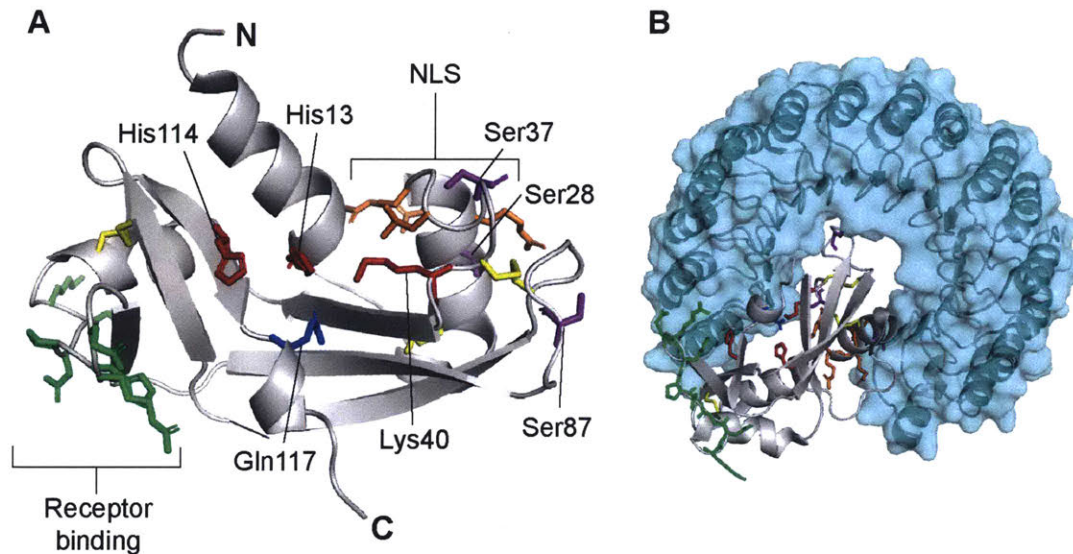


FIGURE 1.5. Ribbon diagrams of the structure of angiogenin. PyMOL renderings are based on PDB entries 1ang and 1a4y. Important side chains are shown as sticks. *A*, Ribbon diagram of angiogenin. Active-site residues His12, Lys41, and His119 are shown in red. Gln117, which occludes the active site, is shown in blue. The three intramolecular disulfide bonds are highlighted in yellow. The nuclear localization signal (NLS) (RRRGL) is shown in orange. The receptor binding domain (KNGNPHRE) is shown in green. Phosphorylation sites at Ser28, Ser37, and Ser87 are shown in purple. *B*, Ribbon diagram of angiogenin in complex with RI, shown in cyan. Note that binding of angiogenin to RI occludes the active site and nuclear localization signal of angiogenin, and that the three phosphorylated serine residues are in contact with the RI-binding interface.

(99). Angiogenin also contains a nuclear-localization signal (RRRGL, at positions 31-35) (100), which drives the accumulation of the enzyme in the nucleolus and is required for its angiogenic activity (101).

Nuclear localization of angiogenin would normally be prevented due to the association of the enzyme with cytosolic RI, to which angiogenin binds with subfemtomolar affinity (21).

Angiogenin avoids association with RI by disruption of its Coulombic interactions through phosphorylation, which is known to occur at Ser28, Ser37, and Ser87, and is mediated through protein kinase C and cyclin-dependent kinase (Figure 1.5, panel B). This phosphorylation event

has also been demonstrated to be essential for nuclear localization and proliferative activity of angiogenin (94).

In the nucleus, angiogenin has been shown to cleave pRNA, which normally associates with TIP5, a member of the NoRC chromatin remodeling complex. pRNA is responsible for recruitment of TIP5 and NoRC to the ribosomal DNA (rDNA) promoter, which results in repression of rDNA transcription (102,103). Cleavage of pRNA prevents its association with TIP5 and impairs recruitment of NoRC to the rDNA promoter, which results in derepression of rDNA and cell growth (94). This signaling pathway is unique among transcription factors, as no other proteins are known to reach the nucleus from the extracellular space and effect transcriptional change.

1.4.2 Angiogenin-mediated cell growth

The angiogenic ability of angiogenin has been studied in the context of cancer for over 50 years, as it was initially identified as a factor capable of stimulating blood vessel growth from human adenocarcinoma (89). Angiogenin has since been shown to be secreted by multiple types of tumors, including prostate cancer (104), oral squamous cell carcinoma (105), and melanoma (106). Its expression from cancer cells appears to be regulated by HIF-1 α (105), suggesting a mechanism of action for tumor neovascularization in response to oxygen starvation. Angiogenin has also been studied as a biomarker in human colorectal cancer (107), bladder cancer (108), and breast cancer (109), as its expression has been correlated with tumor aggressiveness.

Consequently, angiogenin is being explored as a therapeutic target for the treatment of cancer.

Knockdown of angiogenin in bladder cancer cells using siRNA was successful in reducing tumor

growth in a mouse xenograft model (110), and antibody neutralization of angiogenin reduced *in vitro* migration of triple-negative breast cancer cells (111). An experimental small-molecule drug, (8-amino-5-(4'-hydroxybiphenyl-4ylazo)naphthalene-2-sulfonate), that inhibits catalysis by angiogenin, has also been developed, and shows promising results in inhibition of tumor growth and vascularization in mouse xenograft models (112).

Angiogenin has also been demonstrated to act in the placenta, endometrium, and ovarian follicle, tissues that normally undergo extensive angiogenesis in adults (113). Angiogenin is present in ovarian follicular fluid, with expression stimulated by human chorionic gonadotropin – a hormone that promotes luteinization and angiogenesis during formation of the corpus luteum (114). In studies of ovarian follicle transfer, angiogenin was identified to be a crucial factor in mediating the angiogenic and follicle-preserving effect of co-transplanted mesenchymal stem cells (115), underscoring the importance of the enzyme for follicle survival and function. Angiogenin expression in the endometrium reflects the menstrual cycle, with expression approximately doubling in the mid-to-late secretory phases relative to the proliferative phase (116). In pregnancy, angiogenin expression increases over time in the human placenta, with maximal expression at term (117,118). In the placenta, angiogenin is found alongside markers of early vasculogenesis, such as VE-cadherin, CD34, and von Willebrand factor, and is present in developing fetal blood vessels (119).

Angiogenin can act on cells other than in vascular endothelium to promote cell growth. This versatility was first observed in the context of cancer – HeLa cells both secrete angiogenin and take it up, with angiogenin localizing to the nucleus and stimulating cell proliferation

independent of cell density (120). Angiogenin has also demonstrated this activity in PC-3 prostate cancer cells (104). In addition, angiogenin appears to promote growth of hepatocellular carcinoma cells (HCCs) in paracrine. HCCs secrete angiogenin, which is taken up by tumor-associated hepatic stellate cells, spurring their activation, which in turn promotes the growth and metastasis of HCCs by modulation of the extracellular matrix (121,122). Angiogenin also appears to modulate the growth of neurons, as it is expressed in the nervous system during embryonic development in mice and is localized to axonal growth cones, where it appears to promote axonal growth and neurite pathfinding (123).

1.4.3 Angiogenin-mediated protection from cell stress

In addition to stimulating neuronal growth, angiogenin has been also been observed to have a protective effect on motoneurons in the context of amyotrophic lateral sclerosis (ALS). Similarly to the action of angiogenin in hepatocellular carcinoma, this activity is mediated in paracrine, by astrocyte uptake of motoneuron-secreted angiogenin (98). Angiogenin-stimulated astrocytes are then able to protect motoneurons against excitotoxic stress through a mechanism that involves protein expression changes in astrocytes largely related to modulation of the extracellular matrix (124). This finding helps to explain many earlier studies that linked mutations in angiogenin to ALS, many of which are missense mutations that interfere with the catalytic activity of the enzyme (125,126). These studies did not, however, identify specific effector RNA targets for angiogenin.

A possible effector substrate for angiogenin in neurons is tRNA, which has been known to be an angiogenin substrate for many years (93). This activity was first reported as cytotoxicity, as

cleaved tRNA were identified to arrest protein translation. Yet, it has only recently been appreciated that tRNA cleaved at the anticodon loop, termed tiRNA, are a product of catalysis by angiogenin that is induced by cellular stress (127,128). These tiRNAs do promote the formation of stress granules and inhibit protein synthesis, which is suggested to occur via displacement of the initiation factor eIF4G/A from mRNA (129). Nonetheless, tiRNAs also exert a pro-survival effect in cells by binding to apoptotic protease-activating factor 1 (APAF1) in a manner that competitively blocks the binding of cytochrome C and formation of the apoptosome (130).

Angiogenin has also been implicated to play roles in stem cell self-renewal. In hematopoietic stem/progenitor cells (HPSCs), angiogenin has been found to generate tiRNA and reduce protein synthesis, which is suggested to promote stemness and quiescence of these cells, while having a proliferative effect on myeloid progenitor cells (131). The mechanism by which angiogenin differentially regulates these two cell types is unknown.

Additionally, some antimicrobial and anti-inflammatory activity has been demonstrated for angiogenin. It is an acute-phase protein and was initially thought to contribute to angiogenesis as part of the tissue repair process (132), but more recent studies have reported that angiogenin is also toxic to *C. albicans* and *S. pneumoniae*. Closely related proteins in the angiogenin subfamily in mice appear to have broader-spectrum antimicrobial activity (133). Further, angiogenin suppresses the effects of TNF α in fibroblasts, reducing expression of NF κ B, TNF α R1 and TNF α R2, IL6, and IL8 (134) and exerting a net anti-inflammatory effect.

Emerging research on angiogenin suggests that in addition to its well-characterized roles in vascular growth, this enzyme could play broader roles in cell growth and survival (Figure 1.4).

Future research on angiogenin might offer a better understanding of the mechanisms that determine whether angiogenin drives proliferation or quiescence in a cell. Angiogenin has been an attractive drug target for both antiangiogenic therapy in cancer (112) or protection from cellular stress in neurodegeneration (135), and more knowledge of the regulators of its activity could allow more selective targeting of the enzyme in specific biological niches.

1.5 Connections to vertebrate physiology

New roles identified for RNase 1 and angiogenin cluster broadly into the areas of regulating vascular homeostasis and cell growth/survival. Interestingly, some of these roles are tied to the innate physiology of vertebrates, where ptRNase expression is exclusively present – the only enzyme family for which this is the case (136). The distribution of ptRNase subfamilies within vertebrates does vary, however. Lower vertebrate species such as fish express only angiogenin-like enzymes (137,138), and the diversification of the RNase 2 and 3 family occurs only in rodents (11). Some highlights of this evolutionary path are depicted in Figure 1.6.

Angiogenin has been suggested to be the primordial ptRNase family member. This thought is supported by the presence of ptRNase enzymes in fish that are more similar to human angiogenin than to RNase 1 or other ptRNases (138). Additionally, angiogenin has three intramolecular disulfide bonds in contrast to the four in other ptRNases (25). This fourth disulfide bond is more readily reduced than the other three (139), suggesting it is less essential to the enzyme and was likely a later addition (140). Angiogenin, then, is likely as old as vertebrates themselves – reflected by its fundamental roles in cell growth and survival. The functions of angiogenin in the

brain highlight this centrality, as the neural crest, which gives rise to protective glial cells, is not present in invertebrates (141).

One of the other hallmarks of vertebrate physiology is the presence of a closed circulatory system with a continuous endothelial barrier (153), which requires a specialized blood clotting

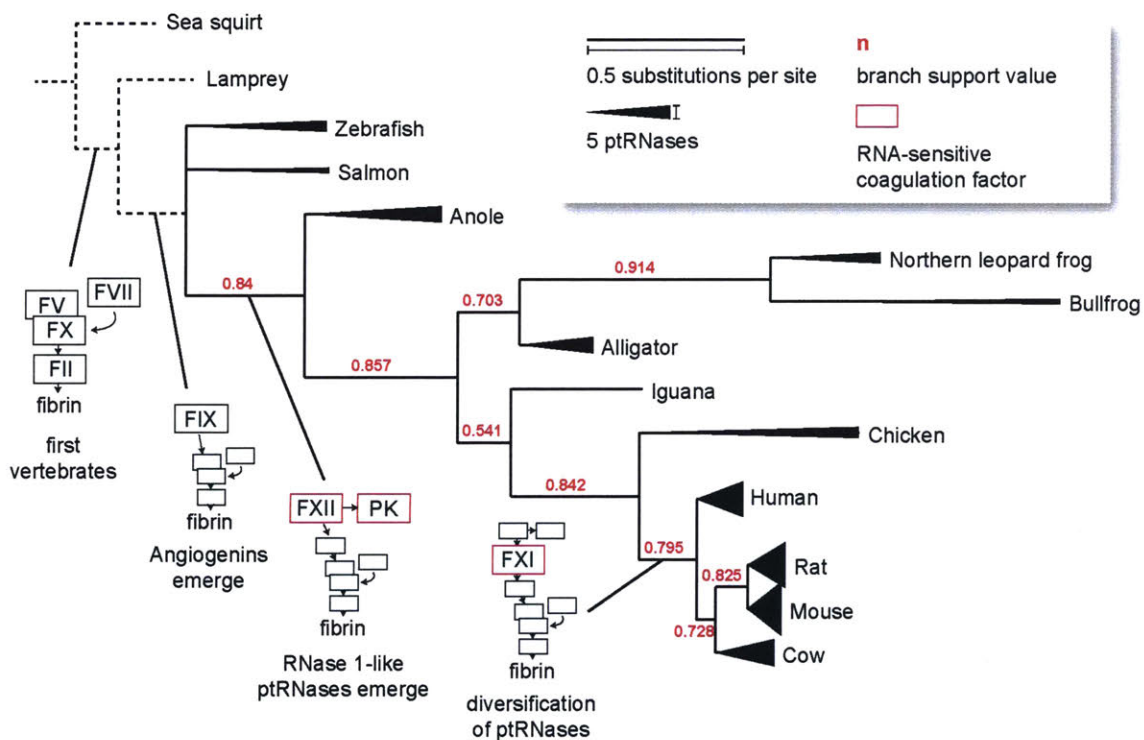


FIGURE 1.6. Phylogenetic tree of species by ptRNase homology, annotated with blood coagulation factors. Protein sequences of RNase 1 homologs from Uniprot entries P07998 (human), P00683 (mouse), P00684 (rat), P61823 (cow), P30374 (chicken), P80287 (iguana), A0A151LY34 (alligator), P11916 (bullfrog), Q8UVX5_LITPI (northern leopard frog), H9GD73_ANOCA (anole), A0A1S3RRZ8 (salmon), and A5HAK0 (zebrafish) were used to generate a phylogenetic tree using the program phylogeny.fr (142-146). The branch support value is shown in red for each junction, and the number of substitutions per site is represented by line length. Line weight at the termini of each leaf represents the number of ptRNase proteins reported to be expressed in each organism (11, 137, 138, 147-150). Species without identified ptRNases are represented by dashed lines and are not to scale; they are included to highlight the emergence of vertebrate coagulation factors. The emergence of angiogenins in fish, RNase 1-like proteins in amphibians, and RNA-sensitive coagulation factors in amphibians and mammals is highlighted at the appropriate junctions (151, 152)

system (152). Lower vertebrates share the common thrombin-catalyzed coagulation pathway present in humans, but lack intrinsic factor proteases such as FXII, FXI, and prekallikrein (154). Intrinsic factors emerged with the evolution of amphibians, with FXI appearing only in mammals (151). Interestingly, the emergence of these RNA-sensitive coagulation factors mirrors the presence of RNase 1. RNase 1 is more highly expressed in reptiles and birds than in fish that do not express these contact factors, and much more highly expressed in mammals (155), suggesting that the evolution of RNA-responsive coagulation proteins and a cognate extracellular ribonuclease to regulate this activity were simultaneous.

Vertebrates also exhibit a much more specialized immune system than that found in invertebrates, with the emergence of major histocompatibility complex proteins, T-cell receptor, and immunoglobulins. The rapid evolution of ptRNases has been used to suggest that these enzymes also are part of the vertebrate-specific immune response (156), as many family members (including angiogenin) are cytotoxic against a variety of microorganisms. RNase 1 alone, however, is not cytotoxic – instead, it modulates a broad array of cytokines and affects the interplay between innate and adaptive immunity via control of eRNA-mediated macrophage polarization. These macrophages can then influence T and B cell activity (88). The polarization of macrophages also appears to be a vertebrate-specific phenomenon as well, as polarization has been observed in fish but not lower animals (157). These effects represent multiple possible avenues by which eRNA (and by extension, RNase 1) might regulate the inflammation associated with cancer, autoimmune disease, and infectious disease.

1.6 Prospectus

Numerous new biological functions of pancreatic-type ribonucleases have been outlined in the past decade. Still, our appreciation of the function of these enzymes in their endogenous environment is lacking. The effects of RNase 1 as an exogenous agent have been characterized in multiple models of cancer, vascular homeostasis, and injury. Angiogenin has been more thoroughly studied, but little information about the phenotype of constitutive knockouts are available. Further study on the biological functions of these enzymes would advance our knowledge of the roles of the ptRNase superfamily and the functions of novel RNA populations, and guide their use as therapeutic targets.

The central aim of this thesis is to describe biological functions for RNase 1 and angiogenin through the study of knockout mouse models lacking these enzymes. I identify that RNase 1 is a natural anticoagulant enzyme in mice, and that angiogenin plays an important role in reproduction and embryonic viability. I have also have worked to generate tools for further study of these enzymes in biological systems by producing proteins for use in a phage-display antibody-generation system. Together, the studies in this thesis provides a previously unappreciated perspective on the biological functions of these two ptRNases, and sets the stage for future study of these dynamic proteins in physiological contexts.

Chapter 2

Loss of ribonuclease 1 produces a hypercoagulable phenotype

Contributions: J.E. Lomax performed the work to generate *Rnase1*^{-/-} mice and designed the genotyping strategy. J.P. Sheehan was involved in experimental design and data interpretation for kinetic coagulation, saphenous vein bleeding, and factor activity assays. D. Gailani and B. Mohammed performed plasma immunoblots and aided in data interpretation. Technical assistance in dissection/surgery was provided by R. Sullivan, T. Hacker, and G. Diarra, and in mouse colony management by C. Feldman and K. Tippins. I designed and carried out all other experiments, and wrote the manuscript.

This chapter has been submitted as *Loss of ribonuclease 1 produces a hypercoagulable phenotype* to the *Journal of Biological Chemistry*.

2.1: Abstract

Ribonuclease 1 (RNase 1) is a small secretory enzyme with unknown biological function. In contrast, recent work has established biological roles for extracellular RNAs (eRNAs). In particular, eRNAs can initiate blood coagulation via activation of intrinsic factor proteases (such as FXII and FXI), and studies using the bovine homolog of RNase 1 (RNase A) have revealed its ability to prevent blood vessel occlusion in mouse models of thrombosis and stroke. We sought to evaluate the biological role of RNase 1 in an organismal context by generating and analyzing RNase 1 knockout (*Rnase1*^{-/-}) mice. These mice are viable, fertile, and appear generally healthy, but *Rnase1*^{-/-} plasma contains more RNA than does the plasma of *Rnase1*^{+/+} mice. In addition, the plasma of *Rnase1*^{-/-} mice form fibrin clots more rapidly. Yet, *Rnase1*^{-/-} mice do not exhibit perturbations in thrombin–antithrombin complex formation, tail or saphenous vein bleeding, or iron-chloride thrombosis assays *in vivo*. These data suggest activation of intrinsic pathway factors, and FXII and FXI activity is indeed elevated in *Rnase1*^{-/-} mice. This phenotype is consistent with known roles of eRNA and the intrinsic pathway in blood coagulation, and mirrors the largely healthy phenotype of FXII knockout mice. Our work identifies RNase 1 as an endogenous regulator of blood coagulation.

2.2: Introduction

Ribonuclease 1 (RNase 1) is a secretory protein with robust and nonspecific ribonucleolytic activity. The physical and catalytic properties of this enzyme are well understood due to its similarity to RNase A, which is a bovine homolog of RNase 1 that served as a model protein for seminal studies in biological chemistry during the 20th century (14,158-160). RNase 1 is conserved in vertebrates and is part of a large enzyme superfamily termed the pancreatic-type ribonucleases (ptRNases) or vertebrate secretory ribonucleases, many of which have been identified to play diverse biological roles (25).

No distinct biological function has been identified for RNase 1. The earliest hypothesized function of RNase 1 was in digestion, as RNase A is highly expressed in the pancreas of cows, and RNase 1 was thought to have negligible function in non-ruminant animals (26). More recent research has challenged this hypothesis, demonstrating a wide range of non-digestive activities for exogenously-administered RNase 1 *in vitro* and *in vivo*, including as an anti-viral agent (161,162) and cancer chemotherapeutic agent (163,164).

Still, the function of endogenous RNase 1 remains elusive. RNase 1 has the highest catalytic activity and the widest expression pattern of any of the ptRNases, and is present in many bodily fluids (165,166). In both humans and mice, RNase 1 circulates at ~0.5 µg/ml (35). The major source is the vascular endothelium (36,38), and the pH optimum for its enzymatic activity is 7.3, which is close to the pH of blood (42). Thus, we reasoned that the endogenous enzyme could play a role within the vascular system.

Recent studies have highlighted the ability of RNase A to exert biological effects via degradation of extracellular RNA (eRNA), which is known to play roles in immunity, cancer, and blood coagulation (73,76,79). RNA has been shown to potentiate the activation of intrinsic coagulation pathway factors XII (FXII) and XI (FXI) via physical interaction with these enzymes (79). Further study suggests that RNA is a particularly effective activator in the conversion of FXII to FXIIa by plasma kallikrein and in the conversion of FXI to FXIa by thrombin (81). Indeed, previous analyses of RNase A have highlighted its ability to reduce eRNA-mediated thrombosis in murine models of carotid thrombosis (79) and stroke (86). eRNA secondary structure is thought to be important for its procoagulant activity (80), and RNase 1, which has higher activity against dsRNA than does RNase A, might be better adapted as an endogenous regulator of eRNA (42).

Evaluation of RNase 1 in an organismal context is indicated to determine its biological function. Here, we report the generation of *Rnase1* knockout mice and characterize the impact of the loss of RNase 1 on blood coagulation *in vitro* and *in vivo*. Our results reveal activation of intrinsic coagulation factors upon loss of RNase 1. These data indicate that RNase 1 serves as an endogenous regulator of blood coagulation.

2.3: Experimental procedures

2.3.1: Materials—Murine ribonuclease 1 (RNase 1) and ribonuclease A were produced in *E. coli* as described previously (167). PNGase F was from New England BioLabs. Human FXI-, FXII-, and PK-deficient plasma was from George King Bio-Medical. Murine FXI- and FXII-deficient plasma was obtained as described previously (168,169), and murine FIX-deficient plasma was

obtained as described previously (170). Soluble tissue factor was a gift from B. S. Schwartz (University of Wisconsin–Madison).

Phosphatidylserine (PS), phosphatidylcholine (PC), and cholesterol were from Avanti Polar Lipids. PC:PS:C (molar ratio, 75:25:20) phospholipid vesicles were prepared by extrusion through a 100-nm polycarbonate filter. Primers, DNA constructs, and 6-FAM–dArUdAdA–6-TAMRA ribonuclease substrate were from Integrated DNA Technologies. Poly(cytidylic acid) and lipopolysaccharide (LPS) were from Sigma–Aldrich.

Equipment—All fluorescence and absorbance measurements were made with a Tecan M1000 fluorescence plate reader, unless stated otherwise.

Conditions—All procedures were performed at ambient temperature (~22°C) and pressure (1.0 atm) unless noted otherwise.

2.3.2: Generation of Rnase 1 knockout mice—All experiments with animals were conducted in accord with an Institution on Animal Care and Use Committee-approved protocol at the University of Wisconsin–Madison. Ribonuclease 1 knockout mice (*Rnase1*^{-/-}) were generated in our laboratory using recombineering methods (171). The *Rnase1* targeting vector was generated via homologous recombination in *E. coli*. To target the mouse *Rnase1* gene for deletion *in vivo*, loxP sites were engineered within intronic sequences to flank exon 2 (which contains the entire coding sequence of the gene), marking this region for eventual excision by Cre recombinase. A neomycin resistance (*Neo*) cassette, flanked by FRT sequences, was inserted for positive

selection, and thymidine kinase (*TK*) was included for negative selection. This targeting vector was introduced into 129Sv/Ev murine embryonic stem (ES) cells, and positively selected ES clones were verified with a Southern blot. Correctly targeted clones were sequenced to confirm that all loxP and FRT sites were present and intact. Male germline chimeras were mated to wild-type C57Bl/6 mice, transmitting the targeted *Rnase1* allele. Karyotype analysis and chromosome counting was performed at the Molecular Cytogenetics Laboratory at Yale University (New Haven, CT). Blastocyst injection was performed by the University of Wisconsin–Madison Transgenic Animal Facility.

Ribonuclease 1-deficient mice (*Rnase1*^{-/-}) were generated in our laboratory with assistance from the University of Wisconsin–Madison Transgenic Animal Facility. The knockout (KO) mice were produced in a C57BL6J (Stock 000664, Jackson Laboratories)/129SvJ (embryonic stem cells, Genome Systems Inc.) background. Neomycin resistance cassettes used for selection were removed by crossing transgenic mice with FLP deleter mice (Stock 009086, Jackson Laboratories), and constitutive knockout of *Rnase1* was achieved by crossing *Rnase1*^{fllox/fllox} mice with ubiquitously-driven CMV-Cre mice (Stock 009086, Jackson Laboratories) (Figure 2.1, panel B). Experiments herein have been conducted on gender-matched littermates resulting from *Rnase1* heterozygote crosses. The genotyping of *Rnase1*^{-/-} mice was determined using a universal primer set for the *Rnase1* locus: forward 5'-TGCAGGGACTAGGGTAGTGG-3' and reverse 5'-CATGACACAGGACAGGAACG-3'. This primer set produces a 797-bp band for the wild-type locus, a 2.77-kb band for the transgenic locus + neomycin-resistance cassette, a 2.08-kb band for the KO locus + neomycin-resistance cassette, a 973-bp band for the transgenic locus

– neomycin-resistance cassette, and a 286-bp band for the KO locus – neomycin-resistance cassette.

2.3.3: Quantitative PCR—Quantitative real-time PCR (qPCR) was conducted to identify gene expression changes in *Rnase1*^{-/-} mice. RNA was isolated from tissue samples homogenized in TriZOL Reagent (Invitrogen) using a Benchmark D1000 homogenizer, purified according to the manufacturer’s protocol, DNase-treated using the TURBO DNA-free kit (Ambion), and subjected to reverse transcription–PCR using the qScript cDNA Synthesis kit (Quanta Biosciences). The resultant cDNA was probed for expression of *Rnase1*, *Rnase4*, *Ang1*, and *Rnh1* using primer pairs shown in Table 2.1. Reactions were run in duplicate using SYBR Green master mix (Quanta Biosciences) with an Applied Biosystems ABI 7500 Fast Real-Time PCR system. Cycling conditions were 95°C for 30 s, 55°C for 30 s, and 72°C for 30 s, repeated for 30 cycles and monitored by melting curves. Threshold cycle values were determined by setting a

Table 2.1. Primers used for qPCR

Target	Forward (5'→3')	Reverse (3'→5')
<i>Rnase1</i>	CTGCAAGAACAGGAAGAGCAAC	GAGTGGTCTTGTAGTCACAGTTGG
<i>Rnase4</i>	AACGGTTCCTTCGACAGCAT	GCGTTTGCCTGGACAGAAG
<i>Ang1</i>	TCTGCAGGGTTCAGACATGT	TCTGGGCTATGAGGGGAGAT
<i>Rnh1</i>	CCCAGCTGTAAGCTCAGGAC	CTCTGCTTGGCTCTGAGGAC
<i>Gapdh</i>	CTCCCACTCTTCCACCTTCG	CCACCACCCTGTTGCTGTAG
<i>Rpl13a</i>	GCTGAAGCCTACCAGAAAGT	TCCGTTTCTCCTCCAGAGT
<i>Hprt1</i>	CTAGTCCTGTGGCCATCTGC	GGGACGCAGCAACTGACATT

constant threshold at 0.6, and fold changes in gene expression were determined by the comparative C_T method (172). Expression was normalized to that of *Gapdh*, *Rpl13a*, and *Hprt1*.

2.3.4: Gross phenotypic analysis—The viability of *Rnase1*^{-/-} mice was determined by a χ^2 -squared test. Fertility was assessed by pairing *Rnase1*^{-/-} male \times *Rnase1*^{+/+} female, *Rnase1*^{+/+} male \times *Rnase1*^{-/-} female, and *Rnase1*^{-/-} \times *Rnase1*^{-/-} mice for mating. In longevity studies, aged mice were euthanized upon exhibiting signs of illness or distress (*e.g.*, significant weight loss, tumors, reduced movement or responsiveness).

Gross physical analysis and histopathological analysis of mice were performed by the University of Wisconsin–Madison Research Animal Resource Center Comparative Pathology Laboratory.

2.3.5: Preparation of plasma samples—Whole blood was collected by cardiac puncture into citrate-rinsed syringes immediately prior to mixing with 3.2% w/v sodium citrate (citrate/blood 1:9). Blood was subjected to centrifugation at 2400g for 10 min at 4°C to prepare platelet-poor plasma for subsequent assays. For mixing tests, blood was drawn from the inferior vena cava and prepared similarly.

2.3.6: Quantitation of RNA in plasma—The size and amount of RNA in mouse plasma was evaluated with a NanoVue Plus spectrometer (GE), Bioanalyzer (Agilent) and RNA denaturing gel. For spectrophotometry, plasma was DNase-treated using the TURBO DNA-free kit (Ambion), and then RNA was isolated by using the TRIzol Liquid Sample Reagent (Invitrogen) according to the manufacturer's instructions, and analyzed with the Small RNA Bioanalyzer chip

system (Agilent), according to the manufacturer's instructions. Alternatively, RNA was prepared with urea loading dye and loaded onto a 12% w/v acrylamide SequaGel (National Diagnostics), and visualized with 1:10000 SYBR Gold (Invitrogen) stain on a Typhoon FLA 7000 imager (GE). ImageJ software was used to evaluate band intensity (173).

2.3.7: Ribonucleolytic activity assay—Assays of ribonucleolytic activity were performed on plasma samples as a proxy for protein concentration, using a ribonuclease substrate described previously (174). The background fluorescence intensity (I_0) of 100 mM Tris-HCl buffer, pH 7.0, containing 6-FAM-dArUdAdA-6-TAMRA (10 μ M), NaCl (100 mM), and acetylated bovine serum albumin (0.1 mg/ml) was measured. A 1- μ l aliquot of plasma was added, and the change in fluorescence intensity (ΔI) over time was monitored. Excess RNase A was added, and maximum fluorescence intensity (I_{\max}) was measured. All measurements were taken at $\lambda_{\text{ex}} = 490$ nm and $\lambda_{\text{em}} = 525$ nm using a Tecan Infinite M1000 plate reader. Recombinant murine RNase 1 was used to measure $k_{\text{cat}}/K_M = 8.6 \times 10^6 \text{ M}^{-1}\text{s}^{-1}$, which is similar to values reported previously (175). This value was, in turn, used to calculate the RNase 1 concentration in mouse plasma with Equation 2.1:

$$[\text{RNase 1}] = \frac{\Delta I}{\frac{I_{\max} - I_0}{\frac{k_{\text{cat}}}{K_M}}} \quad (2.1)$$

2.3.8: Ribonuclease zymogram assay—Zymograms were performed on plasma samples to verify the loss of RNase 1 in *Rnase1^{-/-}* mice, using an assay similar to one reported previously (176). Briefly, a polyacrylamide gel containing SDS (0.1% w/v), Tris (375 mM), and poly(C) (4.5 mg, incubated at 50°C prior to addition) was cast. Samples containing recombinant murine RNase 1 (100 pmol) or murine plasma (0.5 μ l) were prepared with 2 \times Laemmli sample buffer (without

DTT or β -mercaptoethanol, and without boiling). Some samples were prepared from murine plasma pre-treated with by incubating 2 μ l of plasma with 1000 U of PNGase F (New England BioLabs) for 48 h to remove *N*-linked glycans from RNase 1. After electrophoresis, the gel was washed twice in 10 mM Tris-HCl buffer, pH 7.5, containing isopropanol (20% v/v), then once in 10 mM Tris-HCl buffer, pH 7.5, before incubation overnight in 100 mM Tris-HCl buffer, pH 7.5 to allow RNase 1 to refold within the gel. The next day, the gel was washed in 10 mM Tris-HCl buffer, pH 7.5 before staining in an aqueous solution of toluidine (0.2% w/v) for 10 min. The gel was washed with deionized water and destained in 10 mM Tris-HCl buffer, pH 7.5. ImageJ software was used to evaluate band intensity (173).

2.3.9: Kinetic coagulation assay—Coagulation assays were performed on mouse plasma by using a protocol adapted from one reported previously (177). Briefly, assay mixtures contained plasma (10 μ l), human fibrinogen (100 μ g; Sigma-Aldrich), PC:PS:C vesicles (4 μ M), and CaCl₂ (6 mM, added to initiate clotting). The reaction volume was increased to 100 μ l by the addition of 20 mM HEPES-HCl buffer, pH 7.35, containing NaCl (20 mM) and BSA (1% w/v). A variant of the prothrombin time (PT) assay was conducted by adding 5 μ l of Thromborel S solution (Dade), diluted in the same buffer to final concentrations of 2.2 pM (high tissue factor) or 0.22 pM (limiting tissue factor) in the reaction. A variant of the activated partial thromboplastin (aPTT) time assay was conducted by adding 5 μ l of Actin FSL Activated PTT reagent (Dade), at full strength or diluted 1:50 to provide limited intrinsic activation. The value of $A_{405\text{ nm}}$ was recorded over a period of ≤ 1 h to track clot formation. Clotting times are reported as the time at which the value of $A_{405\text{ nm}}$ was half-maximal.

2.3.10: ELISA and immunoblotting—An ELISA was performed to evaluate plasma fibrinogen content. Assays were performed with a Mouse Fibrinogen ELISA Kit (Abcam) according to the manufacturer's instructions.

Relative plasma concentrations for Factor XI, factor XII, PK, and HK were determined by non-reducing immunoblotting using chemiluminescence. Factor XI was detected with biotinylated anti-mouse FXI IgG 14E11 and streptavidin-HRP (178). Factor XII and PK were detected with polyclonal goat anti-human FXII or anti-human PK IgG conjugated to HRP (Affinity Biologicals, Ancaster, Ontario). HK was detected with polyclonal rabbit IgG raised against mHK1-specific sequence, and donkey anti-rabbit IgG-HRP(179). Blots were imaged using a c600 system (Azure Biosystem) and band strength was assessed with ImageJ software (173).

The relative expression level of tissue factor in liver was determined by immunoblotting. Briefly, tissue samples were homogenized with a Benchmark D1000 homogenizer in T-PER Tissue Protein Extraction Reagent (Pierce). Homogenized tissue and plasma samples were tested for protein content by using a bicinchoninic acid assay kit (Pierce) and prepared with denaturing sample buffer prior to SDS-PAGE. Samples were transferred to a membrane using the IBlot 2 Dry Blotting System (Thermo Fisher Scientific) for 1 min at 20 V, 2 min at 23 V, and 1 min at 25 V. Membranes were blocked for 1 h in 5% w/v dry milk in Tris-buffered saline with Tween (TBST, which contained 19 mM Tris base, 137 mM NaCl, 2.7 mM KCl, and 0.1% v/v Tween 20), and incubated overnight at 4°C with antibody. Tissue factor was detected with a rabbit polyclonal IgG (Bioss), and β -actin with a rabbit monoclonal IgG (Cell Signaling). The membrane was washed in TBST before a 1-h incubation at room temperature with a secondary

antibody, diluted with an aqueous solution of dry milk (5% w/v) in TBST, then washed in TBST again before imaging. The blot was treated with SuperSignal West Pico Chemiluminescent substrate (Thermo Fisher Scientific) and imaged with an ImageQuant LAS 4000 imager (GE Healthcare). Band intensity was evaluated with ImageJ software (173). Blots were stripped by using Restore Western Blot Stripping Buffer (Thermo Fisher Scientific) and re-probed.

2.3.11: Thrombin–antithrombin complex formation assay—Thrombin–antithrombin (TAT) complex formation was measured as a marker of clot formation in response to LPS using a protocol adapted from one reported previously (180). Briefly, mice were injected intraperitoneally with LPS (2 mg/kg in sterile saline) or an equivalent volume of saline. After 4 h, mice were euthanized via exsanguination. Plasma was then assayed for TAT complex content by using a Thrombin–Antithrombin Complexes Mouse ELISA Kit (Abcam) according to the manufacturer’s instructions.

2.3.12: Tail-vein bleeding time assay—Tail-bleeding assays were performed as described previously (181). Briefly, mice were anesthetized with isoflurane and placed on a warming pad, and a 2-mm section of distal tail was amputated. Blood was collected into warm saline, and total bleeding time (including all rebleeding events) was recorded using a stopwatch. Collected blood cells were lysed, and the $A_{550\text{ nm}}$ value of the lysate was used as a quantitative measure of blood loss.

2.3.13: Saphenous vein hemostasis assay—Hemostasis in the saphenous vein was assessed by using a protocol adapted from one reported previously (182). Briefly, the left saphenous vein of

an anesthetized mouse was dissected free of membranes and punctured with a 27g needle. Time-to-cessation of bleeding was recorded, and the clot was dislodged by wiping the vein in the direction of blood flow to allow rebleeding. This procedure was repeated for 30 min while recording the number of clots and the average time to clot.

2.3.14: FeCl₃-induced thrombosis assay—Iron-chloride-induced arterial thrombosis assays were carried out with assistance from the University of Wisconsin–Madison Cardiovascular Physiology Core Laboratory. The left carotid artery of anesthetized mice was dissected and blotted before application of an aqueous solution of iron chloride (10% w/v) using a 1 × 2 mm square of tissue). This solution was left in place for 3 min before washing the tissue with phosphate-buffered saline. After removal of the iron solution, an ultrasound gel was applied and Doppler ultrasound was employed to identify the carotid artery and measure blood flow rate for 30 min. A clot was judged to have formed when blood flow dropped to <10% of its initial rate. Mice were euthanized at the conclusion of the experiment, and carotid artery sections were collected into 4% neutral buffered formalin for fixation and staining.

2.3.15: Factor activity assay—Activity assays for FIX, FXI, FXII, and prekallikrein in plasma were carried out by a mixing test using a variation of the kinetic coagulation assay described above. Briefly, 10 µl of factor-deficient human plasma was incubated with 10 µl of sample plasma to complement factor activity absent in the deficient plasma. (Sample was diluted in factor-deficient plasma in ratios ranging from 1:5 to 1:100, yielding samples with 20% to 1% of the normal factor activity.) To assay response to extrinsic pathway stimulation, soluble tissue factor (sTF) was added to reactions to a final concentration of 0.1 or 1 µM. Reactions included

fibrinogen, PC:PS:C, and CaCl₂ as described above, and the volume was brought up to 100 μ l with HEPES buffer. The value of $A_{405 \text{ nm}}$ was recorded over a period of ≤ 1 h to track clot formation.

Some mixing tests were also performed with a Start 4 Hemostasis Analyzer (Diagnostica Stago, Parsippany, NJ). Briefly, 50 μ l of factor-deficient human plasma was incubated with 25 μ l of sample plasma (diluted in factor-deficient plasma) and 50 μ l of Actin FSL Activated PTT reagent for 3 min at 37°C. An aqueous solution of CaCl₂ (17 mM) was added to initiate coagulation, and the time to clot was recorded.

Standard curves of factor activity as a function of plasma clotting time were generated by testing a pooled plasma set of five *Rnase1*^{+/+} mice and plotting clotting time (y) against plasma dilution factor (expressed as percent activity of undiluted plasma) on a log-linear chart, and the y -intercept (b) and slope (m) were calculated. Factor activity in *Rnase1*^{-/-} plasma relative to *Rnase1*^{+/+} plasma was calculated with Equation 2.2:

$$\text{activity} = 10^{\frac{y-b}{m}} \quad (2.2)$$

2.3.16: Statistical analyses—A minimum of three biological replicates were performed for every experiment. All data are expressed as the mean \pm SEM, and statistical evaluation was performed by Wilcoxon rank-sum test, log-rank test, and chi-squared test in GraphPad Prism and Mstat software, with $p < 0.05$ being considered significant.

2.4: Results

2.4.1: Generation of $Rnase1^{-/-}$ mice by Cre-LoxP recombination—Prior to generating $Rnase1^{-/-}$ mice, we sought to validate the use of murine RNase 1 as a model for the human enzyme. We had shown previously that the murine RI·RNase 1 complex is highly similar to its human homolog in sequence and structure (17). Further, murine RNase 1 exhibits ribonucleolytic activity similar to that of the human enzyme. Given that human *Rnase1* is expressed ubiquitously (34), we analyzed 16 mouse tissues for *Rnase1* expression by qPCR and found this gene to be expressed ubiquitously as well (Figure 2.1, panel A). These *in vitro* structure–function data, coupled with a similarly broad expression pattern *in vivo*, instilled confidence in murine RNase 1 as a model for human RNase 1.

Given the unknown biological function of RNase 1, we chose a conditional knockout approach to generate mice lacking *Rnase1* expression. The entire *Rnase1* protein-coding exon was flanked with *loxP* sites in the gene-targeting vector, allowing Cre-mediated recombination to excise this exon and result in an ablation of *Rnase1* expression. Disruption of the *Rnase1* gene was verified by a Southern blot (Supplemental Figure 2.1, panel B).

*2.4.2: $Rnase1^{-/-}$ mice express neither *Rnase1* mRNA nor RNase 1 protein*—qPCR was performed to verify the loss of *Rnase1* expression in $Rnase1^{-/-}$ mice. Sixteen tissue types were tested for *Rnase1* expression in $Rnase1^{-/-}$ and $Rnase1^{+/+}$ mice and levels were normalized to three reference genes. Samples from $Rnase1^{-/-}$ mice exhibited virtually undetectable *Rnase1* expression (average CT value of 34 ± 0.3 cycles in samples with amplification) (Figure 2.2, panel A).

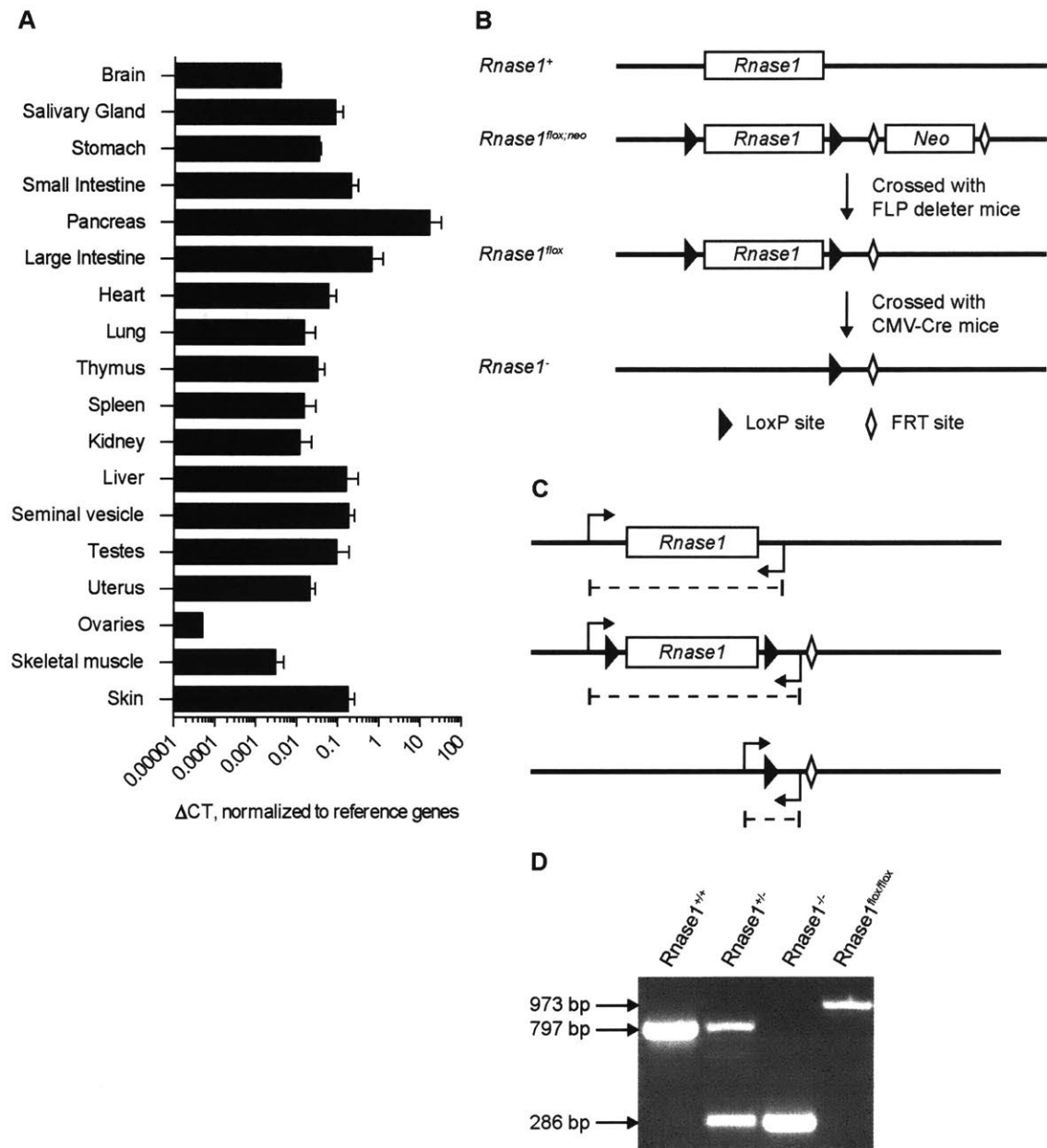


FIGURE 2.1. Generation of *Rnase1* knockout mice. **A**, Bar graph showing the tissue-specific expression of *Rnase1* in wild-type mice as measured by qPCR. Data were normalized to the geometric mean of three reference genes. $n = 3$ per tissue. **B**, Scheme showing the breeding strategy used to generate conditional *Rnase1* knockout mice. *Rnase1* refers to the single coding exon for the *Rnase1* gene; *Neo* refers to a neomycin-resistance cassette. **C**, Scheme showing the genotyping strategy used to identify *Rnase1* alleles. One pair of primers recognizes sites 3' and 5' to the targeted exon, enabling identification of wild-type (top), targeted/floxed (center), and knockout (bottom) individuals. As in panel **B**, black triangles represent loxP sites, and open diamonds represent FRT sites. **D**, A representative genotyping gel, showing bands indicative of wild-type, heterozygous, and *Rnase1*^{-/-} mice, as well as *Rnase1*^{lox/lox} mice.

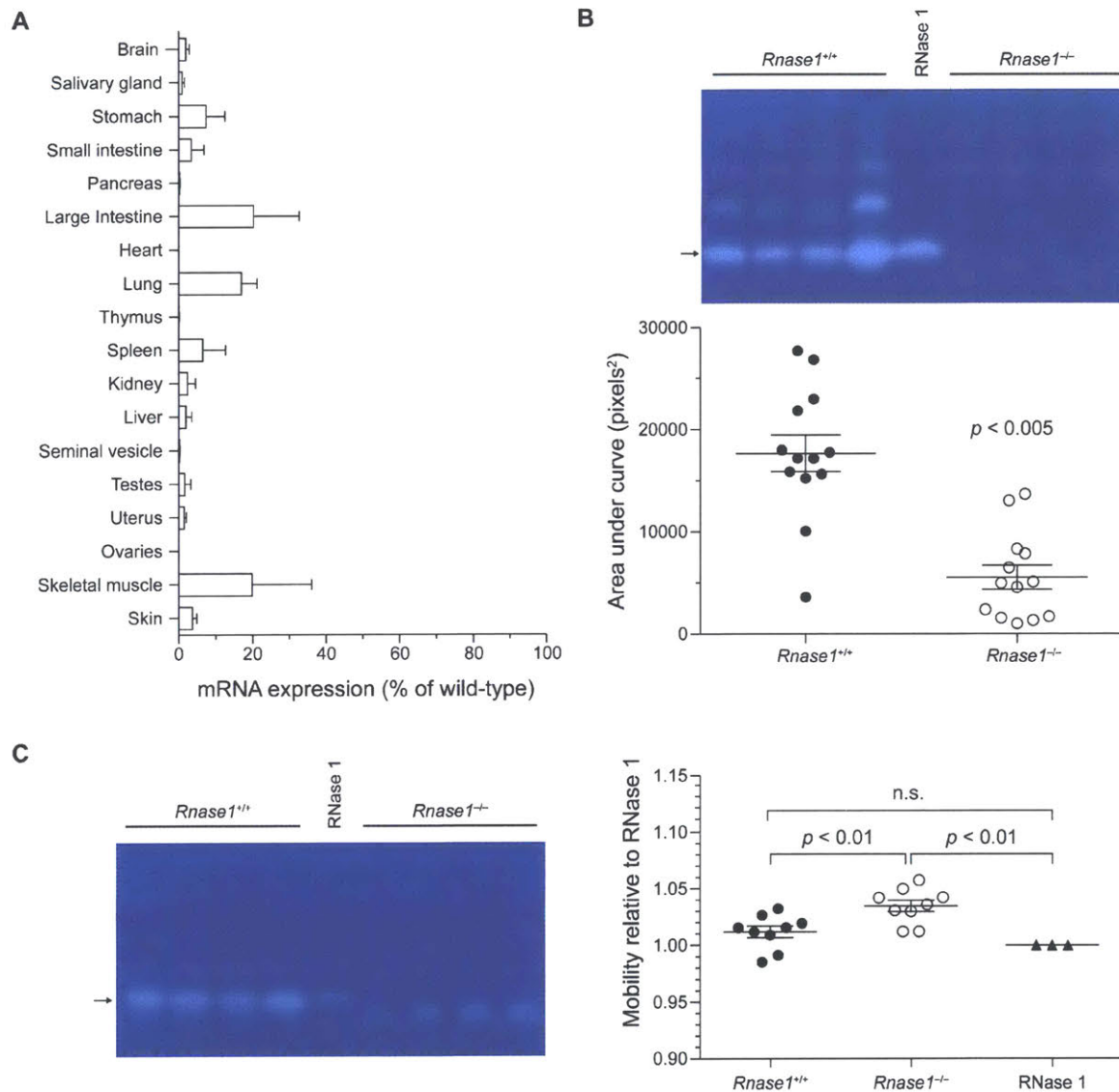


FIGURE 2.2. Verification of the loss of RNase 1 in *Rnase1*^{-/-} mice. **A**, Bar graph showing the tissue-specific expression of *Rnase1* in *Rnase1*^{-/-} mice relative to that in *Rnase1*^{+/+} littermates as measured by qPCR. Mice were matched for sex. $n = 3$ per tissue. Data were normalized to the geometric mean of three reference genes. **B**, Zymogram of plasma samples (0.5 μ l of plasma per lane) from *Rnase1*^{+/+} or *Rnase1*^{-/-} mice used to evaluate ribonucleolytic activity relative to recombinant murine RNase 1 (center lane). Graph showing total ribonucleolytic activity, which was quantified by integration of a densitometry map of each lane and found to be significantly lower in *Rnase1*^{-/-} mice than in *Rnase1*^{+/+} mice. **C**, Zymogram of plasma samples, treated with PNGase F. The mobility was measured from the position of the well, and normalized to the mobility of recombinant murine RNase 1 (center lane). The position of the primary band present in *Rnase1*^{-/-} plasma differs from that in wild-type plasma (arrow).

Antibodies against RNase 1 are likely to cross-react with paralogous secreted ribonucleases, which share high sequence and structural similarity. Thus, we performed zymogram assays of plasma samples to detect RNase 1 by both its ribonucleolytic activity and its electrophoretic mobility. Ribonucleolytic activity as determined by the intensity of all bands was significantly reduced in *Rnase1*^{-/-} samples relative to *Rnase1*^{+/+} samples, representing a (69 ± 6)% loss of ribonucleolytic activity (Figure 2.2, panel B).

We hypothesized that residual ribonucleolytic activity in *Rnase1*^{-/-} plasma is due to other members of the secreted ribonuclease superfamily and not RNase 1. Members of this superfamily exhibit elute at distinct rates during SDS-PAGE due to variation in molecular mass and charge. Given that RNase 1 and other secreted ribonucleases can be glycosylated *in vivo* (183), we treated plasma samples with PNGase F to reduce sample complexity, and measured the mobility of the major ensuing band. Mobility was measured relative to an aglycosylated recombinant murine RNase 1 standard produced in *E. coli*. We found that whereas *Rnase1*^{+/+} plasma produced a band with mobility (101.2 ± 0.5)% of the RNase 1 standard, *Rnase1*^{-/-} plasma does not, with the closest mobility being (103.5 ± 0.5)% of the standard (Figure 2.2, panel C). These results indicate that expression was lost in *Rnase1*^{-/-} mice, and confirm that residual ribonucleolytic activity in these mice is due to expression of other superfamily members. Indeed, qPCR analysis of secreted ribonuclease genes in *Rnase1*^{+/+} and *Rnase1*^{-/-} showed upregulation of many of superfamily genes upon loss of *Rnase1*, notably those of *Rnase4* and *Ang1* (Supplemental Figure 2.2).

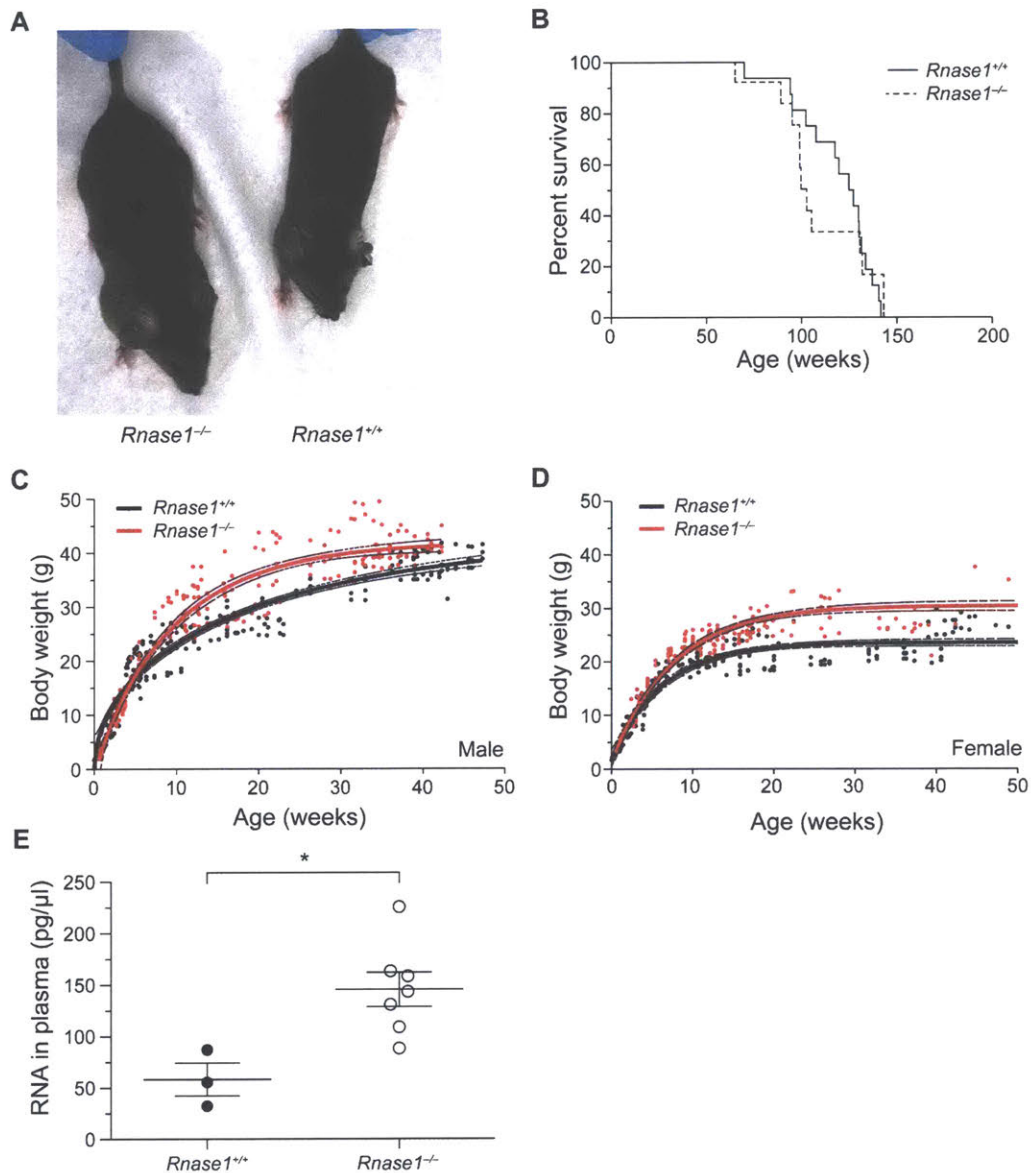


FIGURE 2.3. General phenotyping and longevity studies of *Rnase1^{-/-}* mice. *A*, Photograph of *Rnase1^{-/-}* and *Rnase1^{+/+}* mice that are 8-week-old male littermates. *B*, Graph showing the longevity of *Rnase1^{-/-}* and *Rnase1^{+/+}* mice, revealing no differences between survival by genotype. $n \geq 12$. *C*, Graph showing the weekly weight of male *Rnase1^{-/-}* and *Rnase1^{+/+}* mice, $n \geq 5$. By 8 weeks of age, male *Rnase1^{-/-}* mice (29.7 ± 1 g) were significantly heavier than were male *Rnase1^{+/+}* mice (22.8 ± 1 g). *D*, Graph showing the weekly weight of female *Rnase1^{-/-}* and *Rnase1^{+/+}* mice, $n \geq 5$. By 8 weeks of age, female *Rnase1^{-/-}* mice (23.4 ± 0.5 g) were significantly heavier than were female *Rnase1^{+/+}* mice (19.2 ± 0.4 g). *E*, Graph showing the RNA content of *Rnase1^{-/-}* and *Rnase1^{+/+}* plasma. Data are from purified RNA samples and were normalized to plasma volume. $*p < 0.05$.

2.4.3: *Rnase1*^{-/-} mice are viable and appear physically normal—Genotyping of initial *Rnase1*^{fllox/fllox} × B6.C-Tg(CMV-cre)1Cgn/J progeny revealed that *Rnase1*^{-/-} mice are viable. Heterozygote crosses illustrated further that the *Rnase1*^{-/-} allele was inherited according to expected Mendelian ratios, χ^2 (2, $n = 243$) = 9.62, $p < 0.05$. Additionally, *Rnase1*^{-/-} males and females are both fertile, with crosses of *Rnase1*^{-/-} mice producing litters of identical size and gender distribution (7.4 ± 1 pups per litter, $39 \pm 9\%$ male, $n = 67$) to *Rnase1*^{+/+} mice (7.8 ± 2 pups per litter, $39 \pm 11\%$ male, $n = 39$).

Rnase1^{-/-} mice of both sexes are significantly heavier than are *Rnase1*^{+/+} mice (Figure 2.3, panels C and D), but do not exhibit any other obvious physical phenotype (Figure 2.3, panel A). Gross necropsy and histopathological analyses did not reveal differences between *Rnase1*^{-/-} and *Rnase1*^{+/+} littermates (data not shown). *Rnase1*^{-/-} also exhibit similar longevity to *Rnase1*^{+/+} mice, with a median survival time of 102 weeks versus 126 weeks (Figure 2.3, panel B).

2.4.4: Loss of *Rnase1* results in increased plasma RNA—Given the reduction of ribonucleolytic activity in the plasma with loss of *Rnase1* (Figure 2.2, panel B), we anticipated elevated RNA concentration in the plasma of *Rnase1*^{-/-} mice. We isolated RNA from the plasma of mice and measured the resultant concentration of the purified RNA isolates with a Small RNA Bioanalyzer, normalizing the concentration values to the quantity of input plasma. By this assay,

Rnase1^{-/-} mice do indeed exhibit elevated levels of RNA in their plasma, (145.6 ± 16.7) pg/μl, relative to *Rnase1*^{+/+} mice, (58.3 ± 15.8) pg/μl (Figure 2.3, panel E).

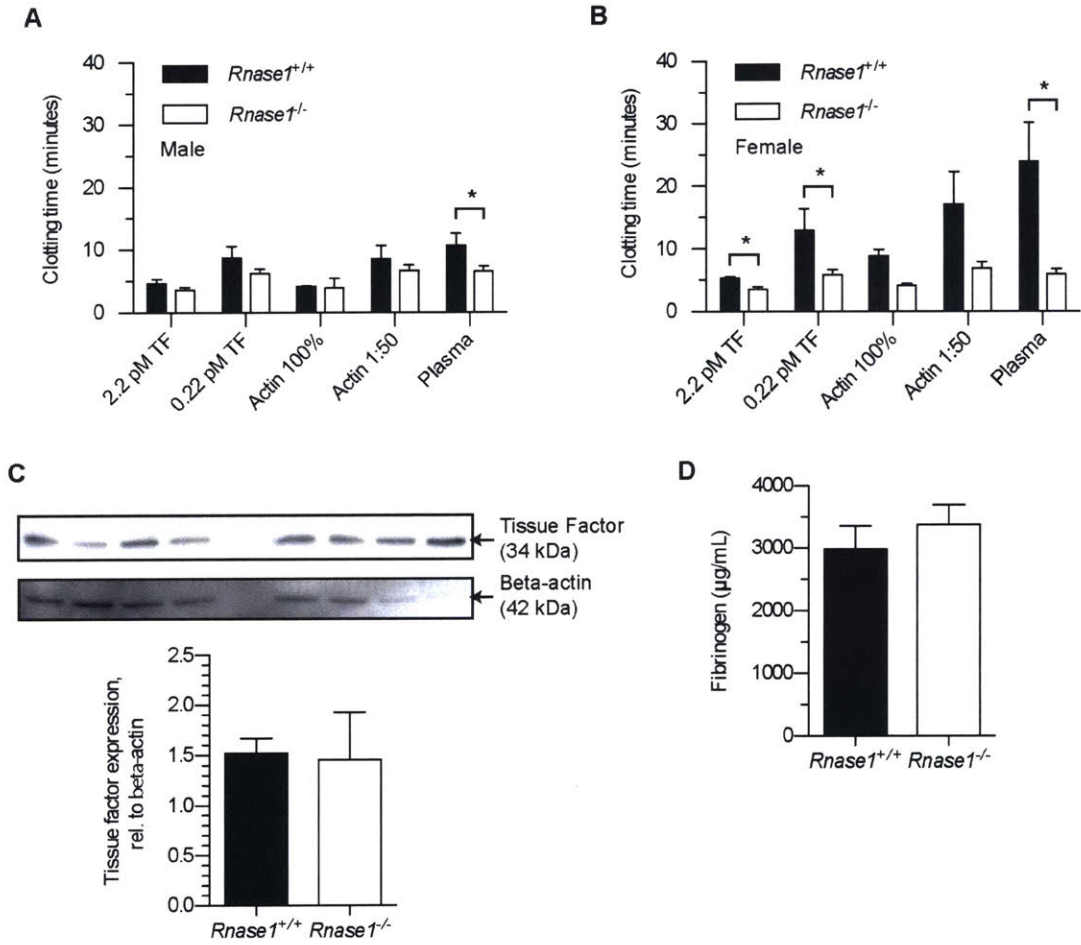


FIGURE 2.4. Effect of *Rnase1* on coagulation *in vitro*. A, Bar graph showing the effect of activators Thromborel S (TF) and Actin FSL aPTT reagent (Actin) on the clotting of plasma from male mice. *Rnase1*^{-/-} plasma from mice clots significantly faster than does *Rnase1*^{+/+} plasma in the absence of added activator. $n \geq 3$. B, Bar graph as in panel A but with female mice. *Rnase1*^{-/-} plasma clots significantly faster than does *Rnase1*^{+/+} plasma in the absence of added activator and in the presence of Thromborel S. $n \geq 3$. C, Representative immunoblot to probe for tissue factor in the liver and bar graph showing the quantitation of band intensities in *Rnase1*^{-/-} and *Rnase1*^{+/+} mice. No significant difference was detected in the tissue factor level by genotype. $n = 4$. D, Bar graph showing the fibrinogen level of plasma as assayed by ELISA in *Rnase1*^{-/-} and *Rnase1*^{+/+} mice. No significant difference was detected in fibrinogen level by genotype. $n = 13$. * $p < 0.05$.

2.4.5: *Rnase1^{-/-}* plasma clots more quickly than does *Rnase1^{+/+}* plasma—Extracellular RNA can stimulate plasma coagulation *in vitro* (79). To evaluate whether increased endogenous RNA seen in *Rnase1^{-/-}* mice results in enhanced plasma coagulation, we carried out a series of kinetic coagulation studies.

Plasma from *Rnase1^{-/-}* mice formed fibrin clots significantly more quickly than did plasma from *Rnase1^{+/+}* mice. The respective values were (7.2 ± 1.0) min and (10.6 ± 2.0) min for males, and (5.9 ± 0.8) min and (23.9 ± 6.2) min for females (Figure 2.4, panels A and B). Stimulation of coagulation via the intrinsic pathway with Actin FSL aPTT reagent reduced clotting time relative to unstimulated plasma, but did not reveal significant differences between clotting in *Rnase1^{-/-}* and *Rnase1^{+/+}* samples. In contrast, stimulation of clotting with Thromborel S to activate coagulation via the extrinsic pathway resulted in significantly shorter clotting times in *Rnase1^{-/-}* samples relative to *Rnase1^{+/+}* in female mice. This effect was apparent for a high concentration of Thromborel S (3.52 ± 0.40 min for *Rnase1^{-/-}* versus 5.26 ± 0.28 min for *Rnase1^{+/+}*) as well as a limiting concentration of Thromborel S (5.81 ± 0.83 min for *Rnase1^{-/-}* versus 12.9 ± 3.5 min for *Rnase1^{+/+}*).

Experiments were performed to detect non-intrinsic causes of the observed phenotypes. For example, tissue factor expression is known to be elevated by obesity (184), and *Rnase1^{-/-}* mice are heavier than are *Rnase1^{+/+}* mice. Nonetheless, *Rnase1^{-/-}* and *Rnase1^{+/+}* mice do not differ in tissue-factor expression (Figure 2.4, panel C). An ELISA was also performed to evaluate changes in fibrinogen level, as the kinetic coagulation assay relies on fibrin generation. No

differences were observed in fibrinogen level between *Rnase1*^{-/-} and *Rnase1*^{+/+} mice (Figure 2.4, panel D).

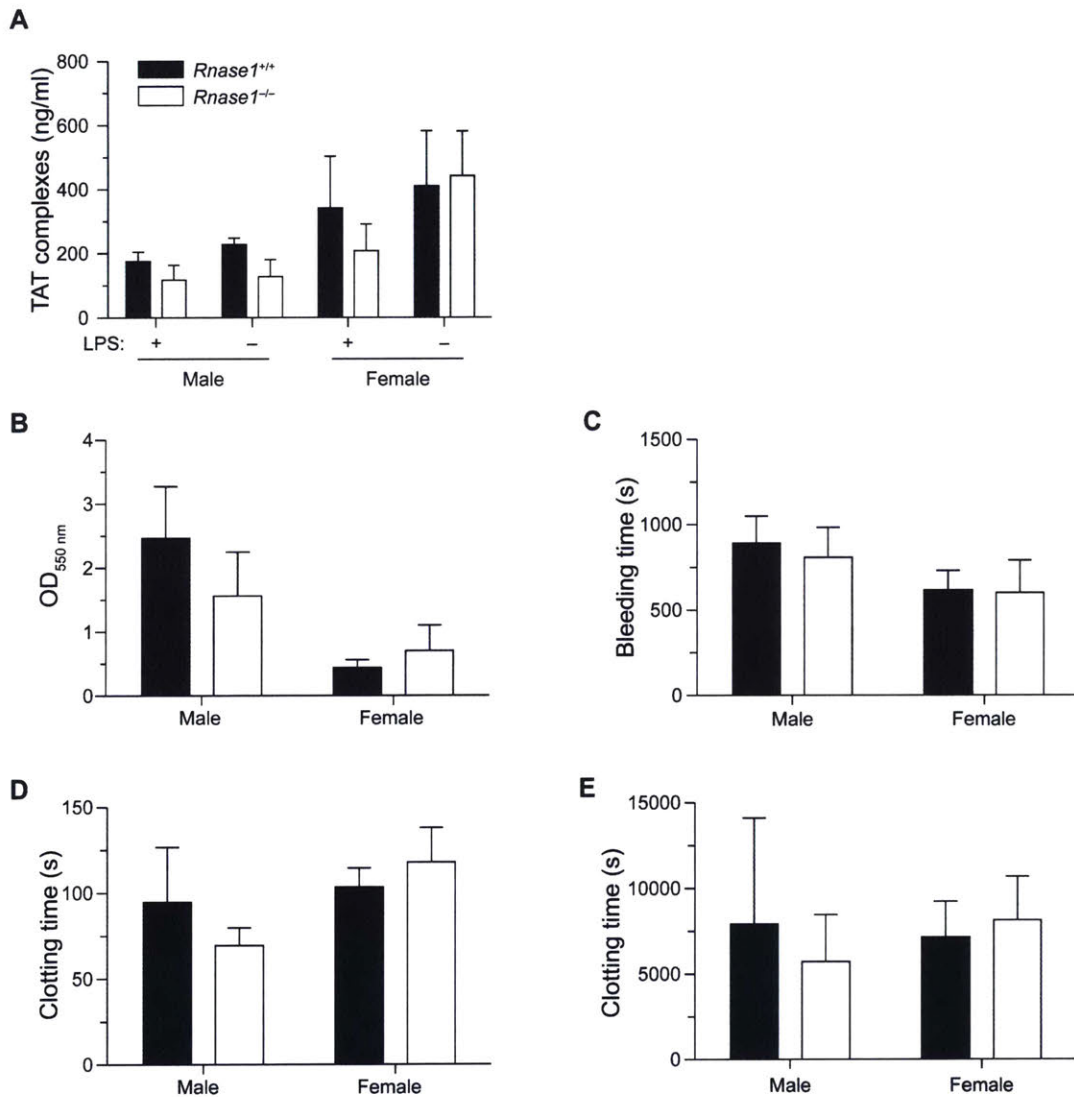


FIGURE 2.5. Effect of *Rnase1* on coagulation *in vivo*. *A*, Bar graph showing the effect of LPS (2 mg/kg) on the level of thrombin–antithrombin complex in the plasma of *Rnase1*^{-/-} and *Rnase1*^{+/+} mice. No significant difference was detected in complex level by genotype. *n* ≥ 3. *B*, Bar graph showing blood loss in tail-vein bleeding assays. Blood was quantified by the absorbance of hemoglobin at 550 nm. No significant difference was detected in blood loss by genotype. *n* ≥ 4. *C*, Bar graph showing bleeding time in tail-vein bleeding assays. No significant difference was detected in bleed time by genotype. *n* ≥ 4. *D*, Bar graph showing clotting time in the carotid artery upon administration of iron chloride. No significant difference was detected in clotting time by genotype. *n* ≥ 4. *E*, Bar graph showing clotting time in the saphenous vein. No significant difference was detected in clotting time by genotype. *n* ≥ 3.

2.4.6: *Rnase1^{-/-} mice do not exhibit coagulation abnormalities in vivo*—We asked whether the changes seen in *in vitro* coagulation assays would be reflected *in vivo*. In four models of bleeding, coagulation, or hemostasis, *Rnase1^{-/-}* mice did not exhibit significant differences from *Rnase1^{+/+}* mice (Figure 2.5). Thrombin–antithrombin complex formation did not differ by genotype after LPS treatment. Tail-bleeding time did not differ by genotype, nor did the amount of blood lost. Bleeding time in the saphenous vein hemostasis assay also did not differ by genotype. No differences in clotting time were noted in iron-chloride-induced arterial thrombosis assays, and fixed sections of the carotid artery revealed a similar distribution of degrees of vessel occlusion in both genotypes.

2.4.7: *Rnase1^{-/-} plasma exhibits elevated FXII and FXI activity*—Given that perturbations in the intrinsic coagulation pathway can produce coagulation abnormalities *in vitro* without significant phenotypes *in vivo* (168,169), we sought to evaluate whether intrinsic coagulation factors are more active in *Rnase1^{-/-}* mice than in *Rnase1^{+/+}* mice. As in initial coagulation assays *in vitro*, Actin FSL aPTT reagent did not detect significant differences between genotypes (Figure 2.6, panel A). FXII activity was, however, elevated significantly in the absence of added activator. In addition, whereas the activity of FXI was not significantly greater in conditions without activator, FXI activity was much greater in *Rnase1^{-/-}* plasma than in *Rnase1^{+/+}* plasma when stimulated with 0.1 μ M soluble tissue factor. FIX activity was also tested as a control, as it should not be stimulated by excess RNA, and its activity was not observed to differ by genotype (Figure 2.6, panel A). In *in vitro* clotting assays, coagulation through the intrinsic pathway is triggered by a process called contact activation. The plasma concentrations of all components of the contact activation system (FXII, FXI, PK and HK) were similar in wild-type and *Rnase1^{-/-}*

mice (Figure 2.6, panels B and C). Hence, the apparent increase in activity of FXII and FXI in *Rnase1*^{-/-} mice is not due to increased plasma concentrations of the proteins. The data indicate, instead, that greater proportions of FXII and FXI in the *Rnase1*^{-/-} mice are in the active form of these proteases (FXIIa and FXIa).

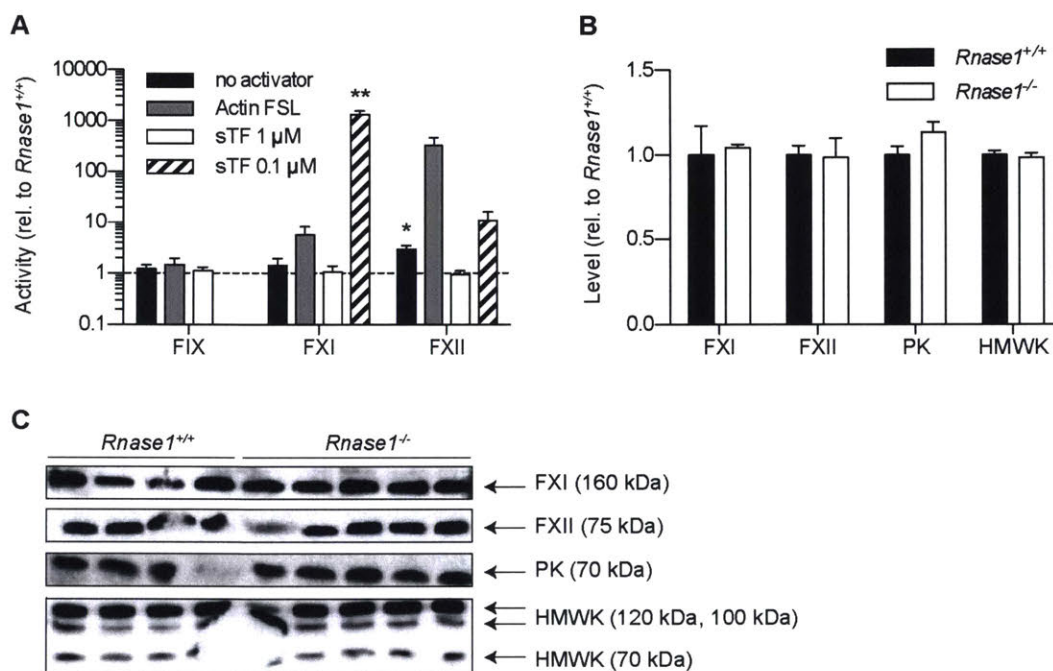


FIGURE 2.6. **Effect of *Rnase1* on the levels of FXII and FXI.** A, Bar graph showing the activity of FIX, FXI, and FXII in the plasma of *Rnase1*^{-/-} relative to that in *Rnase1*^{+/+} mice. $n \geq 3$. B, Bar graph showing the level of FXI, FXII, plasma kallikrein (PK), and high molecular weight kininogen (HMWK) in the plasma of in *Rnase1*^{-/-} and *Rnase1*^{+/+} mice, normalized to the average expression in *Rnase1*^{+/+} mice. $n \geq 3$. C, Representative immunoblots to probe for FXI, FXII, PK, and HMWK. * $p < 0.05$; ** $p < 0.001$.

2.5: Discussion

RNase A has likely been the object of more biochemical and biophysical analyses than any other enzyme (14,158-160). Little is known, however, about the function of RNase A or its homologs *in vivo*. We report on the use of reverse genetics to create an *Rnase1*^{-/-} mouse. We find that *Rnase1*^{-/-} mice are viable and fertile. We also find, however, that the loss of RNase 1 causes increased coagulation *in vitro*, which appears to be mediated through activation of FXII and FXI. This phenotype is consistent with the known role of eRNA, FXII, and FXI in blood coagulation, and links the loss of ribonucleolytic activity to the ability of eRNA to activate these proteases (79,81). Notably, the loss of FXII is not associated with a clinically-relevant phenotype in humans (185). In mice, the loss of FXII leads to prolongation of aPTT but not to deficient coagulation *in vivo* (169).

In all kinetic coagulation assays, *Rnase1*^{-/-} plasma tended to coagulate more rapidly than did *RNase1*^{+/+} plasma. Differences were most robust under conditions with no or low levels of activator (Figure 2.4, panels A and B). Moreover, no samples activated with the Actin FSL aPTT reagent were significantly different by genotype. These data support the hypothesis that the intrinsic coagulation pathway is activated by eRNA in *Rnase1*^{-/-} mice. Other studies have demonstrated that although eRNA is an activator of intrinsic factor proteases (79), its capacity for activation is lower than that of other molecules, such as polyphosphate (81). Actin FSL is a highly robust activator of FXII via its component ellagic acid (186), and thus could saturate the anion-activation pathway and mask activation engendered by eRNA. In contrast, activation of

the intrinsic pathway by eRNA could have an additive effect on coagulation when also activated by Thromborel S.

The one-stage coagulation assays used to measure specific plasma clotting factors are designed to generate a value for plasma factor concentration relative to a control plasma, which is assigned a value of 100%. Use of such an assay is based on the clotting factor being completely (or almost completely) in its inactive precursor form at the start of the assay. Yet, the apparent FXII and FXI levels in the plasma of *Rnase1^{-/-}* mice as determined by one-stage clotting assays are much greater than the levels obtained by immunoblot analysis of factor antigen. Indeed, concentrations of FXII and FXI antigen appear similar in *Rnase1^{+/+}* and *Rnase1^{-/-}* mice by immunoblotting. These observations are consistent with the presence of significant amounts of FXIIa and FXIa in plasma from *Rnase1^{-/-}* mice, likely driven by the elevated plasma level of eRNA (Figure 2.3, panel E). RNA-dependent generation of FXIIa and FXIa could occur *in vivo* and after blood collection, as the citrate anticoagulant that we used would not inhibit RNA-induced FXII and FXI activation. These findings are consistent with the previously reported procoagulant effects produced by infusing RNA into rodents (79).

FXII is suggested to be important for thrombus formation in the iron-chloride arterial thrombosis model also used in our study (187). Still, our data do not identify significant differences between *Rnase1^{-/-}* mice (which have elevated FXII activity) and *Rnase1^{+/+}* mice. It is possible that under normal conditions, the accumulation of eRNA in *Rnase1^{-/-}* mice is insufficient to cause

pathogenic levels of FXII activity. A higher eRNA burden, as in the context of infectious disease or cancer (73,188,189), could predispose these mice to develop thrombosis more freely.

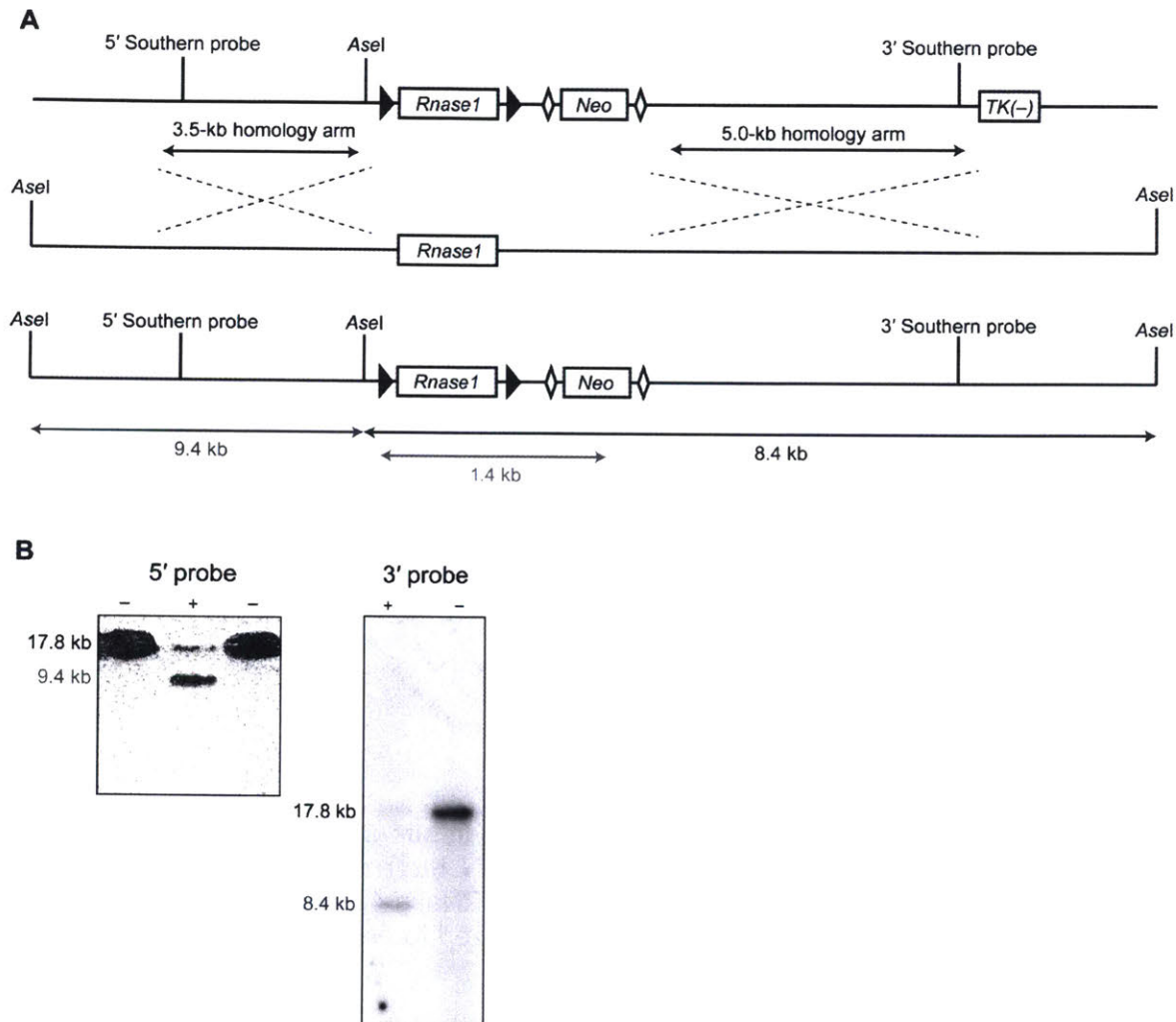
RNase 1 is one of ~25 homologous ptRNases in mice (11). The mild phenotype resulting from the loss of RNase 1 could be due to functional redundancy—homologs could be performing crucial RNA-regulatory functions (190,191). RNase 4, which is upregulated in *Rnase1*^{-/-} mice, is a likely candidate to compensate, as it exhibits similar substrate preferences and is also broadly expressed (25).

The increased body weight of *Rnase1*^{-/-} mice is not explicable by differences in food or water consumption, or body fat. *Rnase1*^{-/-} mice do, however, appear to have slightly longer bodies than do *Rnase1*^{+/+} mice (data not shown). This difference could suggest changes in growth factor activity in *Rnase1*^{-/-} mice. Additionally, differences in coagulation *in vitro* appear to be more robust by genotype in female mice than in male mice. This distinction could be due to hormonal differences between sexes, as hormonal contraceptive use and pregnancy are known risk factors for aberrant blood clot formation (192,193). Our analyses used nulliparous mice, but were performed in sexually mature mice and did not control for the estrus cycle in females, which could have contributed to trends in the data.

Given the roles speculated for RNase 1 in host defense, cancer, and blood coagulation, our findings likely reveal only one of the biological functions of this enzyme. Notably, these three biological activities are related to one another. FXII cleaves plasma kallikrein, which in turn liberates the vasoactive peptide bradykinin (194,195). Bradykinin is an important mediator of

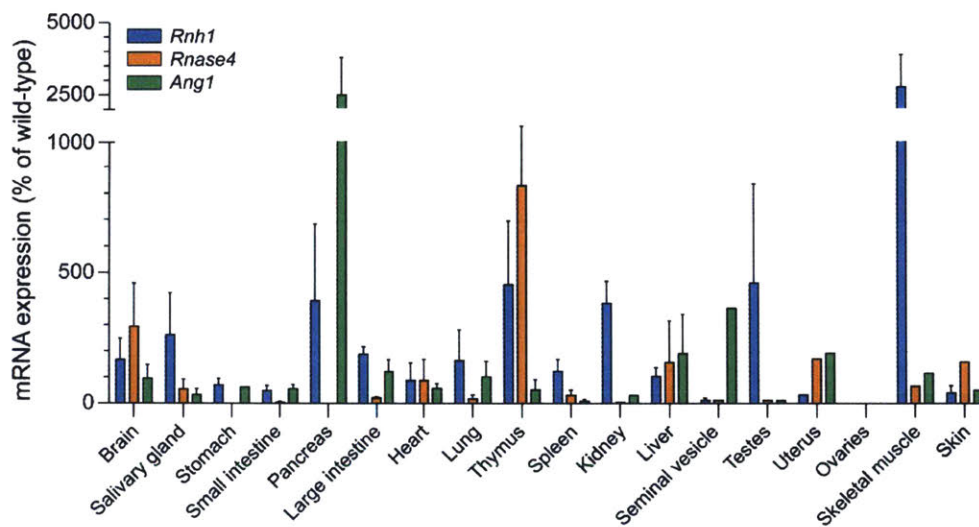
inflammation via its ability to modulate vascular permeability (196). Cancer patients are prone to coagulopathy (197), and tumor-associated and circulating cancer cells have been shown to express tissue factor (198,199) and activate FXII (200). Moreover, RNA is known to stimulate proinflammatory cytokines, including tumor necrosis factor α (TNF α) and vascular endothelial growth factor (VEGF), thus promoting tumor cell growth and immune cell recruitment (73,76). The enzymatic activity of RNase 1 could affect any or all of these biological processes.

2.6: Supplementary information



SUPPLEMENTAL FIGURE 2.1. **Generation of *Rnase1* knockout mice: strategy and results.**

A, Map of the vector to target the *Rnase1* gene. The vector, which was constructed in *Escherichia coli* via homologous recombination, consists of a 5' 3.5-kb homology arm, the *Rnase1* gene flanked by *loxP* sites (black triangles), a *Neo* cassette flanked by FRT sites (open diamonds) in the 3' untranslated region of exon 2 of *Rnase1*, a 3' 5.0-kb homology arm, and a thymidine kinase cassette (*TK*). **B**, Southern blot to identify correctly targeted embryonic stem cell clones. 5' and 3' probes detected either a wild-type band (17.8 kb) or targeted band (9.4 kb for 5'; 8.4 kb for 3') following digestion with *AseI*.



SUPPLEMENTAL FIGURE 2.2. Bar graph showing the tissue-specific expression of relevant genes in *Rnase1*^{-/-} mice relative to that in *Rnase1*^{+/+} littermates as measured by qPCR. *Rnh1* encodes ribonuclease inhibitor, *Rnase4* encodes RNase 4, and *Ang1* encodes angiogenin 1. Mice were matched for sex. *n* = 3. Data were normalized to *Gapdh*.

Chapter 3

Angiogenin is necessary for embryonic development in mice

Contributions: I designed and carried out all experiments. Pathology and histology services were provided by S. Muthupalani at the MIT Comparative Pathology Laboratory and by R. Sullivan at the University of Wisconsin-Madison. Technical assistance with mouse colony management was provided by C. Feldman and K. Tippins.

3.1 Abstract

Angiogenin (Ang) is a member of the secreted ribonuclease superfamily with unique biochemical and biological features. It was first identified in the context of cancer as a pro-angiogenic factor, and is now understood to have more general cell-survival and proliferative functions based on *in vitro* study. Ang is expressed in the developing embryo during periods that align with the vascularization of the embryo and development of the heart, as well as during CNS development, which suggests possible roles in the embryo analogous to roles suggested in adults in angiogenesis and in neuronal survival. Our studies show that *Ang1* is required for survival of embryos, as *Ang1*^{-/-} pups were not found to be produced from heterozygous crosses. Additionally, heterozygosity of *Ang1* is sufficient to significantly impair fertility, resulting in elevated incidence of litter loss in *Ang1*^{+/-} dams and reduced uterine vascularity during pregnancy. We conclude that Ang is essential for support of the embryo during development, and that even minor reduction in Ang expression in the uterine environment results in impaired survival of pups.

3.2 Introduction

Angiogenin (Ang) is a small, secretory enzyme belonging to the pancreatic-type ribonuclease (ptRNase) superfamily (90). Ang was initially identified as a factor produced by human adenocarcinoma that drives angiogenesis by spurring the formation of blood vessels (89), and only later identified to be a ptRNase – an association that has informed extensive biochemical and evolutionary study of the enzyme (91,140). Mechanistic studies have shown that Ang drives endothelial cell proliferation via association with a cell-surface receptor (95,98) and translocates to the nucleolus (100), where it derepresses transcription of ribosomal DNA (94).

The angiogenic activity of Ang is unique among ptRNases, and coincides with unique structural features. The ribonucleolytic activity of Ang is dramatically lower than that of RNase A, the prototypical ptRNase (90), which is attributable in part to the occlusion of its active site by Gln117 (91). Ang also is a more specific ribonuclease than other ptRNases, and has a receptor-binding site and nuclear localization signal. Ang is conserved in vertebrates, like other ptRNases, and is suggested to be the oldest ptRNase due to the absence of other ptRNases in earlier vertebrates (138).

Ang has been widely characterized in the context of cancer (104-106), where it is suggested to act as a driver of neovascularization in response to hypoxia (105). This association has led to considerable interest in targeting Ang for antiangiogenic therapy in cancer (112), and in understanding the role of Ang in other environments where angiogenesis normally takes place, such as the placenta (113,119). Yet, Ang is not a purely angiogenic enzyme. Ang acts as a pro-survival factor in the cellular stress response, which has been demonstrated in the interaction of

astroglia with motoneurons under excitotoxic stress (98) and in hepatic stellate cells with hepatocellular carcinoma (121,122). In response to cell stress, Ang can cleave tRNA to produce tiRNA (127,128), which inhibits protein translation and apoptosis (129,130). This action is thought to be important in response to ER stress (201) and the quiescence or proliferation of stem cells (131).

The accumulated research suggests that Ang could play broad roles in cellular growth and homeostasis. Our studies, using *Ang1* heterozygote mice, demonstrate a fundamental role for Ang 1. We find that homozygosity in the loss of *Ang1* is incompatible with embryonic survival, and that heterozygosity is sufficient to impair survival of pups. These results suggest the activity of Ang is essential for normal growth and development of mice.

3.3 Experimental procedures

3.3.1: Materials—Primers were obtained from Integrated DNA Technologies.

Conditions—All procedures were performed at ambient temperature (~22 C) and pressure (1.0 atm) unless noted otherwise.

*3.3.2: Expansion of *Ang1*^{+/-} mice and genotyping*—All experiments involving animal work were conducted according to an Institution on Animal Care and Use Committee-approved protocol at the University of Wisconsin–Madison and a Committee on Animal Care-approved protocol at the Massachusetts Institute of Technology. One *Ang1*^{tm1.1(KOMP)V1cg} (*Ang1*^{+/-}) mouse was received from the Knockout Mouse Project repository (University of California at Davis, project ID

VG10596) and expanded by crossing with C57BL/6J mice (Stock 000664, Jackson Laboratories). Genotyping of weaned mice was carried out in two separate reactions based on suggested protocols (Velocigene). Amplification of the *Ang1*⁻ allele was performed using forward primer 5' CCAAGGCCAAGATGGAATTAGG 3' and reverse primer 5' GCTGGCTTGGTCTGTCTGTCCTA 3', which produces a band at ~300 bp. The *Ang1*⁺ allele was amplified using forward primer 5' TACTATGGATGATGGTGAACCTAAGG 3' and reverse primer 5' GATCACAACCAGACCCAGCACG 3', which produces a band at ~280 bp (Supplemental Figure 3.1, panel B).

3.3.4: Gross phenotyping analysis—The fertility of *Ang1*^{+/-} mice was evaluated by a heterozygote intercross. The viability of *Ang1*^{-/-} mice was evaluated initially by a chi-squared analysis of genotypes born to heterozygote intercrosses.

3.3.5: Developmental viability studies—To identify the point during gestation that *Ang1*^{-/-} mice are lost, timed mating experiments were conducted. *Ang1*^{+/-} x *Ang1*^{+/-} and *Ang1*^{+/-} x *Ang1*^{+/+} intercrosses were paired for 24 h to allow for mating, then weighed daily to identify pregnancies using a method described previously (202). Pregnant dams were euthanized at embryonic day 7.5, 8.5, or 9.5, and uteri or embryos were isolated. Embryonic development was evaluated according to Theiler staging criteria (203).

Samples were fixed using 10% neutral buffered formalin (37% w/v formaldehyde solution, diluted 1:10 with buffer containing dibasic sodium phosphate (45 mM) and monobasic sodium phosphate (33 mM), pH 7.0) for 48 h prior to histopathological evaluation. Pathological

evaluation was performed at the Comparative Pathology Laboratory at the Massachusetts Institute of Technology.

3.3.6: Quantitative PCR—Quantitative real-time PCR (qPCR) was conducted to identify gene expression changes in *Ang1*^{+/-} mice. RNA was isolated from tissue samples homogenized in TriZOL Reagent (Invitrogen) using a Benchmark D1000 homogenizer, purified according to the manufacturer’s protocol, DNase-treated using the TURBO DNA-free kit (Ambion), and subjected to reverse transcription-PCR using the qScript cDNA Synthesis kit (Quanta Biosciences). The resultant cDNA was probed for expression of *Ang1* using primer pairs shown in Table 3.1. Reactions were run in duplicate using SYBR Green master mix (Quanta Biosciences) on an Applied Biosystems ABI 7500 Fast Real-Time PCR system. Cycling conditions were 95 °C for 30 s, 55 °C for 30 s, and 72 °C for 30 s, repeated for 30 cycles and followed by melt curve analysis. Threshold cycle values were determined by setting a constant threshold at 0.6, and fold changes in gene expression were determined by the ΔC_T method (172). Expression was normalized to that of *Gapdh*, *Rpl13a*, and *Hprt1*.

Table 3.1. Primers used for qPCR

Target	Forward (5'→3')	Reverse (3'→5')
<i>Ang1</i>	TCTGCAGGGTTCAGACATGT	TCTGGGCTATGAGGGGAGAT
<i>Ang2</i>	ACTGCGAAAGTATGATGGTGA	TCCACAGATGGCCTTGATGTT
<i>Ang3</i>	GAGCACGAAGCTAGACACA	GACCAACAACAAAGAACCTGG
<i>Ang4</i>	GAGCCCATGTCCTTTGTTGT	CATAGTGCTGACGTAGGAATTTTC
<i>Gapdh</i>	CTCCCACTCTTCCACCTTCG	CCACCACCCTGTTGCTGTAG
<i>Rpl13a</i>	GCTGAAGCCTACCAGAAAGT	TCCGTTTCTCCTCCAGAGT
<i>Hprt1</i>	CTAGTCCTGTGGCCATCTGC	GGGACGCAGCAACTGACATT

3.3.7: *Ribonuclease zymogram assay*—Zymograms were performed on plasma samples to verify reduction of angiogenin expression in *Ang1*^{+/-} mice, using an assay similar to one reported previously (176). Briefly, a polyacrylamide gel containing SDS (0.1% w/v), Tris (375 mM), and poly(C) (4.5 mg, incubated at 50 C prior to addition) was cast. Samples containing recombinant angiogenin (100 nmol) or murine plasma (0.5 μL) were prepared with 2X Laemmli sample buffer (without DTT or β-mercaptoethanol, and without boiling). Plasma samples were pre-treated by incubating 2 μL plasma with 1000 U PNGase F (New England BioLabs) for 48 h to remove N-linked glycans from secreted ribonucleases in plasma and reduce sample complexity. After electrophoresis, the gel was washed twice in 10 mM Tris-HCl buffer, pH 7.5, containing isopropanol (20% v/v), then once in 10 mM Tris-HCl buffer, pH 7.5 before an incubation overnight in 100 mM Tris-HCl buffer, pH 7.5 to allow RNase 1 to refold within the gel. The next day, the gel was washed in 10 mM Tris-HCl buffer, pH 7.5 before staining in an aqueous solution of toluidine blue (0.2% w/v) for 10 min. The gel was washed with deionized water and destained in 10 mM Tris-HCl buffer, pH 7.5. ImageJ software was used to evaluate band intensity (173).

3.3.8: *Immunoblotting*—An immunoblot was performed to probe expression of angiogenin in *Ang1*^{+/-} mice. Briefly, tissue samples were homogenized using a Benchmark D1000 homogenizer in T-PER Tissue Protein Extraction Reagent (Pierce). Homogenized tissue and plasma samples were tested for protein content by using a bicinchoninic acid assay kit (Pierce) and prepared with denaturing sample buffer prior to SDS-PAGE. Samples were transferred to a membrane using the IBlot 2 Dry Blotting System (Thermo Fisher) for 1 min at 20 V, 2 min at 23

V, and 1 min at 25 V. Membranes were blocked for 1 h in 5% w/v dry milk in Tris-buffered saline with Tween (TBST, which contained 19 mM Tris base, 137 mM NaCl, 2.7 mM KCl, and 0.1% v/v Tween 20), and incubated overnight at 4 °C with a polyclonal antibody against human Ang (R&D Systems) or polyclonal antibody against mouse transferrin (Bethyl Laboratories). The membrane was washed in TBST before a 1-h incubation at room temperature with a secondary antibody, diluted in an aqueous solution of dry milk (5% w/v) in TBST, then washed in TBST again before imaging. The blot was treated with SuperSignal West Pico Chemiluminescent substrate (Thermo Fisher) and imaged on an ImageQuant LAS 4000 imager (GE Healthcare). ImageJ software was used to evaluate band intensity (173). Blots were stripped using Restore Western Blot Stripping Buffer (Thermo Fisher) and re-probed.

3.3.9: Statistical analyses—A minimum of three biological replicates were performed for every experiment. All data are expressed as the mean \pm SEM, and statistical evaluation was performed by Wilcoxon rank-sum test, log-rank test, and chi-squared test in GraphPad Prism and Mstat software, with $p < 0.05$ being considered significant.

3.4 Results

3.4.1: Ang1^{+/-} mice have reduced Ang1 gene expression—We hypothesized that heterozygosity of *Ang1* should result in reduced expression of *Ang1*, as the gene dosage is halved. Analysis of *Ang1* expression in ten tissues by qPCR did not reveal significant changes in gene expression on a tissue-by-tissue basis, yet, overall expression of *Ang1* in *Ang1^{+/-}* mice was 61% that of *Ang^{+/+}* expression (Figure 3.1, panel A).

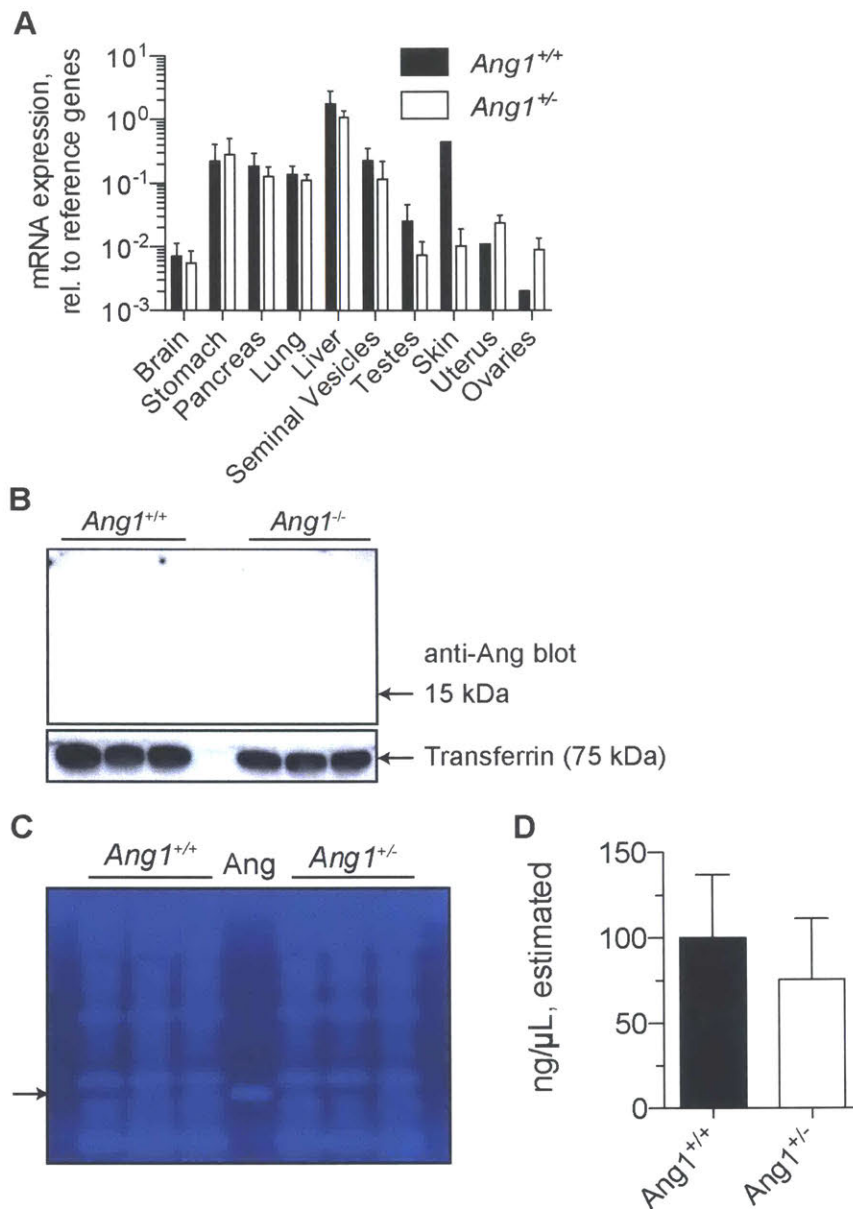


FIGURE 3.1. Verification of the reduction of Ang in *Ang1*^{+/-} mice. **A**, Bar graph showing the tissue-specific expression of *Ang1* in *Ang1*^{+/+} and *Ang1*^{+/-} mice as measured by qPCR. Data were normalized to the geometric mean of three reference genes. *n* = 3 per tissue. **B**, Representative immunoblot probing for Ang in plasma from *Ang1*^{+/+} and *Ang1*^{+/-} mice. **C**, Zymogram of plasma samples (0.5 μl of plasma per lane) from *Ang1*^{+/+} or *Ang1*^{+/-} mice, used to evaluate ribonucleolytic activity relative to recombinant human Ang (center lane). **D**, Bar graph showing estimated ng/μl of Ang present in *Ang1*^{+/+} or *Ang1*^{+/-} plasma samples, measured by quantification of densitometry maps of each lane at the position occupied by Ang (arrow) and normalization to the known quantity of Ang loaded as a standard.

3.4.2: *Ang1*^{+/-} plasma exhibits reduced angiogenin expression and activity—Immunoblotting was carried out to probe for expression of Ang in *Ang1*^{+/+} and *Ang1*^{+/-} mice. An antibody reported to be reactive to human and rat Ang did not react to any protein present in mouse tissues or plasma (Figure 3.1, panel B).

Zymogram analysis of plasma samples was carried out as an alternative, activity-based method to detect circulating Ang. *Ang1*^{+/-} samples exhibited reduced band intensity at the position expected for recombinant Ang, equivalent to 76% of the activity of *Ang1*^{+/+} samples (Figure 3.1, panels C and D).

3.4.3: *Ang1*^{-/-} mice are not produced from *Ang1*^{+/-} intercrosses—In the expansion of *Ang1*^{+/-} mice through a heterozygous intercross, we did not observe any *Ang1*^{-/-} pups born out of 52 pups

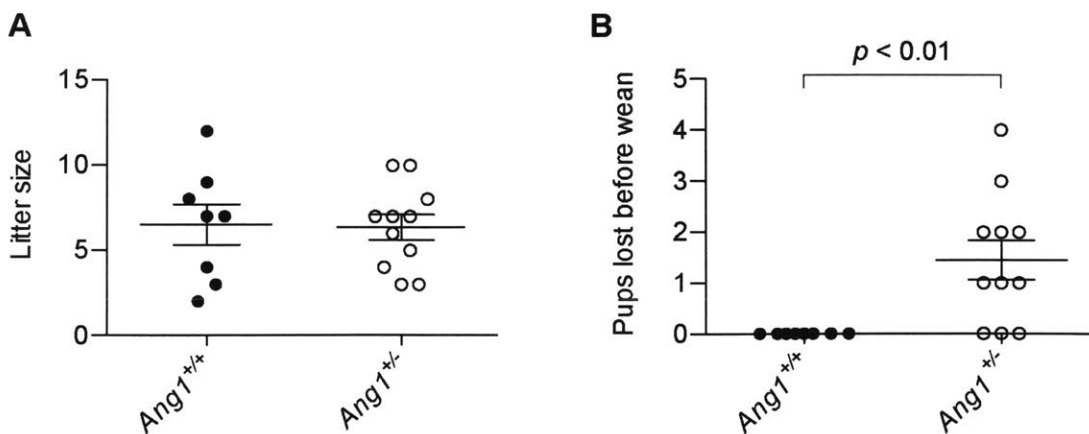


FIGURE 3.2. **Effect of *Ang1* heterozygosity on litter size and survival.** A, Graph showing litter sizes of *Ang1*^{+/+} and *Ang1*^{+/-} dams. B, Graph showing number of pups lost from original litter prior to weaning age from *Ang1*^{+/+} and *Ang1*^{+/-} dams.

surveyed from 10 litters. This complete absence deviates significantly from expected Mendelian inheritance ratios, $\chi^2(2, n = 52) = 19.5, p < 0.005$, and suggests the loss of *Ang1* is lethal.

3.4.4: Ang1^{+/-} mice experience partial litter loss—In the initial expansion of *Ang1^{+/-}* mice, we found that litter sizes of *Ang1^{+/-}* intercrosses (6.4 ± 0.7 pups) were similar to those of *Ang1^{+/+}* intercrosses (6.5 ± 1 pups) (Figure 3.2, panel A). Nevertheless, the survival of pups to weaning age was impaired in *Ang1^{+/-}* dams. Whereas no *Ang1^{+/+}* intercross litters were observed to lose any pups, loss of at least one neonate was typical of *Ang1^{+/-}* litters, with an average of (1.5 ± 0.4) pups lost (Figure 3.2, panel B). Of note, no genotyped neonate carcasses were homozygous for deletion of *Ang1*. Additionally, neonatal death occurred irrespective of the genotype of the pup.

3.4.5: Ang1^{+/-} dams exhibit impaired uterine vascularization and elevated incidence of embryonic loss during pregnancy—Timed mating studies were performed to evaluate development of embryos and uteri during the period of E7.5-E9.5. Embryos were collected at E9.5 and E8.5 (Figure 3.3, panels B and C) and genotyped. No *Ang1^{-/-}* samples were identified. Histological analysis of embryos at E7.5 is underway.

Gross analysis of samples from pregnant mice was conducted using Theiler staging criteria to identify embryonic developmental stages based on morphology. This examination identified a high proportion of underdeveloped (less than Theiler stage 11) or absent embryos at E7.5 in *Ang1^{+/-}* mice (8 of 9 embryos in 1 litter), whereas embryos from *Ang1^{+/+}* dams were normal. Uteri from E8.5 *Ang1^{+/-}* mice were also highly likely to have missing embryos (11 of 18 in 2 litters) or underdeveloped embryos (less than Theiler stage 13, 4 of 18 embryos). Yet, in E9.5

pregnancies, the incidence of underdeveloped (less than Theiler stage 15) or missing embryos decreased (5 of 28 embryos in 3 litters). Additionally, analyses of whole uteri indicate that *Ang*^{+/-} uteri are less vascular than are *Ang*^{+/+} uteri at the same number of days post coitum (Figure 3.3, panels D and E), as determined by fewer visible blood vessels and reduced coloration of the uterus.

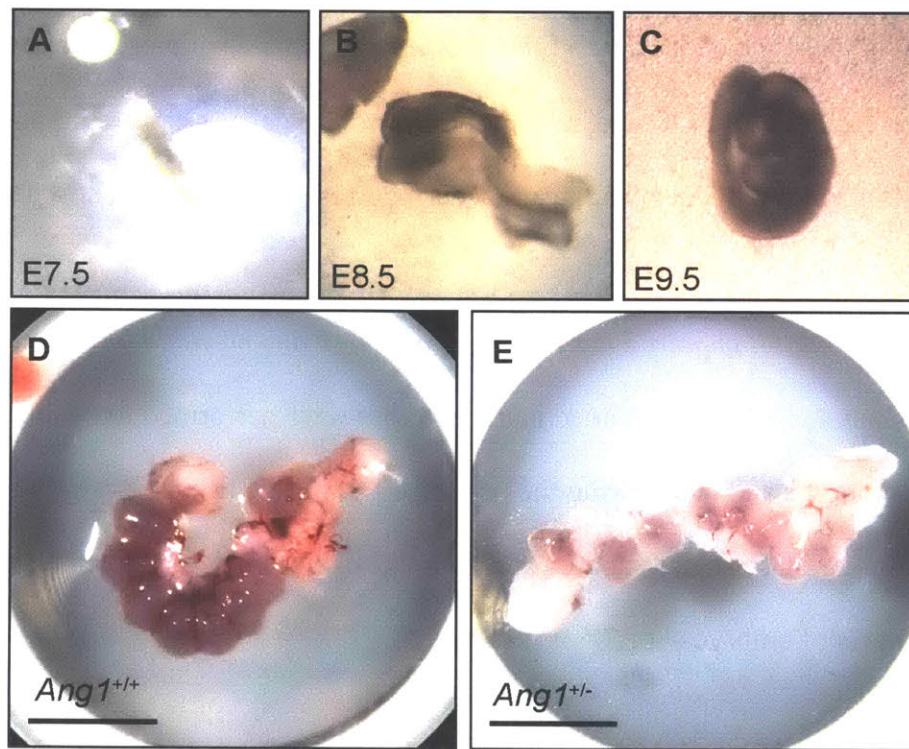


FIGURE 3.3. Embryonic development and effect of *Ang*1 heterozygosity on uterine vascularization. Panels A-C depict normal embryos produced from *Ang*1 intercrosses. A, Photograph of a representative normal mouse embryo at E7.5. B, Photograph of a representative normal mouse embryo at E8.5. C, Photograph of a representative normal mouse embryo at E9.5. Panels D-E depict uteri isolated from pregnant mice at E7.5. Scale bars are 1 cm. D, Photograph of a wild-type uterus at E7.5. E, Photograph of an *Ang*1^{+/-} uterus at E7.5.

3.5 Discussion

Angiogenin (Ang) has long been appreciated to play an important role in the generation of blood vessels. Although this action has been extensively characterized in the context of cancer, we now appreciate that angiogenin also functions in nonmalignant environments. We undertake the characterization of *Ang1*^{+/-} mice, and find that homozygosity for loss of *Ang1* is incompatible with embryonic development. Although *Ang1*^{+/-} mice are fertile, heterozygosity is associated with elevated incidence of litter loss, impaired embryonic survival, and reduced vascularization of the uterus.

Our findings are consistent with previous findings that demonstrate the association of angiogenin with blood vessel growth in the uterus and placenta. Substantial angiogenesis and vascular remodeling takes place in both the maternal and fetal placenta in early gestation (204), and many studies have demonstrated the presence of Ang in these tissues. Ang is expressed in human endometrial cells (119), and this expression fluctuates with the menstrual cycle, with Ang levels elevated by 3- to 4-fold in mid and late secretory phases and in gestation relative to the proliferative phase. Additionally, endometrial Ang expression is induced by progesterone, suggesting that it is important during pregnancy (116). Ang is also associated with fetal chorionic villi in the placenta (118), with expression increasing to double that of first-trimester levels by term (117), suggesting that Ang is also important in the embryo for vascularization of the placenta.

Key vasculogenic and angiogenic events in the mouse embryo take place between day E6.5 and E10 (205,206), which informed our choice to study uteri at E7.5–E9.5. Yet, angiogenin

localization in the embryo has only been reported for the nervous system, where angiogenin is associated with developing neurons and is strongly expressed from E9.5 onward (123). This timing also correlates with CNS blood vessel development (207). In neonates and adults, however, the primary site of angiogenin expression is the liver (208).

The absence of *Ang1*^{-/-} pups suggests that maternal Ang either cannot cross the placental barrier or does so in insufficient quantity to compensate for the loss of the enzyme in the embryo. Although the permeability of murine placenta to protein has been incompletely characterized (209), it exhibits similar structure and behavior to human placenta (210), which is not freely permeable to solutes above 5200 daltons in size (211).

The finding that maternal heterozygosity for *Ang1* is sufficient to increase the risk of neonatal death (Figure 3.2, panel B) suggests that maternal expression of Ang is important to support the survival of pups. Impaired placental angiogenesis has been associated with complications of pregnancy, such as preeclampsia and preterm delivery, in humans; yet, mice are not naturally prone to these conditions (212), and we did not evaluate blood pressure during pregnancy in *Ang1*^{+/-} mice. Although not significantly so, a higher proportion of neonates lost were heterozygous for *Ang1* rather than wildtype (75%, data not shown), which suggests that Ang expression in neonates could compensate to some degree for the reduction in maternal Ang expression.

The high incidence of underdeveloped embryos at E7.5 in *Ang1*^{+/-} mice, and subsequent high incidence of absent embryos at E8.5, suggests that Ang-dependent events at or prior to E7.5 are

important for survival of embryos. Placentation in mice takes place around E8, with extension of maternal spiral arteries occurring as early as E7.5. Meanwhile, absence of fetal villi, as in mice lacking *Gcm1*, is lethal at E10 (213). Hence, partial loss of Ang expression in maternal tissues, which correlates with reduced vascularization of the uterus and placenta (Figure 3.3), has a greater impact on embryonic survival than does partial loss of Ang in embryonic tissues. This distinction agrees with our finding that *Ang1*^{+/-} dams are more likely than *Ang1*^{+/+} dams to lose pups of either *Ang1*^{+/+} or *Ang1*^{+/-} genotypes postnatally.

We find that the number of pups initially delivered by *Ang1*^{+/-} dams does not differ from that of *Ang1*^{+/+} dams (Figure 3.2, panel A), although this does not appear to be correlated with partial loss of initially larger litters *in utero*. *Ang1*^{+/-} uteri dissected at E7.5, E8.5, or E9.5 yielded 8 ± 1 , 9 ± 2 , or 9.3 ± 0.3 pregnancies respectively, while *Ang1*^{+/+} uteri yielded 8.5 ± 0.5 pregnancies at E7.5 (data not shown). Instead, we hypothesize that critical Ang-dependent events are required for survival of embryos beyond E8.5, and that failure to pass this point results in loss of the litter. Indeed, preliminary histological evaluation at E7.5 suggests that embryos from *Ang1*^{+/-} uteri at E7.5 are underdeveloped and dying.

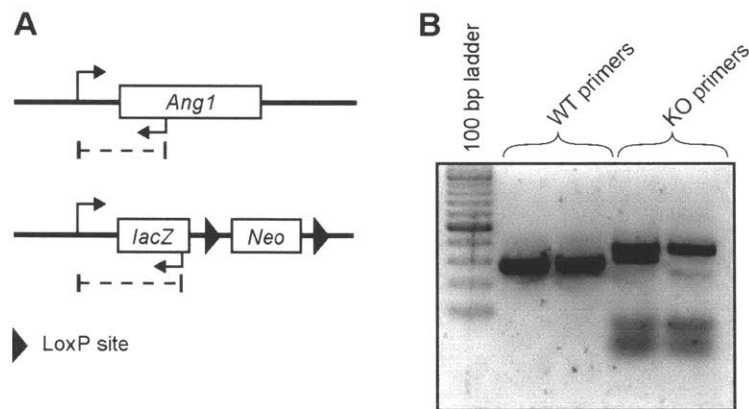
Our results contrast with previous publications, using an independently-generated *Ang* knockout mouse line, that report no significant phenotypes related to fertility and embryonic development (131,201). This mouse line is a constitutive knockout in the C57BL/6 background and was reported using qPCR to detect *Ang* and *Rnase4* expression and immunoblot to detect Ang. Higher expression of *Rnase4* was reported in this *Ang*^{-/-} line, but no other gene expression was evaluated. Differences between the two lines could also be due to effects of gene expression in

the transgenic cassette used to create the knockout, as the strain we characterized expresses a LacZ reporter and neomycin resistance cassette, but the transgenic locus is not described in detail for the other line.

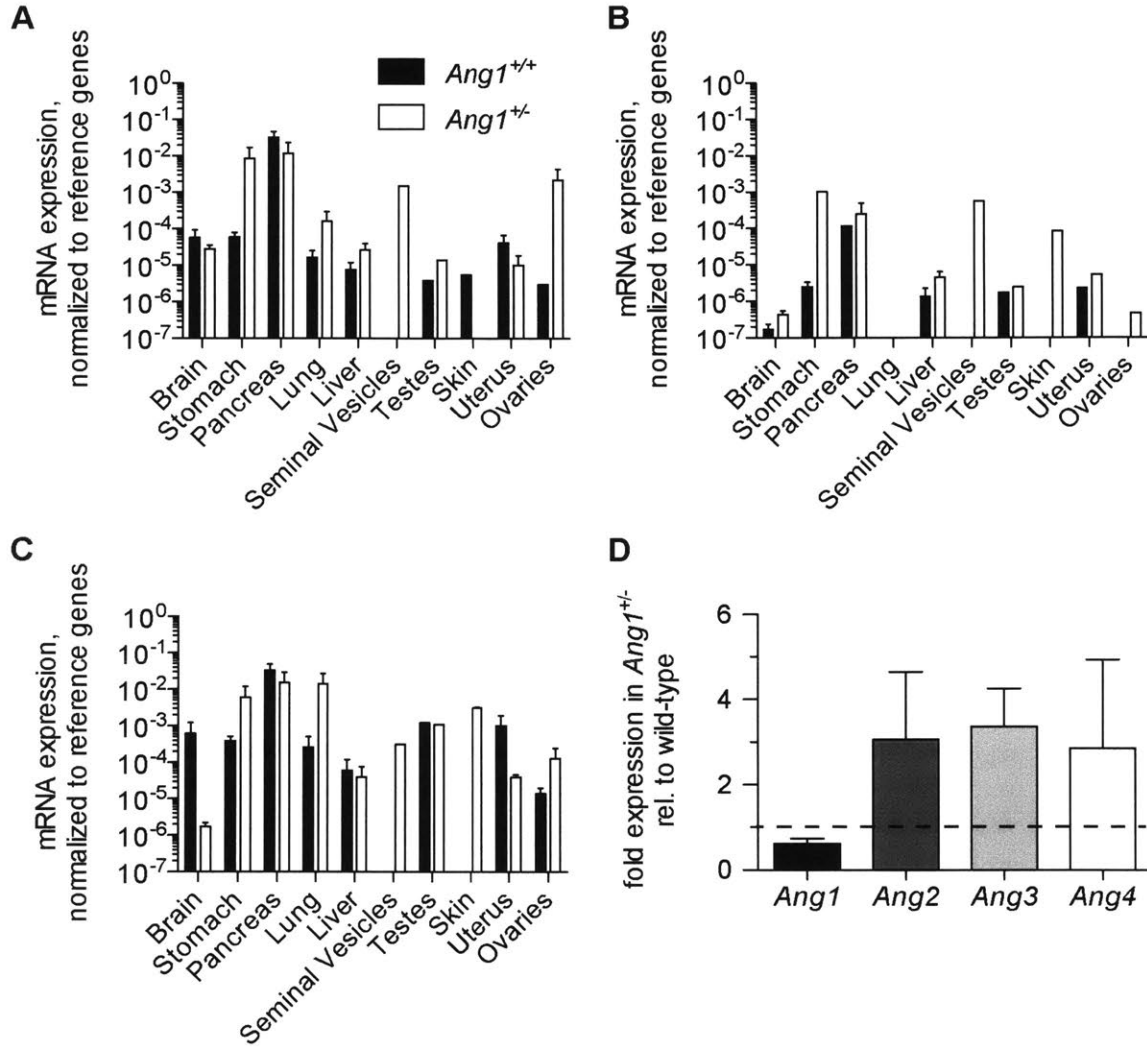
We note that the mouse genome contains six genes encoding angiogenins (140), of which at least at least three of the encoded enzymes (Ang 1, Ang 3, and Ang 4) exhibit angiogenic activity (214). The possibility that the two knockout systems affect multiple or different subsets of these genes could also explain the observed differences, as this is not reported for the other line. In our system, qPCR analysis reveals that while *Ang2*, *Ang3*, and *Ang4* are expressed at very low levels, loss of *Ang1* is not accompanied by loss of other *Ang* genes (Supplemental Figure 3.2). Instead, expression of other *Ang* genes appears slightly elevated in *Ang1*^{+/-} mice, which could explain the relatively high residual amount of Ang that is present in *Ang1*^{+/-} plasma by zymogram analysis.

Other biological roles that have been suggested for Ang could impact the phenotype reported here. Ang participates in the response to oxidative stress by generating tiRNAs, which inhibit apoptosis (129,130). Fetal villous endothelium is particularly sensitive to oxidative stress (215,216). Thus, Ang could serve not only to drive growth of these nascent blood vessels, but as a factor that protects from cell death. Additionally, roles in immunity have been attributed to Ang, which is classified as an acute-phase protein (132), reduces inflammatory cytokine expression in fibroblasts (134), and has antimicrobial activity (133). These activities could be protective of the embryo during its development.

3.6: Supplemental information



SUPPLEMENTAL FIGURE 3.1. **Genotyping for the *Ang1* allele.** A, Schematic of the genotyping strategy used to identify the wild-type *Ang1* allele and mutant cassette. Adapted from KOMP. B, Gel showing the presence of bands using wild-type (~280 bp) and mutant (~300 bp) primer sets in two *Ang1*^{+/-} samples.



SUPPLEMENTAL FIGURE 3.2. **Effect of *Ang1* heterozygosity on expression of other angiogenin genes.** Expression was probed by qPCR and normalized to the geometric mean of three reference genes, n = 3. For missing bars, no expression was detectable. **A**, Bar graph of *Ang2* expression in $Ang1^{+/+}$ and $Ang1^{+/-}$ mice. **B**, Bar graph as in **A**, for expression of *Ang3*. **C**, Bar graph as in **A**, for expression of *Ang4*. **D**, Bar graph showing gene expression of all $Ang1^{+/-}$ samples tested, normalized to gene expression of $Ang1^{+/+}$ samples.

Chapter 4

Towards novel anti-secreted ribonuclease antibodies using phage display

Contributions: I expressed and purified tagged human and murine ribonuclease 1 proteins, performed ribonucleolytic activity assays on all proteins, carried out TEV cleavage experiments, and performed acetylation and MALDI mass spectrometry confirmation. T. Hoang and I worked jointly to design constructs for the expression of human and murine ribonuclease 1 and angiogenin and to perform biotinylation of proteins. T. Hoang expressed and purified human and murine angiogenin proteins and performed MALDI mass spectrometry experiments. We collaborated with M. Hornsby and J. Wells's laboratory at the University of California, San Francisco for antibody generation via phage display.

4.1 Abstract

Protein binding and detection using antibodies is a cornerstone of biological research and is essential to techniques such as Western blotting, ELISA, immunocyto/histochemistry, and immunoprecipitation. Conventional antibody generation processes rely on the adaptive immune response of animals, which result in the inability to generate specific antibodies to all targets of biological interest. One such example is the secretory ribonuclease (ptRNase) superfamily. These proteins are conserved in all vertebrate species, limiting their immunogenicity, and are both small and highly similar between homologs and paralogs, further limiting the selection of possible epitopes that would be useful for differentiation between proteins. As a result, no antibodies currently exist that can reliably detect and differentiate between ptRNases. To address this paucity, we sought to use antibody phage display, a technique developed in the Wells laboratory at the University of California, San Francisco, to generate antibody fragments against ptRNases from a recombinant library. Here, we describe the design and generation of ribonuclease conjugates to be used for antibody phage display.

4.2 Introduction

Biomolecular research relies heavily on antibodies for the detection of proteins. The commercial availability of specific antibodies against biologically relevant targets, along with new techniques to chemically or genetically alter antibodies for specific purposes, have enabled leaps forward in protein detection. Moreover, the future of antibody-based detection promises higher throughput and massive multiplexation to detect many targets simultaneously. Yet, high-quality antibodies are not available against all biologically relevant targets, which limits the quality of data generated using these methods.

Two significant challenges face antibody-based methods at present: the difficulty of antibody generation against non-immunogenic targets, and the tendency of antibodies to exhibit cross-reactivity with non-target proteins. Targets that exhibit poor immunogenicity, such as highly conserved proteins, are difficult to probe using conventional *in vivo* immunization and hybridoma generation due to immune tolerance by the host animal (217,218). Autoimmunity-prone mice, such as the NZB/W strain, have been used successfully to circumvent this problem (219), but resulting antibodies exhibit low affinity and tend to be cross-reactive with other proteins (220). Cross-reactivity is not a problem unique to this system, but is a systemic problem even among antibodies with high binding affinity to their targets (221-223). Generating specific antibodies against targets with conserved sequences or structural epitopes is of growing importance given the increasing demand for high-throughput applications, but current antibody generation methods fall short.

Antibody phage display presents an opportunity to address these problems. In this technique, antibody variable region gene libraries are recombined and expressed in phage (224), yielding surface-displayed F(ab)s with much higher sequence diversity than is naturally present in the B-cell repertoire. This technique has already been used to generate specific antibodies to challenging targets, such as the botulinum neurotoxin (225) and specific protein conformational states (226).

Secretory ribonucleases (ptRNases) are an ideal model system for the generation of specific antibodies. ptRNases are small proteins, approximately 14 kDa in molecular mass, and composed of 124 to 128 amino acid residues. They are highly structurally similar, with a mean TM score of 0.852 for a set of four murine and human homologs and paralogs (RNase 1 and angiogenin) (227,228). This similarity results in a relatively restricted set of possible epitopes that can be used to differentiate between proteins, and results in cross-reactivity of antibodies against RNase 1 with other ptRNases (229). Further, ptRNases are highly cationic proteins, which presents an additional challenge as nonspecific Coulombic interactions must be avoided.

In our study, we evaluate the use of antibody phage display to generate monospecific F(ab)s against a set of four ptRNases: human and murine ribonuclease 1 and angiogenin. We anticipated that phage display could yield antibodies that are not cross-reactive against paralogous or homologous protein. Success would represent a significant advance in antibody generation technology, as such antibodies have yet to be successfully generated, and would present an opportunity to broaden research into the biology of ptRNases using antibody-based methods.

4.3 Experimental procedures

4.3.1: Materials—DNA constructs for the cloning of murine and human ribonuclease 1 (mRNase 1 and hRNase 1) and angiogenin (mAng and hAng) and primers for manipulation of pET22b vector were from Integrated DNA Technologies. ProTEV Plus enzyme and buffer were from Promega. Competent cells for cloning and expression of protein in *E. coli* (XL10-Gold Ultracompetent and BL21-DE3) were from Agilent Technologies and New England BioLabs, respectively.

Equipment—All fluorescence measurements were made with a Tecan M1000 fluorescence plate reader. Liquid chromatography for protein purification was carried out using a GE ÄKTA pure fast protein liquid chromatography (FPLC) system. Gel imaging was performed with a GE AI600 imager. Matrix-assisted laser desorption ionization-time-of-flight (MALDI-TOF) mass spectrometry was performed with a Voyager DE-Pro instrument at the Biophysics Instrumentation Facility at the University of Wisconsin–Madison.

Conditions—All procedures were carried out at ambient temperature (~22 °C) and pressure (1.0 atm) unless noted otherwise.

4.3.2: Design of tagged ribonuclease constructs—Our chosen tag for use with the antibody phage display system is 28 amino acid residues in length and contains a terminal AviTag sequence (GLNDIFEAQKIEWHE) (230), (GlySer)₃ linker (GSGSGS), and a TEV protease recognition sequence (ENLYFQG) proximal to the protein N- or C-terminus.

To verify that appending such a tag to the N- or C-terminus of the sequence of our chosen ribonucleases would not block potentially useful epitopes for antibody discrimination between proteins, the ConSurf server was used to identify regions of the protein structure with high and low degrees of evolutionary conservation (231-235). Maps of protein structures were made in PyMOL (236) using structural information from RCSB Protein Data Bank entries 1z7x (hRNase 1) (20), 3tsr (mRNase 1) (17), 1ang (hAng) (91), and 2bwl (mAng) (237).

4.3.3: Cloning of tagged ribonucleases—The signal peptide prediction program SignalP was used to predict and exclude signal peptide sequences from recombinant proteins. Constructs of hRNase 1 (residues 28–156) (238), mRNase 1 (residues 26–149) (17), hAng (residues 25–147) (239), and mAng (residues 26–145, Gene ID: 11727) with the peptide tag sequence appended to the C-terminus of the enzyme were designed. Overlap sequences were appended to the 5' (5' TTTGTTTAACTTTAAGAAGGAGATATACAT 3') and 3' (5' GATCTCAGTGGTGGTGGTGGTGGTGCTCGAG 3') end of the construct to enable Gibson assembly into the pET22b expression vector (Novagen). pET22b was linearized by PCR with forward primer: 5' AAGCCCGAAAGGAAGCTGAGTTGGCTGC 3' and reverse primer: 5' ATGTATATCTCCTTCTTAAAGTTAAACAA 3'. Gibson assembly was performed using Gibson Assembly Master mix (NEB) following the manufacturer's protocols with 50 ng of each linearized plasmid and ribonuclease construct insert (240). Correct DNA sequences of the resultant vectors were verified by Sanger sequencing at the University of Wisconsin–Madison Biotechnology Center.

4.3.4: Production of tagged ribonucleases—pET22b plasmids encoding the peptide-tagged hRNase 1, mRNase 1, hAng, or mAng were used for protein production in BL21(DE3) cells. Ribonucleases were harvested from inclusion bodies as described previously (241).

Ribonucleases were purified by FPLC using a GE ÄKTA pure system. Aliquots of protein-containing fractions were prepared with 6X Laemmli loading dye for SDS-PAGE analysis to verify purity of the tagged ribonuclease preparations. Gels were stained with Coomassie Blue stain (Pierce) and imaged. Protein identity was confirmed by matrix-assisted laser desorption ionization-time-of-flight (MALDI-TOF) mass spectrometry.

4.3.5: Biotinylation of tagged ribonucleases—Biotin was appended to the peptide tag of ribonucleases to facilitate binding to the streptavidin column used in antibody phage display screening. This was performed using the enzyme BirA, in a reaction that has been described previously (242).

A BirA-maltose binding fusion protein (MBP-BirA) was cloned and purified using a method described previously (243). MBP-BirA and all tagged ribonucleases were dialyzed into bicine buffer (50 mM bicine, pH 8.3).

Biotinylation was carried out using the following parameters: tagged ribonuclease substrate and MBP-BirA were combined in a 1:4 molar ratio in bicine buffer containing magnesium acetate (10 mM), ATP (10 mM), and D-biotin (60 μ M). The reaction mixture was incubated with rotation overnight at 4 °C.

Biotinylated ribonucleases were purified from the reaction mixture by FPLC using a HiTrap SP column, and their purity was assessed by SDS–PAGE. The correct molecular mass of biotinylated protein was confirmed by MALDI–TOF mass spectrometry.

4.3.6: Ribonucleolytic activity assays—Assays of ribonucleolytic activity were performed on tagged ribonucleases using a ribonuclease substrate described previously (174). Protein concentration was measured using a bicinchoninic acid assay kit (Pierce) according to the manufacturer’s instructions. The background fluorescence intensity (I_0) of 100 mM Tris buffer, pH 7.0, containing 6-FAM-dArUdAdA-6-TAMRA (10 μ M), NaCl (100 mM), and acetylated bovine serum albumin (0.1 mg/mL), was measured. A 1- μ L aliquot of RNase was added, and the change in fluorescence intensity (ΔI) monitored over time. Excess RNase A was added, and maximum fluorescence (I_{\max}) was measured. All measurements were taken at $\lambda_{\text{ex}} = 490$ nm and $\lambda_{\text{em}} = 525$ nm. This value was, in turn, used to calculate the activity of RNases based on known concentration with Equation 4.1.

$$[\text{RNase 1}] = \frac{\Delta I}{\frac{I_{\max} - I_0}{\frac{k_{\text{cat}}}{K_M}}} \quad (4.1)$$

4.3.7: TEV protease cleavage assays—To verify effective removal of the peptide tag from the ribonucleases, TEV protease cleavage assays were carried out using the ProTEV Plus kit (Promega) and according to the manufacturer’s instructions. Aliquots of sample were prepared with 6X Laemmli loading dye for SDS–PAGE analysis, and extent of cleavage determined by appearance of the cleavage product on the gel by Coomassie Blue staining (Pierce).

4.3.8: Acetylation of RNase—Lysine acetylation of mRNase 1 was performed to remove positive charges from the protein, following a method published previously (244). Briefly, 10 nmol mRNase was diluted into 50 mM ammonium bicarbonate, pH 7.5 to a total of 3 mL, and 10 μ mol acetic anhydride added while stirring. The pH of the mixture was corrected to ≥ 7.0 , and left to stir for one hour. Residual reagents were removed by overnight dialysis in buffer containing NaCl (137 mM), KCl (2.7 mM), Na₂HPO₄ (10 mM), and KH₂PO₄ (1.8 mM), pH 7.4. Acetylation was confirmed by MALDI–TOF mass spectrometry.

4.3.9: Statistical analyses—A minimum of three replicates were performed for activity and TEV cleavage experiments. All data are expressed as the mean \pm SEM, and statistical evaluation was performed by Wilcoxon rank-sum test in GraphPad Prism and Mstat software, with $p < 0.05$ being considered significant.

4.4 Results

4.4.1: Evolutionarily divergent residues in ptRNases are not present near the amino acid termini—The four ptRNases in our study share relatively low sequence identity despite their high structural agreement (Table 4.1), suggesting that useful epitopes for antibody generation could exist on the proteins. The phage display strategy requires attachment of our target protein to a column via streptavidin–biotin interaction, necessitating the introduction of a peptide tag to which biotin can be ligated. We sought to verify that this tag would not preclude antibody binding if cloned on to the N- or C-terminus of the proteins.

Table 4.1. Sequence and structure identity and similarity between ptRNases.

ptRNase sequence identity (%)				
	mRNase 1	mAng	hRNase 1	hAng
mRNase 1	100	35.46	70.47	34.51
mAng	35.46	100	36.81	73.39
hRNase 1	70.47	36.81	100	35.62
hAng	34.51	73.79	35.62	100

ptRNase sequence similarity (%)				
	mRNase 1	mAng	hRNase 1	hAng
mRNase 1	100	49.7	78.8	50
mAng		100	50.9	84.4
hRNase 1			100	48.8
hAng				100

RMSD between structures				
	mRNase 1 (3tsr)	mAng (2bwl)	hRNase 1 (1z7x)	hAng (1ang)
mRNase 1 (3tsr)	0	2.859	0.77	3.865
mAng (2bwl)		0	4.584	1.473
hRNase 1 (1z7x)			0	5.87
hAng (1ang)				0

Our evaluation of the evolutionary conservedness of residues in these four proteins show that divergent regions in ptRNases are distributed around the perimeter of the protein, away from the active site in the central cleft. We find that many of the divergent residues are present in unstructured loops distal to the active site and to the N- and C-termini of the protein (Figure 4.1). We subsequently generated tagged ptRNase constructs for expression of the four proteins with tags appended to the C-terminus of the enzyme (Figure 4.2).

4.4.2: Tagged ptRNases express in E. coli, are of expected molecular weight, and retain ribonuclease activity—Our expression system for the four ptRNases readily yielded sufficient quantity of protein for downstream analysis. Purity of the resultant protein was high after column

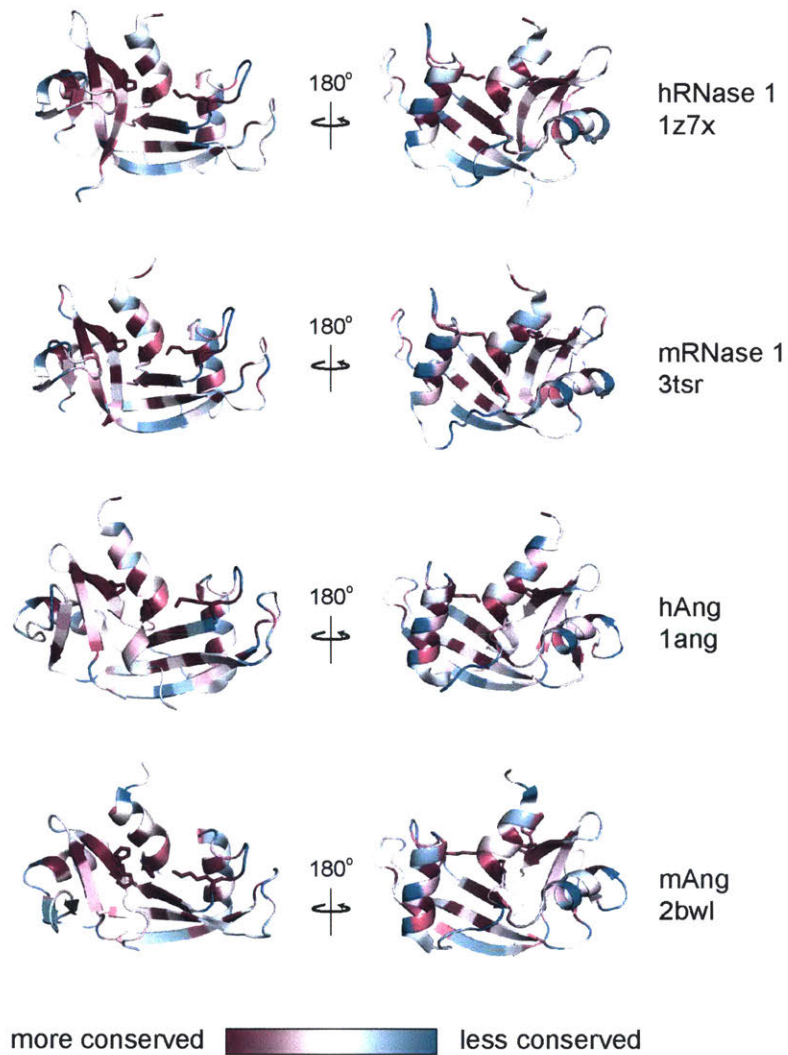
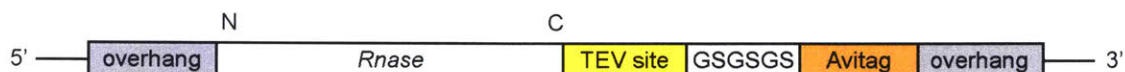


FIGURE 4.1. PyMOL renderings of RNases, with evolutionary conservation mapped by residue. Ribonuclease active site residue side chains are shown.



hRNase 1

MKESRAKKFQRQHMDSDSSPSSSSTYCNQMMRRRNMTQGRCKPVNTFVHEPLVDVQN
 VCFQEKVTCKNGQGNCYKSNSSMHITDCRLTNGSRYPNCAVRTSPKERHIIVACEGSPYV
 PVHFDASVEDSTENLYFQGGSGSGSGSGMSGLNDIFEAQKIEWHEG

mRNase 1

MRESAAQKFQRQHMDPDGSSINSPTYCNQMMKRRDMTNGSCKPVNTFVHEPLADVQA-
 VCSQENVTCKNRKSNKYKSSSALHITDCHLKGNSKYPNCDYKTTQYQKHIIIVACEGNPYV
 PVHFDATVENLYFQGGSGSGSGSGMSGLNDIFEAQKIEWHEG

hAng

MQDNSRYTHFLTQHDAKPQGRDDRYCESIMRRRGLTSPCKDINTFIHGNKRSIKAICEN-
 KNGNPHRENLRISKSSFQVTTCKLHGGSPWPPCQYRATAGFRNVVACENGLPVHLDQS
 IFRPVENLYFQGGSGSGSGSGMSGLNDIFEAQKIEWHEG

mAng

MQDDSRYTFLTQHDAKPKGRDDRYCERMMKRRSLTSPCKDVNTFIHGNKSNKAIC-
 GANGSPYRENLRMSKSPFQVTTCKHTGGSPRPPCQYRASAGFRHVVIACENGLPVHFD
 ESFFSLENLYFQGGSGSGSGSGMSGLNDIFEAQKIEWHEG

FIGURE 4.2: Design schematic for tagged ribonuclease constructs. The 5' and 3' end of the constructs are 30-bp overlaps with the pET22b vector. Genes encoding each of the four ribonucleases were inserted between these overlaps, with a TEV protease cleavage site appended to the C-terminus of the enzyme, a glycine-serine linker, and a terminal Avitag appended before the stop codon. The respective amino acid sequences for each ribonuclease construct are shown, with construct features highlighted.

chromatography (Figure 4.3, panel A). Identity of the ptRNases was confirmed with MALDI–TOF mass spectrometry, which yielded molecular masses consistent with the expected protein mass after peptide tag addition. With the C-terminal peptide tag, observed masses were 18136 Da for hRNase 1, 17571 Da for mRNase 1, 17699 Da for hAng, and 17319 Da for mAng (Table 4.2).

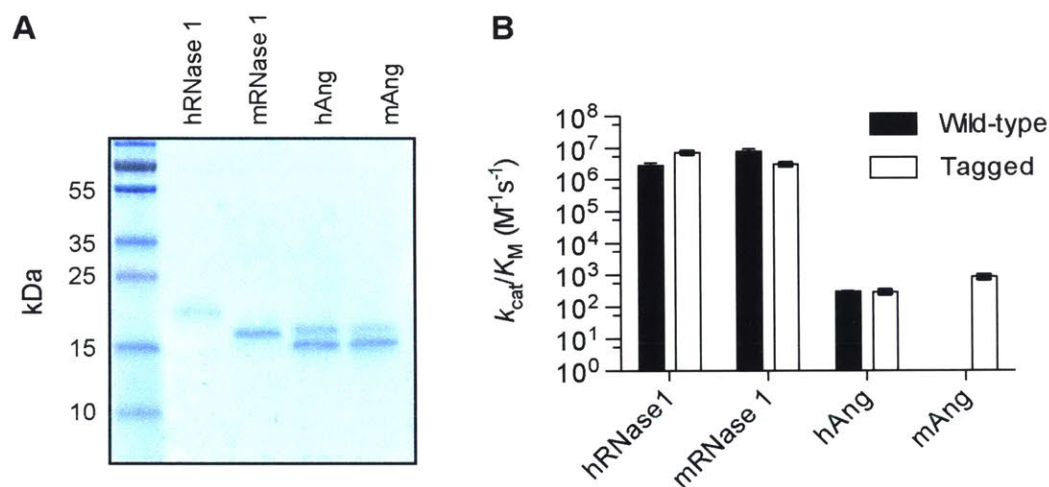


FIGURE 4.3. **Tagged ribonucleases are readily purified and retain activity.** A, Gel showing migration and banding pattern of purified tagged RNases. Coomassie stain was used to visualize protein bands. B, Graph of ribonucleolytic activity of wild-type and tagged ptRNases. Wild-type activity values are from published sources for hRNase 1 (175), mRNase 1 (175), and hAng (239). Tagged activity values were determined experimentally under conditions identical to those published, $n \geq 4$.

Table 4.2. **Molecular weights of tagged ribonucleases.**

Protein	c-Avitag protein		Biotinylated c-Avitag protein	
	Calculated MW (Da)	Observed MW (Da)	Calculated MW (Da)	Observed MW (Da)
hRNase 1	18133	18136	18359	18350
mRNase 1	17577	17571	17803	17805
hAng	17701	17699	17927	17923
mAng	17325	17319	17551	17547

Tagged ptRNases were determined to be properly folded based on the retention of wild-type ribonucleolytic activity. The respective values were $(7.5 \pm 1.8) \times 10^6 \text{ M}^{-1}\text{s}^{-1}$ for tagged hRNase 1 and $(3.2 \pm 0.8) \times 10^6 \text{ M}^{-1}\text{s}^{-1}$ for tagged mRNase 1 (Figure 4.3, panel B), relative to the previously published values of $(3 \pm 1) \times 10^6 \text{ M}^{-1}\text{s}^{-1}$ for wild-type hRNase 1 and $(8 \pm 3) \times 10^6 \text{ M}^{-1}\text{s}^{-1}$ for wild-type mRNase 1 (175). Human and murine angiogenin also exhibited similar activity to wild-type enzymes. Respective values were $(2.9 \pm 1) \times 10^2 \text{ M}^{-1}\text{s}^{-1}$ for tagged hAng and $(8.6 \pm 3) \times 10^2 \text{ M}^{-1}\text{s}^{-1}$ for tagged mAng (Figure 4.3, panel B), relative to previously published activity of $(3.1 \pm 0.1) \times 10^2 \text{ M}^{-1}\text{s}^{-1}$ for wild-type hAng (239).

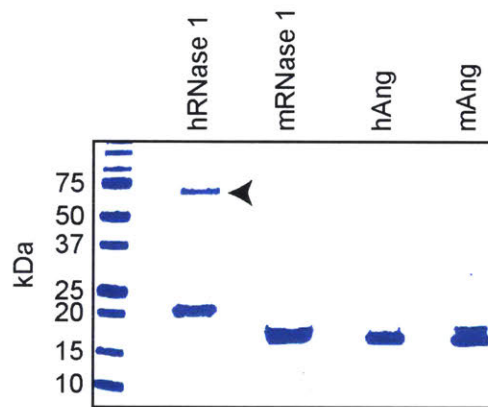


FIGURE 4.4. **Gel showing purity of biotinylated ribonucleases.** Protein bands were visualized by using Coomassie staining. Residual MBP-BirA is present in the hRNase 1 lane, and is marked by a black arrowhead.

4.4.3: Tagged ptRNases are successfully biotinylated, and the tag successfully cleaved—

Biotinylation reactions were carried out on tagged ptRNases, and the resultant proteins tested for successful biotin incorporation. Purity of tagged, biotinylated ptRNases was high after column chromatography (Figure 4.4). Biotinylation was verified with MALDI-TOF mass spectrometry,

revealing an average mass shift of 225 Da. With biotin, observed masses were 18350 Da for hRNase 1, 17805 Da for mRNase 1, 17923 Da for hAng, and 17547 Da for mAng (Table 4.2).

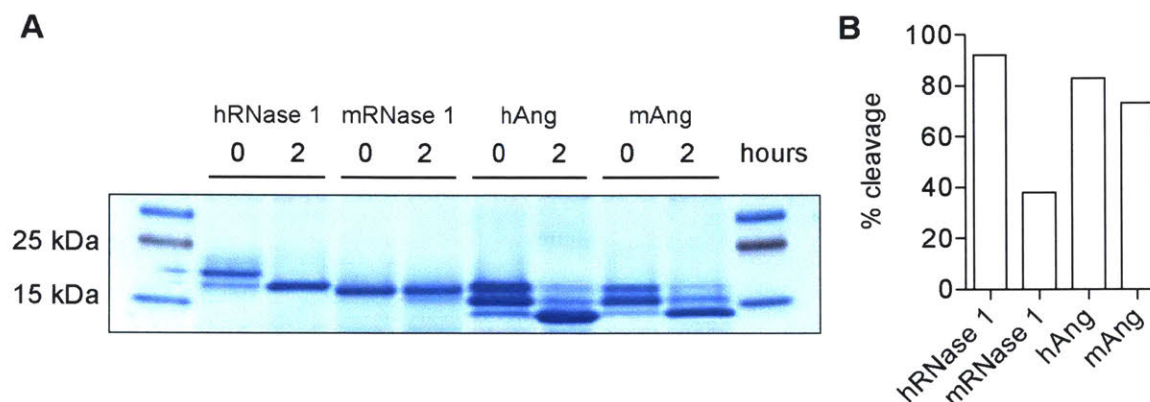


FIGURE 4.5. **TEV protease cleaves the C-terminal peptide tag of ribonucleases.** A, Gel showing mobility shift of RNases after 0 or 2 hours of treatment with TEV protease. B, Graph showing quantitation of protein cleavage by TEV protease from Panel A.

TEV protease cleavage assay was carried out to verify successful cleavage of the protein tag, which is critical for the recovery of tightly bound F(ab)s after affinity chromatography while excluding recovery of anti-biotin F(ab)s. The tag was cleaved from all ptRNases after 2 hours as demonstrated by a shift in protein mobility by SDS-PAGE (Figure 4.5).

4.4.4: mRNase 1 is successfully acetylated—Acetylation of mRNase 1 was carried out as a pilot study to determine whether masking of positive charges on the protein would yield greater specificity of antibody binding. The reaction of acetic anhydride with lysine residues resulted in successful addition of five to eight acetyl groups to mRNase 1 (Figure 4.6).

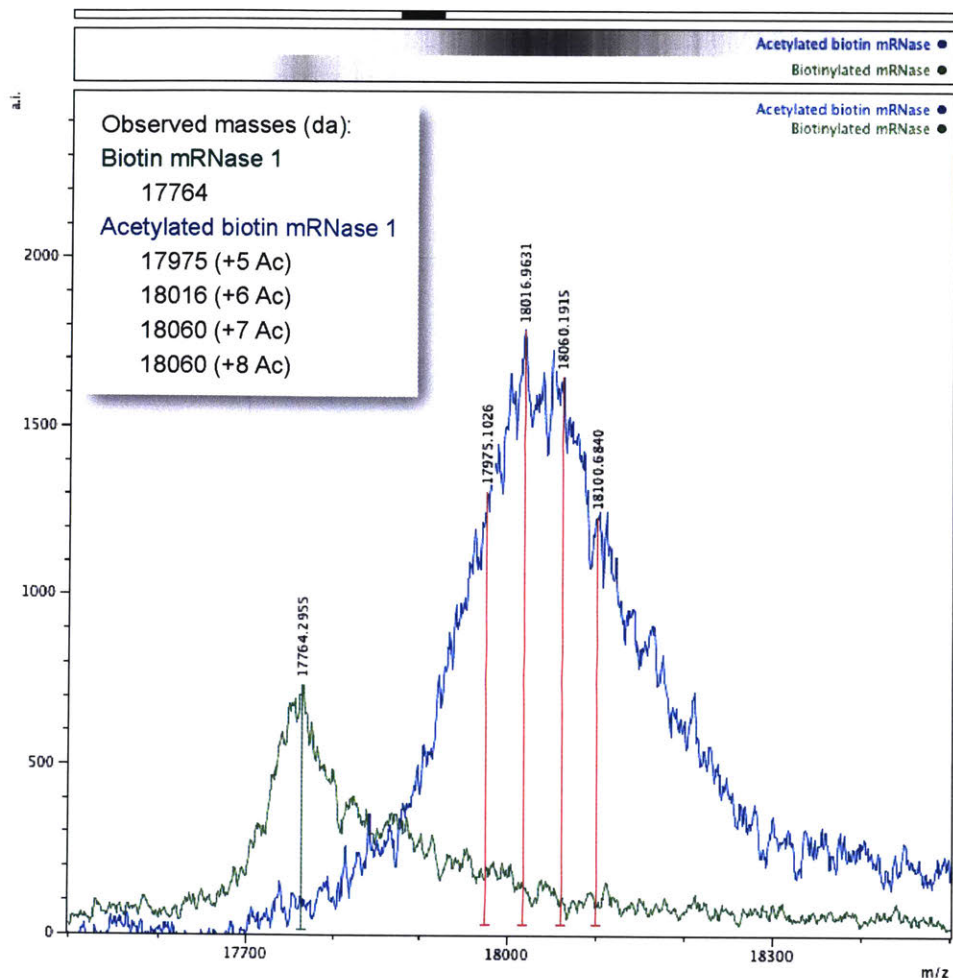


FIGURE 4.6. **Mass spectrum of mRNase 1 acetylation.** The mass spectra of pre- and post-acetylation biotinylated mRNase 1 were collected. Based on an expected mass shift of 42 da with acetylation, our procedure added 5-8 acetyl groups per protein.

4.5 Discussion

In this study, we have generated a set of four ptRNases (human RNase 1, human angiogenin, murine RNase 1, and murine angiogenin) by heterologous expression to be used for antibody generation via antibody phage display. These proteins are of expected molecular mass and retain ribonucleolytic activity, indicating successful production of tagged protein that is likely folded in a manner similar to that of each wild-type enzyme. Further, the tag is cleavable by TEV protease

and accepts biotin as expected, indicating the suitability of these proteins for use in the antibody phage display system.

The goal of this study, to generate specific anti-ptRNase antibodies, is motivated by the cross-reactivity of commercially-available anti-ptRNase antibodies. Other studies have shown that antibodies against RNase 1 cross-react with RNases 2 and 3 (229). This cross-reactivity makes reliance on antibodies to study ptRNases in the murine system particularly difficult given that gene duplication events have vastly increased the number of paralogous enzymes expressed in mice. Our studies in probing the biological activity of RNase 1 have therefore been limited to non-immunological methods. We anticipate the generation of specific antibodies would enable new directions in biological research on ptRNases, and could lead to similar advances in the study of other protein families where gene duplication has led to close similarity among paralogs.

Another goal of this study is to generate specific antibodies to closely-related homologous proteins. Many commercially-available antibodies cross-react between proteins from different species, this cross-reactivity is apparent with RNase 1 (Figure 4.7). Species-specific antibodies are useful for many applications, especially in evaluation of multi-species co-culture cell systems (245) and in pathogen identification (246), and facile generation of these antibodies would allow advances in both research and medical diagnostics.

The phage display workflow subsequent to the protein production and characterization reported here is in progress. Initial efforts to generate specific antibodies have found that the cationicity of ptRNases engenders a large number of nonspecific Coulombic interactions; indeed, previously reported data indicates greater success in antibody selection for proteins with $pI < 8$ (247). This finding highlights one shortcoming of the phage display technique that must be overcome for general applicability of this workflow for other targets. An approach to combat this problem could be to acetylate lysine residues of ptRNases (human RNase 1 has nine lysine residues, angiogenin has seven), thus masking their positive charge and reducing opportunity for nonspecific interactions. Acetylation with acetic anhydride is a facile method to acetylate protein (248), and our pilot experiment with mRNase 1 reveals that five to eight of the nine lysine residues are successfully modified (Figure 4.6). The charge of wild-type mRNase 1 at physiological pH is +4 (175), so the acetylation yields a slightly anionic character and could result in better success with phage display. This workflow could, however, result in the generation of antibodies that recognize the acetylated lysines, so careful re-screening with wild-type proteins would need to be carried out to ensure that recognition of natural epitopes is preserved.

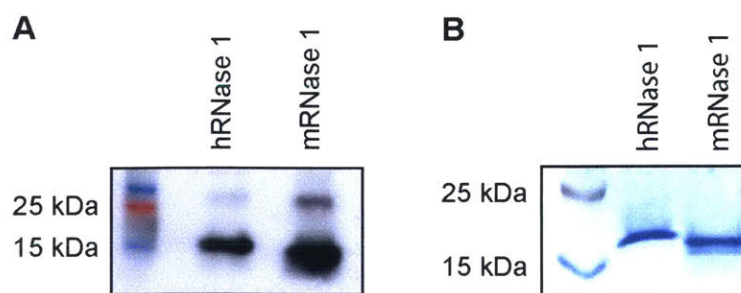


FIGURE 4.7. Reactivity of an anti-RNase 1 antibody across species. *A*, Immunoblot showing reactivity of anti-RNase 1 primary antibody (Santa Cruz) against recombinant RNase 1 of human and murine origin. *B*, Gel showing loading control of the same samples as in Panel *A*, using Coomassie stain to visualize protein bands.

Chapter 5

Conclusions and future directions

5.1 Conclusions

The field of pancreatic-type ribonuclease superfamily biology has exploded in the past 30 years, leading to a renaissance of understanding of the roles of these vertebrate-specific enzymes.

Ongoing research suggests that these proteins could play central roles in the pathogenesis or treatment of a variety of conditions, ranging from neurodegeneration (135) to blood coagulation (79) to cancer (73,249,250). Yet, many unanswered questions remain regarding the physiological function of ptRNases, and new tools to probe ptRNase biology are needed. The primary goal of this thesis was to illuminate unappreciated physiological roles for two members of the ptRNase superfamily that have been well-studied *in vitro*: RNase 1 and angiogenin.

In Chapter 2, I describe the finding that RNase 1 is a modulator of blood coagulation in mice, using a novel *Rnase1* knockout mouse line that was generated in our laboratory. Previous studies demonstrated that eRNA is an activator of coagulation proteases *in vitro* and *in vivo* (79,81), and suggested that RNase 1 could block this activity. My studies confirm this hypothesis in the context of a whole organism, demonstrating that loss of RNase 1 results in accumulation of eRNA and activation of coagulation factors FXI and FXII. Interestingly, coagulopathies are commonly comorbid with other disease states in which eRNA and RNase 1 have been suggested to play a role, such as cancer and infectious disease (197,251). This correlation suggests that blood coagulation likely represents only one of a number of linked biological processes modulated by RNase 1.

In Chapter 3, I identify that angiogenin exhibits a pro-survival function in embryonic development and reproduction through characterization of an *Ang1* knockout mouse. Angiogenin

has long been studied as a pro-proliferative and pro-survival signaling protein in the context of cancer (122,249,252) and amyotrophic lateral sclerosis (98,124), but in addition, it is known to participate in vasculogenesis in the ovary (114,253) and placenta (119). I observed no homozygous *Ang1* knockouts in breeding experiments, and found that the fertility of *Ang1* heterozygotes was significantly reduced, resulting in frequent litter loss. This loss of fertility was associated with impaired placental vasculogenesis during embryonic development. This finding underscores the importance of angiogenin in cell growth and survival. The severe impairment of fertility and absence of *Ang* knockouts observed in our studies were not reported in previous publications citing the use of an *Ang* knockout mouse (99,131,201) – but in these publications, no general phenotyping information is reported about the putative *Ang* knockout.

In Chapter 4, I describe efforts to provide new tools for the biological study of RNases through generation of specific antibodies through phage display. The study of ptRNases in biology is made more complicated by the large number of closely-related family members and the high degree of homology shared by proteins across species (25). The ability to differentiate between RNases of different species and between paralogous proteins will open new doors in the visualization of these enzymes and the characterization of their localization and interactome. We successfully generated tagged ptRNases for use in antibody phage display, which are of expected molecular weight and retain wild-type activity, demonstrating that the tag for phage display was successfully incorporated and does not adversely affect protein folding. The process of antibody generation is still ongoing. Difficulties in generating cognate antibodies to our proteins may highlight a limitation of antibody phage display, as ptRNases are highly cationic.

5.2: Future directions

My work demonstrates a new biological role for RNase 1 and highlights the importance of angiogenin for growth and development in an organism. However, other studies have suggested multiple other possible roles for RNase 1 that merit further investigation, and the broad impacts of eRNA-degrading enzymes are still being determined. I propose additional directions in which my work could lead, which would help paint a more complete picture of the biological functions of ptRNases. These experiments include examination of the growth of *Rnase1*^{-/-} mice, investigations of the function of RNase 1 in cancer and inflammatory processes, removing a compensatory ptRNase from *Rnase1*^{-/-} mice to examine the role of eRNA more generally, and characterization of anti-ptRNase antibodies for future biological study.

5.2.1: Roles for RNase 1 in growth—We identified that loss of RNase 1 results in heavier and longer mice. These results, described in Chapter 6, demonstrate that although *Rnase1*^{-/-} mice are larger than wild-type mice, this difference in size and weight is not explained by differences in food or water intake, and is not associated with increased body fat as measured by the weight of two adipose tissue deposits. No obvious explanation for increased body weight and length was observed in our data.

Reports over the last 50 years have shown that RNase 1 is unlikely to act as a digestive enzyme in animals other than ruminants, and accordingly, our data do not show changes in metabolism in *Rnase1*^{-/-} mice. However, emerging literature suggests that the gut microbiome can profoundly impact multiple arenas of health and disease, including body composition (254) and bone growth (255). While RNase 1 is not by itself cytotoxic to bacteria, it does appear to have some effects on immunity. RNase 1 stimulates cytokine production from dendritic cells (256) and has

demonstrated efficacy *in vitro* against a handful of viruses, including tick-borne encephalitis (161), influenza virus, and HIV (162). It is possible that loss of RNase 1 leads to alterations in microbiome composition, which could in turn cause changes in growth. To test this hypothesis, sequencing of the microbiome could be used to compare bacterial populations present in wild-type and *Rnase1*^{-/-} mice. Body composition analysis, such as DEXA, could be used to provide quantitative measurement of body fat and bone density, to which microbiome data could be cross-referenced.

5.2.2: Roles for RNase 1 in cancer—Multiple studies have highlighted the amazing ability of RNase 1 to act as an anti-cancer agent. Whereas wild-type RNase 1 has been reported to exhibit no cytotoxicity against cancer cells (58), RI-evasive engineered variants of the enzyme are currently undergoing clinical trials as alternatives to standard-of-care chemotherapy for cancer patients (60). Yet, recent studies in our laboratory and others have identified that wild-type RNase 1 binds Globo H, a cancer cell antigen (43), might naturally evade RI in the cytosol under conditions of stress and become cytotoxic (24), and degrades inflammatory RNAs in the extracellular environment that would otherwise promote tumor cell growth (73). Cancer cells are also known to secrete a higher amount of eRNA than do normal cells (65,257), which would further drive a tumorigenic environment (258).

Our hypothesis was that loss of RNase 1 could drive tumor growth in mice by permitting the accumulation of a higher eRNA burden. Yet, my characterization of *Rnase1*^{-/-} mice, described in Chapter 2 and Appendix 1, did not reveal differences in the longevity of these mice or the incidence of tumors with age. As with the studies that I performed to characterize blood coagulation in *Rnase1*^{-/-} mice, I propose that the eRNA burden conferred by loss of RNase 1 is

insufficient to be pathogenic. Instead, inducing tumors in the *Rnase1*^{-/-} background, either through chemical or genetic methods, could result in a more aggressive tumor growth phenotype.

5.2.3: Roles for RNase 1 in inflammation—Other inflammatory processes could also be affected by RNase 1. Ribonucleolytic activity has beneficial effects in systemic lupus erythematosus (SLE) (85), as inflammation secondary to activation of toll-like receptor signaling by nucleic acids appears to be important in SLE. Loss of DNase I activity is been associated with SLE (259), and overexpression of RNase A was able to ameliorate inflammatory symptoms in a mouse model of SLE (85). The mouse model used in this study, which overexpresses *Tlr7*, is characterized by increased myeloid cell load, particularly higher B cell burden. These B cells could be activated by macrophages, which are themselves activated by eRNA, a process that has been demonstrated in a rat model of heart transplantation (88).

Atherosclerosis is commonly coincident with SLE (260), and is also mediated by proinflammatory macrophages, which are recruited to the vascular endothelium and adhere there, forming plaques (261). One study has shown that eRNA also mediates this process, accumulating in atherosclerotic plaques and driving the expression of adhesion factors, such as Vcam-1, Icam-1, and P-selectin, on smooth muscle (77).

Although I do find elevated Il-6 gene expression in adipose tissue deposits of *Rnase1*^{-/-} mice, my studies (described in Appendix 1) did not detect significant inflammatory phenotypes with loss of RNase 1. These studies were not exhaustive, however, and broader cytokine panels could reveal changes in factors associated with SLE or atherosclerosis as described above. Studies to

confirm the role of RNase 1 in these systems could be performed using genetic crosses with *ApoE*^{-/-} mice or *Tlr7* knock-in mice.

Unpublished studies from our laboratory have shown that RNase 1 acts in a synergistic manner with the human cathelicidin-related antimicrobial peptide LL37 to kill *E. coli* (262). LL37 is a 37-residue α -helical protein with cationic character, and is secreted from a variety of cell types and found in body fluids (263). It is thought to form pores in microbial membranes, and has demonstrated antimicrobial activity against fungi, virus, and parasites (264). These activities suggest that loss of RNase 1 could reduce the resistance of a host to bacterial infection. Future studies could use an *E. coli* infection model in RNase 1 knockout mice to evaluate the effect of the enzyme on resistance to infection. Mice express a homologous peptide, CRAMP, that is 48% identical to the human peptide (265), meaning that they could serve as a suitable model system for studying this synergism. Alternatively, if human LL37 is specifically required for synergism with RNase 1, a mouse model would offer the opportunity to study the effects of LL37 and RNase 1 on bacterial infection independently as well as together.

5.2.4: Fundamental roles for nonspecific, extracellular ribonucleolytic activity—RNase 1 is one of approximately 22 ptRNases expressed in mice (11). Most of these are restricted in expression in some manner, for example, to the eosinophils, skin, or placenta. Whereas six angiogenin genes are encoded, the ribonucleolytic activity of these enzymes is miniscule in comparison to RNase 1. RNase 4 is, however, a ubiquitously expressed ptRNase present in mice and has activity similar to that of RNase 1 (266). I hypothesize that it is responsible for the residual ribonucleolytic activity observed in the plasma of *Rnase1*^{-/-} mice. Any fundamental need for

degradation of extracellular RNAs is likely compensated for by RNase 4 in our system, which could explain why the phenotype of *Rnase1*^{-/-} mice is relatively mild.

Future studies could elucidate which biological processes broadly require nonspecific, extracellular ribonucleolytic activity by knocking out additional ptRNases, with RNase 4 being a logical first target. Our generation of the RNase 1 knockout mouse, conducted using homologous recombination, could be replicated in a more rapid and facile manner with the use of CRISPR-Cas9 systems. Loss of this secondary major serum ribonuclease could result in more dramatic phenotypes, perhaps related to the cancer, inflammatory, or infectious disease processes discussed above.

5.2.5: Mechanisms of impaired fertility and embryonic development in Ang1^{+/-} mice—As described in Chapter 3, we find that the total loss of *Ang1* is incompatible with embryonic development, and further, that the partial loss of *Ang1* is sufficient to significantly impair fertility. Histopathological studies to identify specific changes that precipitate these phenotypes are underway. Future studies could include immunohistochemical analysis of uteri and embryos to identify zones of angiogenin loss and examine the impact of *Ang1* heterozygosity on other markers of development. These data could corroborate earlier studies demonstrating the presence of angiogenin alongside developing vasculature in the placenta (119) and embryo. Angiogenin is known to be highly expressed in at day E9.5 in mouse embryos, at which time extensive development of the vascular and nervous system occurs (123,267). A conditional knockout of *Ang1* would also be useful for evaluation of the physiological effects of this protein.

Further characterization of the *Ang1*^{+/-} strain used for my studies is also warranted, as the phenotype we observe is different from that reported by another group that generated their own *Ang1*^{-/-} mice (99,131,201). As angiogenin and RNase 4 are expressed from the same promoter (266), and mice express six genes encoding angiogenin proteins (140), the possibility that the more severe phenotype we observe is due to differential gene expression in the two knockout systems. In our case, I have identified that gene expression of *Ang2*, *Ang3*, and *Ang4* are not negatively impacted by the knockout. Gene expression in our *Ang1*^{+/-} strain, however, might be affected by the presence of the LacZ cassette and neomycin resistance cassette present in the mutant allele. A direct comparison of the two lines of *Ang1*^{-/-} mice would be useful.

5.2.6: Characterization of anti-ptRNase antibodies—As described in Chapter 4, generation of specific anti-ptRNase antibodies is underway. When these antibodies are generated, characterization of their binding affinity, selectivity, and applications will need to be performed. Affinity of the antibodies for their cognate ptRNases can be performed by surface plasmon resonance, which can also be used to verify that a single antibody exhibits specific binding to only its cognate ptRNase and not homologous or paralogous proteins. Antibodies should also be tested for their utility in detecting and binding ptRNases in a variety of biochemical techniques, including immunohistochemistry immunoblotting, immunoprecipitation, and ribonucleolytic activity assay. It would be useful to know whether the antibodies recognize only folded protein (as opposed to denatured protein), only recombinant protein (and not protein that has been posttranslationally modified), and whether the antibodies exhibit any inhibitory effect on the activity of ptRNases.

The availability of specific antibodies would be useful for further biological characterization of the roles and localization of ptRNases. Further, if antibodies can bind modified ptRNases, they could be a useful tool for the characterization of novel post-translational modifications identified on native ptRNases. Understanding these modifications could be important for understanding the biology of ptRNases, as they appear to impact ptRNase function: glycosylation of RNase 1 varies between malignant and nonmalignant cells (268), and phosphorylation of angiogenin permits its dissociation from RI (94).

Appendix 1

Evaluation of metabolic and inflammatory phenotypes in *Rnase1*^{-/-} mice.

Contributions: I designed all experiments, performed metabolism cage studies, and analyzed all data. Technical assistance with dissection was provided by R. Sullivan. C. Feldman provided technical assistance with mouse colony management and performed qPCR studies on inflammatory markers.

6.1 Abstract

The earliest biological study of RNase A suggested a role of the enzyme in digestion in ruminants, owing to the high expression of RNase A in the bovine exocrine pancreas, and little to no appreciable function in non-ruminant animals. More recent studies of RNase 1 have called this hypothesis into question, instead suggesting functions in a variety of biological spheres. In initial phenotyping of *Rnase1*^{-/-} mice, we noted these mice are significantly heavier than their wild-type counterparts, an observation that holds true for all age groups. We hypothesized that this difference might be due to changes in metabolism or in body fat accumulation. We probed for possible causes of this difference by measuring a variety of metabolic and inflammatory parameters. Our studies identified no obvious causes of the increased body weight seen in *Rnase1*^{-/-} mice. Future studies could evaluate other possible causes of increased body weight in these mice, such as changes in the gut microbiota or in growth factor signaling.

6.2 Introduction

Our biochemical understanding of the pancreatic-type ribonuclease (ptRNase) superfamily is owed to the high expression and simple purification of the prototypical family member, Ribonuclease A (RNase A), from the pancreas of cows (14). Due to this tissue-of-origin, early biological characterization of RNase A focused on the gut, culminating in the hypothesis that RNase A was a digestive enzyme in ruminants and that its homologs in other species were of little biological relevance (26). Yet, later study found that this proposed role in digestion was not supported; characterization of Ribonuclease 1 (RNase 1 – a homolog of RNase A in humans and other species) failed to find connections to digestion (269), but suggested a variety of other biological roles in immunity (270), cancer (43,73), blood coagulation (79), and inflammation (76,256).

Despite no effects on digestion, RNase 1 could modulate metabolism, as deleterious changes in metabolism are precipitated by inflammation (271). Natural killer T cells and activated T cells are recruited to adipose tissue (272) and tumor necrosis factor- α (TNF α) is expressed constitutively. This process ultimately reduces signaling downstream of insulin receptors and leads to insulin resistance (273).

These processes could be mediated by eRNA, as it has been demonstrated to spur the production of TNF α (76), the polarization of macrophages to an M1 phenotype (258), and the recruitment of macrophages to atherosclerotic plaques (77). In these systems, RNase 1 was found to disrupt the RNA-mediated inflammatory signaling. In other systems, RNase 1 appears to participate in regulation of inflammation – it has been shown to modulate the activity of dendritic cells *in vitro*

(274), and elevated ribonucleolytic activity resulted reduction of inflammation in a mouse model of systemic lupus erythematosus (85).

Our initial characterization of *Rnase1*^{-/-} mice revealed that loss of RNase 1 results in increased body weight of mice relative to wild-type animals, so we sought to characterize the effect of RNase 1 on metabolism in these mice. We found that *Rnase1*^{-/-} mice are larger than *Rnase1*^{+/+} mice, but do not exhibit increased adiposity and do not exhibit obvious perturbations in food or water consumption or metabolism. We also do not detect significant inflammatory phenotypes in *Rnase1*^{-/-} mice.

6.3 Experimental procedures

6.3.1: Materials—Primers were from Integrated DNA Technologies (Coralville, IA).

Equipment—All fluorescence and absorbance measurements were made with a Tecan M1000 fluorescence plate reader, unless stated otherwise.

6.3.2: Body weight and length measurements—All experiments with animals were conducted in accord with an Institution on Animal Care and Use Committee-approved protocol at the University of Wisconsin–Madison. *Rnase1*^{-/-} mice were generated in our laboratory as described previously (Chapter 2). *Rnase1*^{+/+} and *Rnase1*^{-/-} mice were generated by heterozygote crosses and experiments were performed using gender-matched littermates.

Animals were weighed once weekly from weaning age. Growth curves were approximated in Graphpad Prism software using the Gompertz growth model (275) (Equation 6.1). *A* is the

mature weight of mice, B is an integration constant, and k is a growth rate constant. These parameters were fitted in Prism using nonlinear regression.

$$Y = A \cdot e^{-B \cdot e^{-kx}} \quad (6.1)$$

Body length was measured of adult mice (>12 weeks of age) from the base of the tail to the nose when the mouse's body was fully extended. Measurements were repeated in at least triplicate and averaged.

6.3.3: Food and water consumption studies—Food and water intake of mice was measured using wire-bottomed metabolism cages. Animals were acclimated for 48 h prior to data collection. A chow bin and water bottle were weighed at the start and end of a 24 h period for each individual. Urine and feces were also collected and weighed at the end of a 24 h period.

6.3.4: Urinary protein and glucose excretion studies—A Bradford Protein Assay kit (Pierce) was used to measure protein content of urine, according to the manufacturer's instructions. Glucose content of urine was measured using the Infinity Glucose Oxidase Liquid Stable reagent kit (Thermo Scientific), according to the manufacturer's instructions. Briefly, 3 μL of urine was added to 450 μL Infinity reagent, and the resulting solution was mixed and incubated for 5 min at 37 $^{\circ}\text{C}$ before measuring the $A_{500 \text{ nm}}$ of a 200 μL aliquot.

6.3.5: Fecal lipid content studies—Gravimetric analysis was performed to analyze fecal lipid content by mass. In a borosilicate glass tube, 50 mg of feces was homogenized with 2 mL of 2:1

chloroform:methanol (C:M) using a Benchmark D1000 homogenizer. The homogenizer probe was rinsed into the tube using C:M. This homogenate was decanted into a 15-mL conical tube. Residual matter was removed from the homogenizer probe by running the homogenizer in a clean 2-mL tube with a small volume of C:M, and transferring this liquid to the 15-mL tube. Residual matter was removed from the borosilicate tube by the addition of 1 mL C:M, vortexing, and decanting into the 15-mL tube. To this 15-mL tube, 2 mL ddH₂O was added and vortexed, then the tube was subjected to centrifugation at 6000 rpm for 10 min to precipitate solids and separate organic and aqueous phases. A syringe was used to collect the organic layer from the 15-mL conical, and this layer was transferred to a new, weighed glass tube. Solvent was evaporated from this tube in a chemical fume hood with a heat block set at 50 °C, and the mass of the tube with lipid residue was weighed once dry.

6.3.6: Plasma cholesterol measurement—Whole blood was collected by cardiac puncture into citrate-rinsed syringes immediately prior to mixing with 3.2% w/v sodium citrate (citrate/blood 1:9). Blood was subjected to centrifugation at 2400g for 10 min at 4 °C to prepare platelet-poor plasma for subsequent assays. Plasma cholesterol was measured using the Amplex Red Cholesterol Assay kit (Invitrogen) according to the manufacturer's instructions.

6.3.7: Visceral adipose tissue measurement—Visceral adipose tissue mass was estimated by dissection and weighing of two easily identifiable fat deposits in the mouse: the gonadal fat pad, which is associated with the ovaries or testes, and the subcutaneous fat pad. Fat pads were dissected free of surrounding tissue and wet weights measured. Fat pad weights were calculated as a percentage of total body weight.

Table 6.1. Primers used for qPCR.

Target	Forward primer (5'→3')	Reverse primer (3'→5')
<i>Tnfa</i>	CTGATTGCCCGCTTACAGT	GAAAGAAGCCGTGGGTTGGA
<i>Il6</i>	AGACAAAGCCAGAGTCCTTCA	CACTGCATGAGAGATGGGGAA
<i>Il10</i>	AAAGGGGGCGAGTGTAACAA	GCAGAGGAGGTCACACCATT
<i>Ifng</i>	CCATCAGCAACAACATAAGCGT	GCAATGCCGTCTCACCTCAA
<i>Gapdh</i>	CTCCCACTCTTCCACCTTCG	CCACCACCCTGTTGCTGTAG
<i>Rpl13a</i>	GCTGAAGCCTACCAGAAAGT	TCCGTTTCTCCTCCAGAGT
<i>Hprt1</i>	CTAGTCCTGTGGCCATCTGC	GGGACGCAGCAACTGACATT
<i>Ccl2</i>	CCCAATGAGTAGGCTGGAGA	TCTGGACCCATTCTTCTTG

6.3.8: *Quantitative PCR*—Quantitative real-time PCR (qPCR) was conducted to identify gene expression changes in *Rnase1^{-/-}* mice. Adipose tissue from the gonadal fat pad and the buffy coat layer appearing after initial centrifugation of whole blood were used for these experiments. RNA was isolated from tissue samples that were homogenized in TriZOL Reagent (Invitrogen) using a Benchmark D1000 homogenizer, purified according to the manufacturer’s protocol, DNase-treated using the TURBO DNA-free kit (Ambion), and subjected to reverse transcription-PCR using the qScript cDNA Synthesis kit (Quanta Biosciences). The resultant cDNA was probed for expression of *Tnfa*, *Ifng*, *Il6*, and *Ccl2* using primer pairs shown in Table 6.1. Reactions were run in duplicate using SYBR Green master mix (Quanta Biosciences) on an Applied Biosystems ABI 7500 Fast Real-Time PCR system. Cycling conditions were 95 °C for 30 s, 55 °C for 30 s, and 72 °C for 30 s, and were repeated for 30 cycles and followed by melt curve analysis. Threshold cycle values were determined by setting a constant threshold at 0.6, and fold changes in gene expression were determined by the comparative C_T method (172). Expression was normalized to the geometric mean of *Gapdh*, *Rpl13a*, and *Hprt1*.

3.3.9: *Statistical analyses*—A minimum of three biological replicates were performed for every experiment. All data are expressed as the mean \pm SEM, and statistical evaluation was performed by Wilcoxon rank-sum test in GraphPad Prism and Mstat software, with $p < 0.05$ being considered significant.

6.4 Results

6.4.1: *Rnase1^{-/-} mice are heavier and larger than Rnase1^{+/+} mice*—Mice were weighed weekly as part of initial phenotyping efforts to characterize *Rnase1^{-/-}* mice. We identified *Rnase1^{-/-}* mice as being heavier than their *Rnase1^{+/+}* littermates, with mature male *Rnase1^{-/-}* mice weighing (40.3 ± 0.5) g and *Rnase1^{+/+}* mice (37.9 ± 0.8) g, and mature female *Rnase1^{-/-}* mice weighing (29.5 ± 0.4) g and *Rnase1^{+/+}* mice (23.0 ± 0.3) g (Figure 6.1, panel A). This trend was evident as early as eight weeks of age, at which time the difference in weight is statistically significant (Figure 6.1, panel B).

Body length of mice was also measured to address whether increased body mass was due to larger size. Measurements of adult mice showed that *Rnase1^{-/-}* mice do have significantly longer bodies than do *Rnase1^{+/+}* mice (10.8 ± 0.2 cm versus 10.3 ± 0.2 cm). Yet, when comparing mouse body weight to body length, *Rnase1^{-/-}* mice are not significantly heavier per cm of body length than are *Rnase1^{+/+}* mice (Figure 6.1, panel C).

6.4.2: *Rnase1^{-/-} mice are metabolically similar to Rnase1^{+/+} mice*—Metabolism cage studies were carried out to assess differences in feeding and excretion in *Rnase1^{-/-}* mice and *Rnase1^{+/+}*

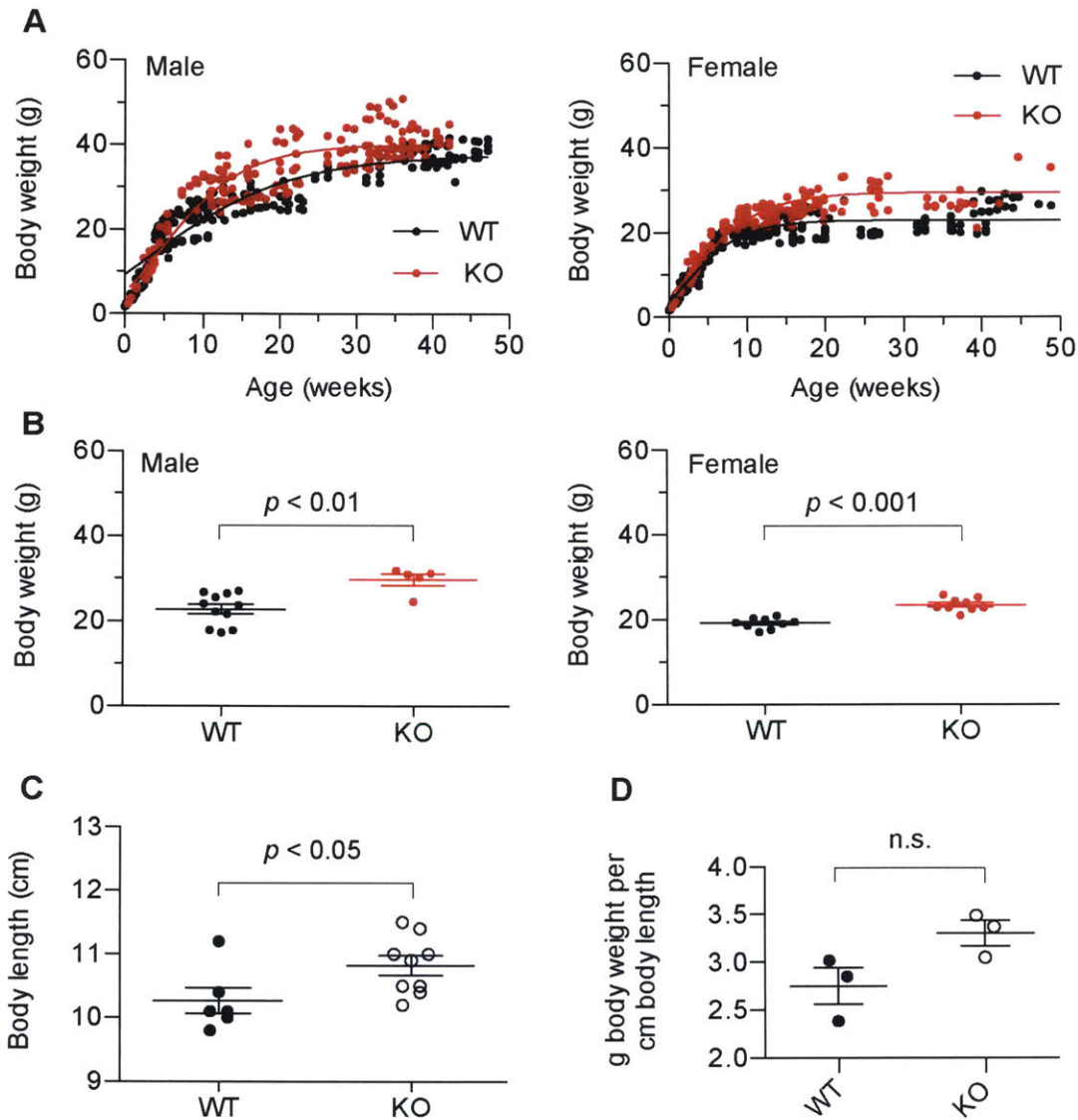


FIGURE 6.1. **Effect of *Rnase1* on mouse body weight and length.** A, Graphs showing the weekly weight of male and female *Rnase1*^{-/-} and *Rnase1*^{+/+} mice, $n \geq 5$. B, Graphs of body weight at 8 weeks of age for male and female mice. C, Graph of body length (nose to base of tail) of mature mice, both sexes. D, Graph of body weight to length ratio, calculated using body weight at the time of body length measurement.

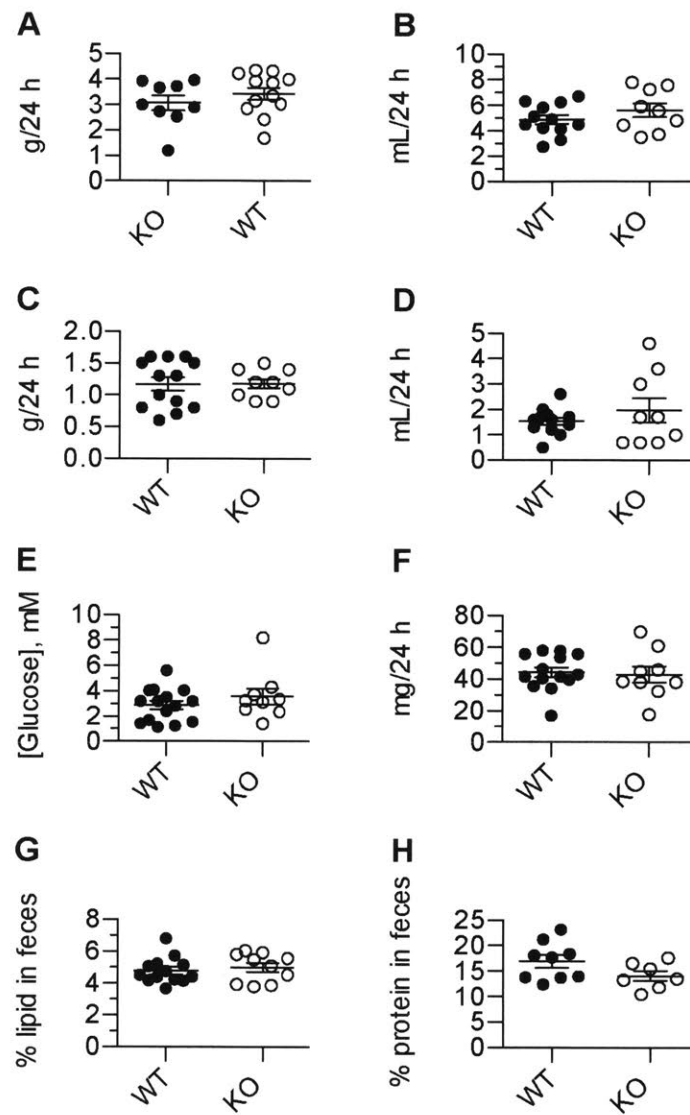


FIGURE 6.2. Effect of *Rnase1* on consumption and metabolism. $n \geq 7$ for all panels. *A*, Graph of food consumption over 24 hours. *B*, Graph of water consumption over 24 hours. *C*, Graph of feces excretion over 24 hours. *D*, Graph of urine excretion over 24 hours. *E*, Graph of urinary glucose concentration from 24-hour collection. *F*, Graph of urinary protein concentration from 24-hour collection, total protein measured by BCA. *G*, Graph of fecal lipid content from 24-hour collection, measured gravimetrically and expressed as % lipid by weight. *H*, Graph of fecal protein content, measured from homogenate by BCA and expressed as % protein by weight.

mice. After a 48-hour acclimation period, there were no differences in food consumption, water consumption, or excretion of urine or feces by genotype (Figure 6.2, panels A-D).

Assays were conducted to analyze protein and glucose content of urine, as well as protein and lipid content of feces. These assays did not reveal differences between *Rnase1*^{-/-} and *Rnase1*^{+/+} mice (Figure 6.2, panels E-H).

6.4.3: Rnase1^{-/-} mice do not exhibit elevated plasma cholesterol or increased body fat—Plasma cholesterol was assayed in *Rnase1*^{-/-} and *Rnase1*^{+/+} mice as an additional measure of lipid metabolism. This did not reveal differences by genotype (Figure 6.3, panels A and B).

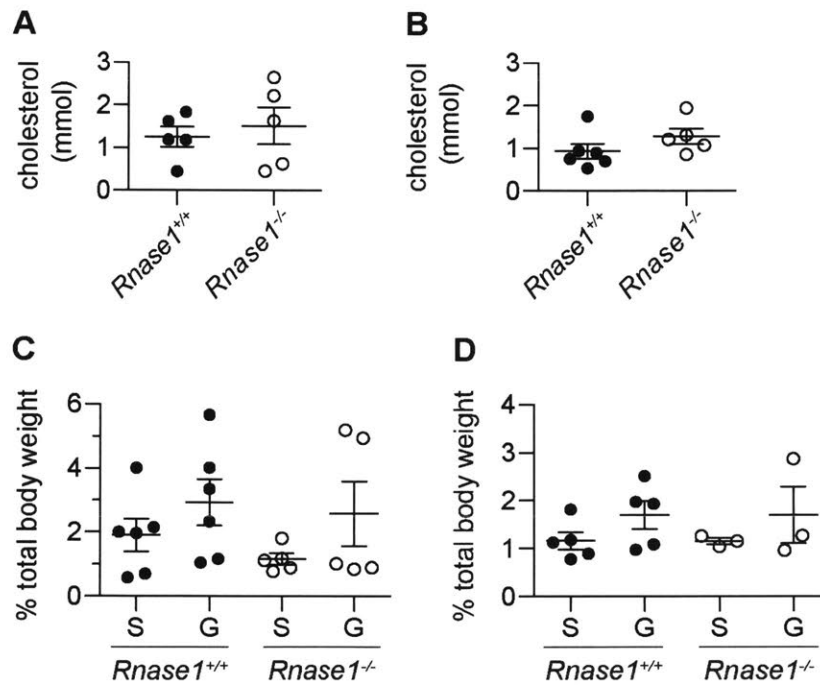


FIGURE 6.3. Effect of *Rnase1* on plasma lipids and body fat. A, Graph showing plasma cholesterol in male *Rnase1*^{+/+} and *Rnase1*^{-/-} mice. *n* = 5. B, Graph as in panel A, but with female mice. *n* = 5. C, Graph showing percentage of total body weight comprised by subcutaneous (S) and gonadal (G) fat pads in male *Rnase1*^{+/+} and *Rnase1*^{-/-} mice. *n* ≥ 4. D, Graph as in panel C, but with female mice. *n* ≥ 3.

Body composition of mice was estimated by dissection and weighing of two easily identifiable fat pads, the gonadal fat pad in the abdominal cavity and the subcutaneous inguinal fat pad. *Rnase1^{-/-}* mice, regardless of sex, did not have larger adipose tissue depots than *Rnase1^{+/+}* mice in either location (Figure 6.3, panels C and D).

6.4.4: Rnase1^{-/-} mice do not have altered inflammatory factor expression relative to Rnase1^{+/+} mice—Gene expression of *Tnfa*, *Il6*, *Il10*, and *Ifng* was assayed in cells from the buffy coat and the gonadal fat pad to compare inflammatory markers between *Rnase1^{-/-}* and *Rnase1^{+/+}* tissue. Although trends towards increased gene expression of *Ifng*, *Il6*, and *Il10* in *Rnase1^{-/-}* mice exist relative to *Rnase1^{+/+}* mice, we did not detect statistically significant effects of genotype for any of the genes tested in buffy coat. Testing of adipose tissue gene expression revealed a trend towards decreased expression of *Tnfa* and significantly elevated *Il6* expression in *Rnase1^{-/-}* mice relative to *Rnase1^{+/+}* mice, but no other significant differences were detected (Figure 6.4).

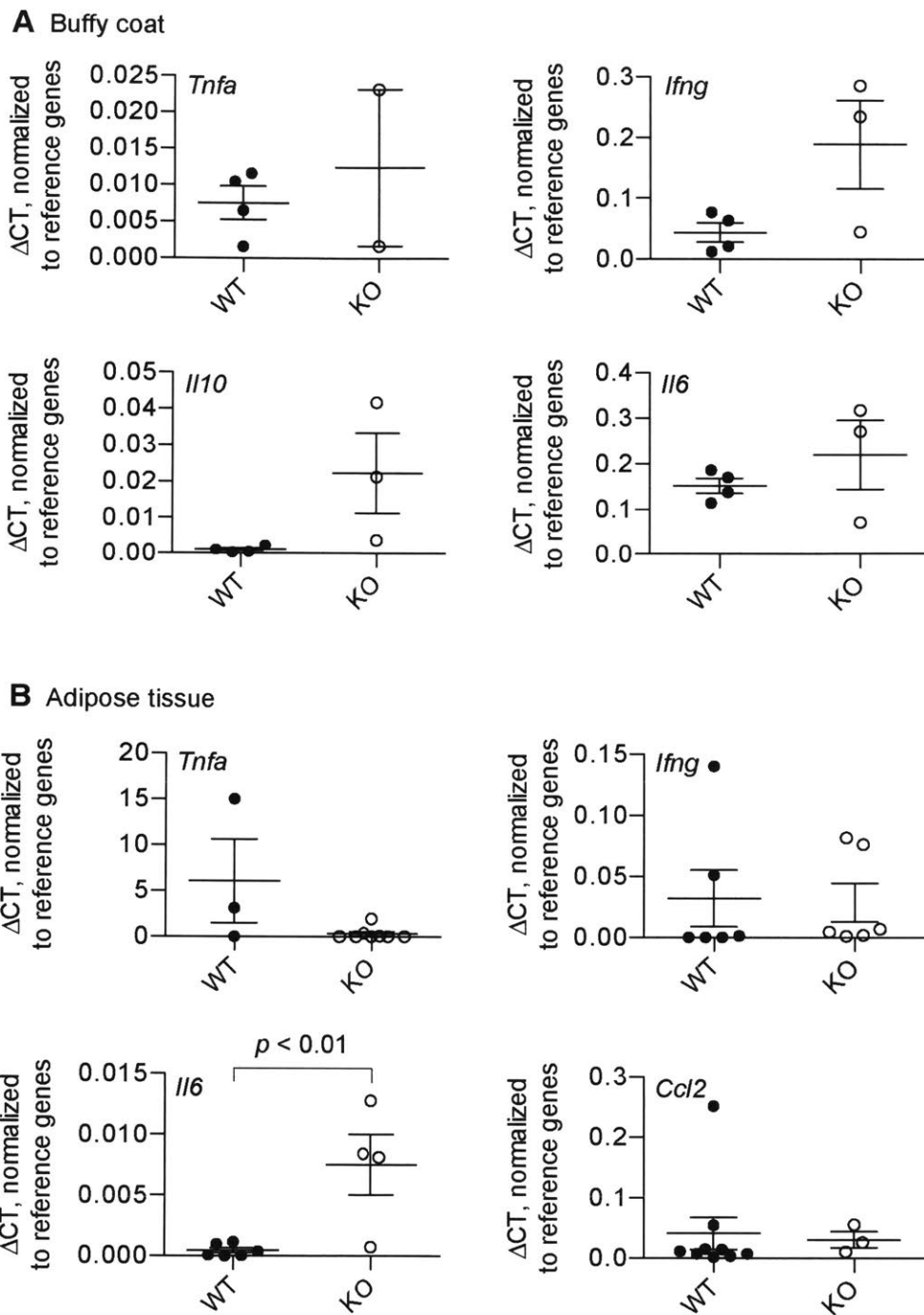


FIGURE 6.4. Effect of *Rnase1* on gene expression of inflammatory markers. A, Graphs of buffy coat expression of *Tnfa* (Tumor necrosis factor α), *Ifng* (Interferon γ), *Il10* (Interleukin 10) and *Il6* (Interleukin 6). Data were normalized to three reference genes, $n \geq 3$. B, Graphs of adipose tissue inflammatory expression as in panel A. *Ccl2* encodes for monocyte chemoattractant protein 1 (MCP1). Data were normalized to three reference genes, $n \geq 3$.

6.5 Discussion

The earliest hypothesis regarding the biological function of RNase 1 was that it serves as a digestive function in ruminants. We characterized *Rnase1*^{-/-} mice and identified that loss of RNase 1 results in increased body weight in mice. As such, we thought it prudent to evaluate murine metabolic markers to evaluate this hypothesis in context of our model system. Our experiments show that *Rnase1*^{-/-} mice are metabolically similar to *Rnase1*^{+/+} mice. As more contemporary research has suggested other roles for RNase 1 in inflammation, immunity, and blood coagulation, this result is unsurprising.

Our studies were not exhaustive in evaluating metabolism. We did not evaluate metabolism on the level of energy expenditure by measuring respiration. A timed glucose-tolerance test was not performed, and weights of two fat pads were used as a proxy for evaluating body composition in place of DEXA or more comprehensive dissection. However, the degree to which *Rnase1*^{-/-} mice were heavier than *Rnase1*^{+/+} was mild (Figure 6.1), and not comparable to mouse models of obesity such as the Ob/Ob mouse, with respective plateau weights (40.3 ± 0.5) g and ~55 g for males (276). Additionally, a veterinary pathologist was unable to distinguish between genotypes based on dissection of *Rnase1*^{-/-} and *Rnase1*^{+/+} mice (data not shown). Further experiments could identify metabolic changes that were not observed in our studies, but the metabolism of these mice appears to be essentially that of wild-type animals, and no literature on the functions of RNase 1 refers to effects on metabolism or growth.

One area that could merit study is the effect of *Rnase1* on the microbiome. RNase 1 and other members of the secreted ribonuclease superfamily have been referenced in the literature as

natural antimicrobial and immune-active agents (133,270), with the potential to kill a variety of pathogenic bacterial targets (277-279). It is possible that RNase 1 could also affect commensal bacterial populations in the gut. This effect could be important in the murine system, as the optimal pH for murine RNase 1 activity is more acidic than that of human RNase 1 (6.4 versus 7.3) (175). Given that the balance of microbiota in the gut has been demonstrated to play a major role in body weight and disease (280,281), it is possible that perturbation of gut flora by the absence of RNase 1 could have caused weight gain in *Rnase1*^{-/-} mice.

Another possibility to explain weight gain in *Rnase1*^{-/-} mice could be in the roles ascribed to RNase 1 as an anti-inflammatory agent, which the enzyme is reported to mediate via degradation of pro-inflammatory extracellular RNAs (73,76) and modulation of dendritic cell activity (274). We probed for this phenotype by evaluating gene expression of several inflammatory markers. Our experiments did not reveal significant differences in the gene expression of *Tnfa*, *Il6*, *Il10*, or *Ifng* in the buffy coat, and only indicated a significant elevation of *Il6* in adipose tissue (Figure 6.4, panel B). IL-6 expression has been demonstrated to be upregulated in adipose tissue with obesity (282) and in monocytes in response to extracellular RNA exposure (258), and *Rnase1*^{-/-} mice do exhibit elevated eRNA levels in plasma. Yet, significant inflammation and adiposity were not detected in *Rnase1*^{-/-} mice. Our findings could reflect minor, non-pathogenic, inflammation with the loss of RNase 1.

References

1. Reijns, M. A., Rabe, B., Rigby, R. E., Mill, P., Astell, K. R., Lettice, L. A., Boyle, S., Leitch, A., Keighren, M., Kilanowski, F., Devenney, P. S., Sexton, D., Grimes, G., Holt, I. J., Hill, R. E., Taylor, M. S., Lawson, K. A., Dorin, J. R., and Jackson, A. P. (2012) Enzymatic removal of ribonucleotides from DNA is essential for mammalian genome integrity and development. *Cell* **149**, 1008-1022
2. Altman, S. (2011) Ribonuclease P. *Philos Trans R Soc Lond B Biol Sci* **366**, 2936-2941
3. Bernstein, E., Kim, S. Y., Carmell, M. A., Murchison, E. P., Alcorn, H., Li, M. Z., Mills, A. A., Elledge, S. J., Anderson, K. V., and Hannon, G. J. (2003) Dicer is essential for mouse development. *Nat Genet* **35**, 215-217
4. Wang, Y., Medvid, R., Melton, C., Jaenisch, R., and Blelloch, R. (2007) DGCR8 is essential for microRNA biogenesis and silencing of embryonic stem cell self-renewal. *Nat Genet* **39**, 380-385
5. Hirs, C., Moore, S., and Stein, W. H. (1960) The sequence of the amino acid residues in performic acid-oxidized ribonuclease. *J Biol Chem* **235**, 633-647
6. Herries, D. G., Mathias, A. P., and Rabin, B. R. (1962) The active site and mechanism of action of bovine pancreatic ribonuclease. 3. The pH-dependence of the kinetic parameters for the hydrolysis of cytidine 2',3'-phosphate. *Biochem J* **85**, 127-134
7. Avey, H. P., Boles, M. O., Carlisle, C. H., Evans, S. A., Morris, S. J., Palmer, R. A., Woolhouse, B. A., and Shall, S. (1967) Structure of ribonuclease. *Nature* **213**, 557-562
8. Anfinsen, C. B. (1973) Principles that govern the folding of protein chains. *Science* **181**, 223-230
9. Moore, S., and Stein, W. H. (1973) Chemical structures of pancreatic ribonuclease and deoxyribonuclease. *Science* **180**, 458-464
10. Merrifield, R. B. (1986) Solid phase synthesis. *Science* **232**, 341-348
11. Cho, S., Beintema, J. J., and Zhang, J. (2005) The ribonuclease A superfamily of mammals and birds: identifying new members and tracing evolutionary histories. *Genomics* **85**, 208-220
12. Zhang, J., Dyer, K. D., and Rosenberg, H. F. (2002) RNase 8, a novel RNase A superfamily ribonuclease expressed uniquely in placenta. *Nucleic Acids Res* **30**, 1169-1175
13. Baker, N. A., Sept, D., Joseph, S., Holst, M. J., and McCammon, J. A. (2001) Electrostatics of nanosystems: Application to microtubules and the ribosome. *Proc Natl Acad Sci* **98**, 10037-10041
14. Raines, R. T. (1998) Ribonuclease A. *Chem Rev* **98**, 1045-1066
15. Sorrentino, S., and Libonati, M. (1994) Human pancreatic-type and nonpancreatic-type ribonucleases: a direct side-by-side comparison of their catalytic properties. *Arch Biochem Biophys* **312**, 340-348
16. Klink, T. A., Woycechowsky, K. J., Taylor, K. M., and Raines, R. T. (2000) Contribution of disulfide bonds to the conformational stability and catalytic activity of ribonuclease A. *Eur J Biochem* **267**, 566-572
17. Lomax, J. E., Bianchetti, C. M., Chang, A., Phillips, G. N., Jr., Fox, B. G., and Raines, R. T. (2014) Functional evolution of ribonuclease inhibitor: insights from birds and reptiles. *Journal of molecular biology* **426**, 3041-3056
18. Lee, F. S., and Vallee, B. L. (1993) Structure and action of mammalian ribonuclease (angiogenin) inhibitor. *Prog Nucleic Acid Res Mol Biol* **44**, 1-30
19. Kobe, B., and Deisenhofer, J. (1993) Crystal structure of porcine ribonuclease inhibitor, a protein with leucine-rich repeats. *Nature* **366**, 751-756
20. Johnson, R. J., McCoy, J. G., Bingman, C. A., Phillips, G. N., Jr., and Raines, R. T. (2007) Inhibition of human pancreatic ribonuclease by the human ribonuclease inhibitor protein. *J Mol Biol* **368**, 434-449
21. Lee, F. S., Shapiro, R., and Vallee, B. L. (1989) Tight-binding inhibition of angiogenin and ribonuclease A by placental ribonuclease inhibitor. *Biochemistry* **28**, 225-230

22. Spencer, J. D., Schwaderer, A. L., Eichler, T., Wang, H., Kline, J., Justice, S. S., Cohen, D. M., and Hains, D. S. (2014) An endogenous ribonuclease inhibitor regulates the antimicrobial activity of ribonuclease 7 in the human urinary tract. *Kidney Int* **85**, 1179-1191
23. Domachowske, J. B., Dyer, K. D., Adams, A. G., Leto, T. L., and Rosenberg, H. F. (1998) Eosinophil cationic protein/RNase 3 is another RNase A-family ribonuclease with direct antiviral activity. *Nucleic Acids Res* **26**, 3358-3363
24. Thomas, S. P., Kim, E., Kim, J.-S., and Raines, R. T. (2016) Knockout of the ribonuclease inhibitor gene leaves human cells vulnerable to secretory ribonucleases. *Biochemistry* **55**, 6359-6362
25. Sorrentino, S. (2010) The eight human “canonical” ribonucleases: Molecular diversity, catalytic properties, and special biological actions of the enzyme proteins. *FEBS Lett* **584**, 2194-2200
26. Barnard, E. A. (1969) Biological function of pancreatic ribonuclease. *Nature* **221**, 340-344
27. Domachowske, J. B., Dyer, K. D., Bonville, C. A., and Rosenberg, H. F. (1998) Recombinant human eosinophil-derived neurotoxin/RNase 2 functions as an effective antiviral agent against respiratory syncytial virus. *J Infect Dis* **177**, 1458-1464
28. Lehrer, R. I., Szklarek, D., Barton, A., Ganz, T., Hamann, K. J., and Gleich, G. J. (1989) Antibacterial properties of eosinophil major basic protein and eosinophil cationic protein. *The Journal of Immunology* **142**, 4428-4434
29. Ackerman, S. J., Gleich, G. J., Loegering, D. A., Richardson, B. A., and Butterworth, A. E. (1985) Comparative toxicity of purified human eosinophil granule cationic proteins for schistosomula of *Schistosoma mansoni*. *Am J Trop Med Hyg* **34**, 735-745
30. Molina, H. A., Kierszenbaum, F., Hamann, K. J., and Gleich, G. J. (1988) Toxic effects produced or mediated by human eosinophil granule components on *Trypanosoma cruzi*. *Am J Trop Med Hyg* **38**, 327-334
31. Harder, J., and Schroder, J. M. (2002) RNase 7, a novel innate immune defense antimicrobial protein of healthy human skin. *J Biol Chem* **277**, 46779-46784
32. Krutskikh, A., Poliandri, A., Cabrera-Sharp, V., Dacheux, J. L., Poutanen, M., and Huhtaniemi, I. (2012) Epididymal protein Rnase10 is required for post-testicular sperm maturation and male fertility. *FASEB Journal* **26**, 4198-4209
33. Westmuckett, A. D., Nguyen, E. B., Herlea-Pana, O. M., Alvau, A., Salicioni, A. M., and Moore, K. L. (2014) Impaired sperm maturation in RNASE9 knockout mice. *Biol Reprod* **90**, 120
34. Futami, J., Tsushima, Y., Murato, Y., Tada, H., Sasaki, J., Seno, M., and Yamada, H. (1997) Tissue-specific expression of pancreatic-type RNases and RNase inhibitor in humans. *DNA Cell Biol* **16**, 413-419
35. Weickmann, J. L., Olson, E. M., and Glitz, D. G. (1984) Immunological assay of pancreatic ribonuclease in serum as an indicator of pancreatic cancer. *Cancer Res* **44**, 1682-1687
36. Landre, J. B., Hewett, P. W., Olivot, J. M., Friedl, P., Ko, Y., Sachinidis, A., and Moenner, M. (2002) Human endothelial cells selectively express large amounts of pancreatic-type ribonuclease (RNase 1). *J Cell Biochem* **86**, 540-552
37. Barrabes, S., Pages-Pons, L., Radcliffe, C. M., Tabares, G., Fort, E., Royle, L., Harvey, D. J., Moenner, M., Dwek, R. A., Rudd, P. M., De Llorens, R., and Peracaula, R. (2007) Glycosylation of serum ribonuclease 1 indicates a major endothelial origin and reveals an increase in core fucosylation in pancreatic cancer. *Glycobiology* **17**, 388-400
38. Fischer, S., Nishio, M., Dadkhahi, S., Gansler, J., Saffarzadeh, M., Shibamiyama, A., Kral, N., Baal, N., Koyama, T., Deindl, E., and Preissner, K. T. (2011) Expression and localisation of vascular ribonucleases in endothelial cells. *Thromb Haemost* **105**, 345-355
39. Beintema, J. J. (1986) Evolutionary role of posttranslational modifications of proteins, as illustrated by the glycosylation characteristics of the digestive enzyme pancreatic ribonuclease. *J Mol Evol* **24**, 118-120

40. Mizuta, K., Awazu, S., Yasuda, T., and Kishi, K. (1990) Purification and characterization of three ribonucleases from human kidney: comparison with urine ribonucleases. *Arch Biochem Biophys* **281**, 144-151
41. Yasuda, T., Nadano, D., Takeshita, H., and Kishi, K. (1993) Two distinct secretory ribonucleases from human cerebrum: purification, characterization and relationships to other ribonucleases. *Biochem J* **296 (Pt 3)**, 617-625
42. Eller, C. H., Lomax, J. E., and Raines, R. T. (2014) Bovine brain ribonuclease is the functional homolog of human ribonuclease 1. *J Biol Chem* **289**, 25996-26006
43. Eller, C. H., Chao, T. Y., Singarapu, K. K., Ouerfelli, O., Yang, G., Markley, J. L., Danishefsky, S. J., and Raines, R. T. (2015) Human cancer antigen Globo H Is a cell-surface ligand for human Ribonuclease 1. *ACS Cent Sci* **1**, 181-190
44. Reddi, K. K., and Holland, J. F. (1976) Elevated serum ribonuclease in patients with pancreatic cancer. *Proc Natl Acad Sci U S A* **73**, 2308-2310
45. Maor, D., and Mardiney, M. R., Jr. (1978) Alteration of human serum ribonuclease activity in malignancy. *CRC Crit Rev Clin Lab Sci* **10**, 89-111
46. Isaacs, P. (1981) Non-specificity of elevated serum ribonuclease as a pancreatic tumour marker. *Digestion* **22**, 101-107
47. Kutas, V., Bertök, L., and Szabó, L. (1969) Effect of endotoxin on the serum ribonuclease activity in rats. *J Bacteriol* **100**, 550-551
48. Maor, D., Klein, M. E., Kenady, D. E., Chretien, P. B., and Mardiney, M. R. (1978) Carcinoma of the lung and cigarette smoking: Effect on serum ribonuclease activity. *JAMA* **239**, 2766-2768
49. Coombes, E. J., Shakespeare, P. G., and Batstone, G. F. (1978) Observations on serum and urine alkaline ribonuclease activity and urate after burn injury in man. *Clin Chim Acta* **86**, 279-290
50. Barlow, G. B., Whitear, S. H., and Wilkinson, A. W. (1979) The excretion of alkaline ribonuclease by children undergoing surgery. *Br J Surg* **66**, 412-414
51. Sznajd, J., Magdoń, M., Naskalski, J., Uracz, R., and Wojcikiewicz, O. (1981) Serum ribonuclease activity in acute myocardial infarction. *Cor Vasa* **23**, 241-247
52. Coombes, E., Shakespeare, P., and Batstone, G. (1977) Age and sex related reference values for serum ribonuclease. *Clin Chim Acta* **79**, 271-275
53. Sajdel-Sulkowska, E. M., and Marotta, C. A. (1984) Alzheimer's disease brain: alterations in RNA levels and in a ribonuclease-inhibitor complex. *Science* **225**, 947-949
54. Sigulem, D. M., Brasel, J. A., Velasco, E. G., Rosso, P., and Winick, M. (1973) Plasma and urine ribonuclease as a measure of nutritional status in children. *Am J Clin Nutr* **26**, 793-797
55. Oribe, M. (1984) [Serum ribonuclease in rheumatic disease. I. Serum alkaline ribonuclease activities in rheumatic diseases, especially in malignant rheumatoid arthritis]. *Fukuoka Igaku Zasshi* **75**, 524-533
56. Darzynkiewicz, Z., Carter, S. P., Mikulski, S. M., Ardelt, W. J., and Shogen, K. (1988) Cytostatic and cytotoxic effects of Pannon (P-30 Protein), a novel anticancer agent. *Cell Tissue Kinet* **21**, 169-182
57. Wu, Y., Mikulski, S. M., Ardelt, W., Rybak, S. M., and Youle, R. J. (1993) A cytotoxic ribonuclease. Study of the mechanism of onconase cytotoxicity. *J Biol Chem* **268**, 10686-10693
58. Leland, P. A., Staniszewski, K. E., Kim, B. M., and Raines, R. T. (2001) Endowing human pancreatic ribonuclease with toxicity for cancer cells. *J Biol Chem* **276**, 43095-43102
59. Vasandani, V. M., Wu, Y. N., Mikulski, S. M., Youle, R. J., and Sung, C. (1996) Molecular determinants in the plasma clearance and tissue distribution of ribonucleases of the ribonuclease A superfamily. *Cancer Res* **56**, 4180-4186
60. Strong, L. E., Kink, J. A., Mei, B., Shahan, M. N., and Raines, R. T. (2010) Abstract 5390: QBI-139, a human RNase variant in a phase I trial, works in combination. *Cancer Res* **70**, 5390-5390
61. Strong, L. E., Kink, J. A., Pensinger, D., Mei, B., Shahan, M. N., and Raines, R. T. (2011) Abstract 2573: Combinations of QBI-139, a clinical stage ribonuclease drug. *Cancer Res* **71**, 2573-2573

62. Kamm, R. C., and Smith, A. G. (1972) Nucleic acid concentrations in normal human plasma. *Clin Chem* **18**, 519-522
63. Lo, K. W., Lo, Y. M., Leung, S. F., Tsang, Y. S., Chan, L. Y., Johnson, P. J., Hjelm, N. M., Lee, J. C., and Huang, D. P. (1999) Analysis of cell-free Epstein-Barr virus associated RNA in the plasma of patients with nasopharyngeal carcinoma. *Clin Chem* **45**, 1292-1294
64. Hasselmann, D. O., Rapp, G., Tilgen, W., and Reinhold, U. (2001) Extracellular tyrosinase mRNA within apoptotic bodies is protected from degradation in human serum. *Clin Chem* **47**, 1488-1489
65. Yuan, T., Huang, X., Woodcock, M., Du, M., Dittmar, R., Wang, Y., Tsai, S., Kohli, M., Boardman, L., Patel, T., and Wang, L. (2016) Plasma extracellular RNA profiles in healthy and cancer patients. *Sci Rep* **6**, 19413
66. Huang, X., Yuan, T., Tschannen, M., Sun, Z., Jacob, H., Du, M., Liang, M., Dittmar, R. L., Liu, Y., and Liang, M. (2013) Characterization of human plasma-derived exosomal RNAs by deep sequencing. *BMC Genomics* **14**, 319
67. Savelyeva, A. V., Kuligina, E. V., Bariakin, D. N., Kozlov, V. V., Ryabchikova, E. I., Richter, V. A., and Semenov, D. V. (2017) Variety of RNAs in peripheral blood cells, plasma, and plasma fractions. *Biomed Res Int* **2017**, 10
68. Yáñez-Mó, M., Siljander, P. R.-M., Andreu, Z., Bedina Zavec, A., Borràs, F. E., Buzas, E. I., Buzas, K., Casal, E., Cappello, F., and Carvalho, J. (2015) Biological properties of extracellular vesicles and their physiological functions. *J Extracell Vesicles* **4**, 27066
69. Turchinovich, A., Weiz, L., Langheinz, A., and Burwinkel, B. (2011) Characterization of extracellular circulating microRNA. *Nucleic Acids Res* **39**, 7223-7233
70. Vickers, K. C., Palmisano, B. T., Shoucri, B. M., Shamburek, R. D., and Remaley, A. T. (2011) MicroRNAs are transported in plasma and delivered to recipient cells by high-density lipoproteins. *Nat Cell Biol* **13**, 423
71. Stroun, M., Anker, P., Beljanski, M., Henri, J., Lederrey, C., Ojha, M., and Maurice, P. A. (1978) Presence of RNA in the nucleoprotein complex spontaneously released by human lymphocytes and frog auricles in culture. *Cancer Res* **38**, 3546-3554
72. Wieczorek, A. J., Rhyner, C., and Block, L. H. (1985) Isolation and characterization of an RNA-proteolipid complex associated with the malignant state in humans. *Proc Natl Acad Sci* **82**, 3455-3459
73. Fischer, S., Gesierich, S., Griemert, B., Schanzer, A., Acker, T., Augustin, H. G., Olsson, A. K., and Preissner, K. T. (2013) Extracellular RNA liberates tumor necrosis factor-alpha to promote tumor cell trafficking and progression. *Cancer Res* **73**, 5080-5089
74. Valadi, H., Ekstrom, K., Bossios, A., Sjostrand, M., Lee, J. J., and Lotvall, J. O. (2007) Exosome-mediated transfer of mRNAs and microRNAs is a novel mechanism of genetic exchange between cells. *Nat Cell Biol* **9**, 654-659
75. Mittelbrunn, M., Gutierrez-Vazquez, C., Villarroya-Beltri, C., Gonzalez, S., Sanchez-Cabo, F., Gonzalez, M. A., Bernad, A., and Sanchez-Madrid, F. (2011) Unidirectional transfer of microRNA-loaded exosomes from T cells to antigen-presenting cells. *Nat Commun* **2**, 282
76. Fischer, S., Grantzow, T., Pagel, J. I., Tschernatsch, M., Sperandio, M., Preissner, K. T., and Deindl, E. (2012) Extracellular RNA promotes leukocyte recruitment in the vascular system by mobilising proinflammatory cytokines. *Thromb Haemost* **108**, 730-741
77. Simsekylmaz, S., Cabrera-Fuentes, H. A., Meiler, S., Kostin, S., Baumer, Y., Liehn, E. A., Weber, C., Boisvert, W. A., Preissner, K. T., and Zerneck, A. (2014) Role of extracellular RNA in atherosclerotic plaque formation in mice. *Circulation* **129**, 598-606
78. Nakazawa, F., Kannemeier, C., Shibamiya, A., Song, Y., Tzima, E., Schubert, U., Koyama, T., Niepmann, M., Trusheim, H., Engelmann, B., and Preissner, K. T. (2005) Extracellular RNA is a natural cofactor for the (auto-)activation of Factor VII-activating protease (FSAP). *Biochem J* **385**, 831-838

79. Kannemeier, C., Shibamiya, A., Nakazawa, F., Trusheim, H., Ruppert, C., Markart, P., Song, Y., Tzima, E., Kennerknecht, E., Niepmann, M., von Bruehl, M. L., Sedding, D., Massberg, S., Gunther, A., Engelmann, B., and Preissner, K. T. (2007) Extracellular RNA constitutes a natural procoagulant cofactor in blood coagulation. *Proc Natl Acad Sci U S A* **104**, 6388-6393
80. Gansler, J., Jaax, M., Leiting, S., Appel, B., Greinacher, A., Fischer, S., and Preissner, K. T. (2012) Structural requirements for the procoagulant activity of nucleic acids. *PLoS One* **7**, e50399
81. Gajsiewicz, J. M., Smith, S. A., and Morrissey, J. H. (2017) Polyphosphate and RNA differentially modulate the contact pathway of blood clotting. *J Biol Chem* **292**, 1808-1814
82. Cabrera-Fuentes, H. A., Niemann, B., Grieshaber, P., Wollbrueck, M., Gehron, J., Preissner, K. T., and Boning, A. (2015) RNase1 as a potential mediator of remote ischaemic preconditioning for cardioprotection. *Eur J Cardiothorac Surg* **48**, 732-737; discussion 737
83. Cabrera-Fuentes, H. A., Ruiz-Meana, M., Simsekylmaz, S., Kostin, S., Inserte, J., Saffarzadeh, M., Galuska, S. P., Vijayan, V., Barba, I., Barreto, G., Fischer, S., Lochnit, G., Ilinskaya, O. N., Baumgart-Vogt, E., Boning, A., Lecour, S., Hausenloy, D. J., Liehn, E. A., Garcia-Dorado, D., Schluter, K. D., and Preissner, K. T. (2014) RNase1 prevents the damaging interplay between extracellular RNA and tumour necrosis factor-alpha in cardiac ischaemia/reperfusion injury. *Thromb Haemost* **112**, 1110-1119
84. Stieger, P., Daniel, J. M., Tholen, C., Dutzmann, J., Knopp, K., Gunduz, D., Aslam, M., Kampschulte, M., Langheinrich, A., Fischer, S., Cabrera-Fuentes, H., Wang, Y., Wollert, K. C., Bauersachs, J., Braun-Dullaeus, R., Preissner, K. T., and Sedding, D. G. (2017) Targeting of extracellular RNA reduces edema formation and infarct size and improves survival after myocardial infarction in mice. *J Am Heart Assoc* **6**
85. Sun, X., Wiedeman, A., Agrawal, N., Teal, T. H., Tanaka, L., Hudkins, K. L., Alpers, C. E., Bolland, S., Buechler, M. B., Hamerman, J. A., Ledbetter, J. A., Liggitt, D., and Elkon, K. B. (2013) Increased ribonuclease expression reduces inflammation and prolongs survival in TLR7 transgenic mice. *J Immunol* **190**, 2536-2543
86. Walberer, M., Tschernatsch, M., Fischer, S., Ritschel, N., Volk, K., Friedrich, C., Bachmann, G., Mueller, C., Kaps, M., Nedelmann, M., Blaes, F., Preissner, K. T., and Gerriets, T. (2009) RNase therapy assessed by magnetic resonance imaging reduces cerebral edema and infarction size in acute stroke. *Curr Neurovasc Res* **6**, 12-19
87. Fischer, S., Gerriets, T., Wessels, C., Walberer, M., Kostin, S., Stolz, E., Zheleva, K., Hocke, A., Hippenstiel, S., and Preissner, K. T. (2007) Extracellular RNA mediates endothelial-cell permeability via vascular endothelial growth factor. *Blood* **110**, 2457-2465
88. Kleinert, E., Langenmayer, M. C., Reichart, B., Kindermann, J., Griemert, B., Blutke, A., Troidl, K., Mayr, T., Grantzow, T., Noyan, F., Abicht, J. M., Fischer, S., Preissner, K. T., Wanke, R., Deindl, E., and Guethoff, S. (2016) Ribonuclease (RNase) prolongs survival of grafts in experimental heart transplantation. *J Am Heart Assoc* **5**
89. Fett, J. W., Strydom, D. J., Lobb, R. R., Alderman, E. M., Bethune, J. L., Riordan, J. F., and Vallee, B. L. (1985) Isolation and characterization of angiogenin, an angiogenic protein from human carcinoma cells. *Biochemistry* **24**, 5480-5486
90. Shapiro, R., Riordan, J. F., and Vallee, B. L. (1986) Characteristic ribonucleolytic activity of human angiogenin. *Biochemistry* **25**, 3527-3532
91. Acharya, K. R., Shapiro, R., Allen, S. C., Riordan, J. F., and Vallee, B. L. (1994) Crystal structure of human angiogenin reveals the structural basis for its functional divergence from ribonuclease. *Proc Natl Acad Sci U S A* **91**, 2915-2919
92. Russo, N., Shapiro, R., Acharya, K. R., Riordan, J. F., and Vallee, B. L. (1994) Role of glutamine-117 in the ribonucleolytic activity of human angiogenin. *Proc Natl Acad Sci USA* **91**, 2920-2924
93. Saxena, S. K., Rybak, S. M., Davey, R. T., Jr., Youle, R. J., and Ackerman, E. J. (1992) Angiogenin is a cytotoxic, tRNA-specific ribonuclease in the RNase A superfamily. *J Biol Chem* **267**, 21982-21986

94. Hoang, T. T., and Raines, R. T. (2017) Molecular basis for the autonomous promotion of cell proliferation by angiogenin. *Nucleic Acids Res* **45**, 818-831
95. Hallahan, T. W., Shapiro, R., and Vallee, B. L. (1991) Dual site model for the organogenic activity of angiogenin. *Proc Natl Acad Sci U S A* **88**, 2222-2226
96. Bicknell, R., and Vallee, B. L. (1988) Angiogenin activates endothelial cell phospholipase C. *Proc Natl Acad Sci* **85**, 5961-5965
97. Hu, G., Xu, C., and Riordan, J. F. (2000) Human angiogenin is rapidly translocated to the nucleus of human umbilical vein endothelial cells and binds to DNA. *J Cell Biochem* **76**, 452-462
98. Skorupa, A., King, M. A., Aparicio, I. M., Dussmann, H., Coughlan, K., Breen, B., Kieran, D., Concannon, C. G., Marin, P., and Prehn, J. H. (2012) Motoneurons secrete angiogenin to induce RNA cleavage in astroglia. *J Neurosci* **32**, 5024-5038
99. Yu, W., Goncalves, K. A., Li, S., Kishikawa, H., Sun, G., Yang, H., Vanli, N., Wu, Y., Jiang, Y., Hu, M. G., Friedel, R. H., and Hu, G. F. (2017) Plexin-B2 mediates physiologic and pathologic functions of angiogenin. *Cell* **171**, 849-864.e825
100. Moroianu, J., and Riordan, J. F. (1994) Identification of the nucleolar targeting signal of human angiogenin. *Biochem Biophys Res Commun* **203**, 1765-1772
101. Xu, Z.-p., Tsuji, T., Riordan, J. F., and Hu, G.-f. (2002) The nuclear function of angiogenin in endothelial cells is related to rRNA production. *Biochem Biophys Res Commun* **294**, 287-292
102. Mayer, C., Schmitz, K. M., Li, J., Grummt, I., and Santoro, R. (2006) Intergenic transcripts regulate the epigenetic state of rRNA genes. *Mol Cell* **22**, 351-361
103. Mayer, C., Neubert, M., and Grummt, I. (2008) The structure of NoRC-associated RNA is crucial for targeting the chromatin remodelling complex NoRC to the nucleolus. *EMBO Rep* **9**, 774-780
104. Yoshioka, N., Wang, L., Kishimoto, K., Tsuji, T., and Hu, G. F. (2006) A therapeutic target for prostate cancer based on angiogenin-stimulated angiogenesis and cancer cell proliferation. *Proc Natl Acad Sci U S A* **103**, 14519-14524
105. Kishimoto, K., Yoshida, S., Ibaragi, S., Yoshioka, N., Okui, T., Hu, G. F., and Sasaki, A. (2012) Hypoxia-induced up-regulation of angiogenin, besides VEGF, is related to progression of oral cancer. *Oral Oncol* **48**, 1120-1127
106. Hartmann, A., Kunz, M., Köstlin, S., Gillitzer, R., Toksoy, A., Bröcker, E.-B., and Klein, C. E. (1999) Hypoxia-induced up-regulation of angiogenin in human malignant melanoma. *Cancer Res* **59**, 1578-1583
107. Ramcharan, S. K., Lip, G. Y., Stonelake, P. S., and Blann, A. D. (2013) Angiogenin outperforms VEGF, EPCs and CECs in predicting Dukes' and AJCC stage in colorectal cancer. *Eur J Clin Invest* **43**, 801-808
108. Urquidi, V., Goodison, S., Kim, J., Chang, M., Dai, Y., and Rosser, C. J. (2012) Vascular endothelial growth factor, carbonic anhydrase 9, and angiogenin as urinary biomarkers for bladder cancer detection. *Urology* **79**, 1185.e1181-1186
109. He, T., Qi, F., Jia, L., Wang, S., Wang, C., Song, N., Fu, Y., Li, L., and Luo, Y. (2015) Tumor cell-secreted angiogenin induces angiogenic activity of endothelial cells by suppressing miR-542-3p. *Cancer Lett* **368**, 115-125
110. Shu, J., Huang, M., Tian, Q., Shui, Q., Zhou, Y., and Chen, J. (2015) Downregulation of angiogenin inhibits the growth and induces apoptosis in human bladder cancer cells through regulating AKT/mTOR signaling pathway. *J Mol Histol* **46**, 157-171
111. Dutta, S., Bandyopadhyay, C., Bottero, V., Veetil, M. V., Wilson, L., Pins, M. R., Johnson, K. E., Warshall, C., and Chandran, B. (2014) Angiogenin interacts with the plasminogen activation system at the cell surface of breast cancer cells to regulate plasmin formation and cell migration. *Mol Oncol* **8**, 483-507
112. Kao, R. Y. T., Jenkins, J. L., Olson, K. A., Key, M. E., Fett, J. W., and Shapiro, R. (2002) A small-molecule inhibitor of the ribonucleolytic activity of human angiogenin that possesses antitumor activity. *Proc Natl Acad Sci* **99**, 10066-10071

113. Reynolds, L. P., Grazul-Bilska, A. T., and Redmer, D. A. (2002) Angiogenesis in the female reproductive organs: pathological implications. *Int J Exp Path* **83**, 151-163
114. Koga, K., Osuga, Y., Tsutsumi, O., Momoeda, M., Suenaga, A., Kugu, K., Fujiwara, T., Takai, Y., Yano, T., and Taketani, Y. (2000) Evidence for the presence of angiogenin in human follicular fluid and the up-regulation of its production by human chorionic gonadotropin and hypoxia. *J Clin Endocrinol Metab* **85**, 3352-3355
115. Zhang, Y., Xia, X., Yan, J., Yan, L., Lu, C., Zhu, X., Wang, T., Yin, T., Li, R., Chang, H. M., and Qiao, J. (2017) Mesenchymal stem cell-derived angiogenin promotes primordial follicle survival and angiogenesis in transplanted human ovarian tissue. *Reprod Biol Endocrinol* **15**, 18
116. Koga, K., Osuga, Y., Tsutsumi, O., Yano, T., Yoshino, O., Takai, Y., Matsumi, H., Hiroi, H., Kugu, K., Momoeda, M., Fujiwara, T., and Taketani, Y. (2001) Demonstration of angiogenin in human endometrium and its enhanced expression in endometrial tissues in the secretory phase and the decidua. *J Clin Endocrinol Metab* **86**, 5609-5614
117. Rajashekhar, G., Loganath, A., Roy, A. C., and Wong, Y. C. (2002) Expression and localization of angiogenin in placenta: enhanced levels at term over first trimester villi. *Mol Reprod Dev* **62**, 159-166
118. Pavlov, N., Hatzi, E., Bassaglia, Y., Frenedo, J. L., Evain Brion, D., and Badet, J. (2003) Angiogenin distribution in human term placenta, and expression by cultured trophoblastic cells. *Angiogenesis* **6**, 317-330
119. Pavlov, N., Frenedo, J. L., Guibourdenche, J., Degrelle, S. A., Evain-Brion, D., and Badet, J. (2014) Angiogenin expression during early human placental development; association with blood vessel formation. *Biomed Res Int* **2014**, 781632
120. Tsuji, T., Sun, Y., Kishimoto, K., Olson, K. A., Liu, S., Hirukawa, S., and Hu, G.-f. (2005) Angiogenin is translocated to the nucleus of HeLa cells and is involved in ribosomal RNA transcription and cell proliferation. *Cancer Res* **65**, 1352-1360
121. Han, S., Han, L., Yao, Y., Sun, H., Zan, X., and Liu, Q. (2014) Activated hepatic stellate cells promote hepatocellular carcinoma cell migration and invasion via the activation of FAK-MMP9 signaling. *Oncol Rep* **31**, 641-648
122. Barcena, C., Stefanovic, M., Tutusaus, A., Martinez-Nieto, G. A., Martinez, L., Garcia-Ruiz, C., de Mingo, A., Caballeria, J., Fernandez-Checa, J. C., Mari, M., and Morales, A. (2015) Angiogenin secretion from hepatoma cells activates hepatic stellate cells to amplify a self-sustained cycle promoting liver cancer. *Sci Rep* **5**, 7916
123. Subramanian, V., and Feng, Y. (2007) A new role for angiogenin in neurite growth and pathfinding: implications for amyotrophic lateral sclerosis. *Hum Mol Gen* **16**, 1445-1453
124. Skorupa, A., Urbach, S., Vigy, O., King, M. A., Chaumont-Dubel, S., Prehn, J. H., and Marin, P. (2013) Angiogenin induces modifications in the astrocyte secretome: relevance to amyotrophic lateral sclerosis. *J Proteomics* **91**, 274-285
125. Gellera, C., Colombrita, C., Ticozzi, N., Castellotti, B., Bragato, C., Ratti, A., Taroni, F., and Silani, V. (2008) Identification of new ANG gene mutations in a large cohort of Italian patients with amyotrophic lateral sclerosis. *Neurogenetics* **9**, 33-40
126. Greenway, M. J., Andersen, P. M., Russ, C., Ennis, S., Cashman, S., Donaghy, C., Patterson, V., Swingler, R., Kieran, D., Prehn, J., Morrison, K. E., Green, A., Acharya, K. R., Brown, R. H., Jr., and Hardiman, O. (2006) ANG mutations segregate with familial and 'sporadic' amyotrophic lateral sclerosis. *Nat Genet* **38**, 411-413
127. Yamasaki, S., Ivanov, P., Hu, G. F., and Anderson, P. (2009) Angiogenin cleaves tRNA and promotes stress-induced translational repression. *J Cell Biol* **185**, 35-42
128. Fu, H., Feng, J., Liu, Q., Sun, F., Tie, Y., Zhu, J., Xing, R., Sun, Z., and Zheng, X. (2009) Stress induces tRNA cleavage by angiogenin in mammalian cells. *FEBS Lett* **583**, 437-442
129. Ivanov, P., Emara, M. M., Villen, J., Gygi, S. P., and Anderson, P. (2011) Angiogenin-induced tRNA fragments inhibit translation initiation. *Mol Cell* **43**, 613-623

130. Saikia, M., Jobava, R., Parisien, M., Putnam, A., Krokowski, D., Gao, X. H., Guan, B. J., Yuan, Y., Jankowsky, E., Feng, Z., Hu, G. F., Puzstai-Carey, M., Gorla, M., Sepuri, N. B., Pan, T., and Hatzoglou, M. (2014) Angiogenin-cleaved tRNA halves interact with cytochrome c, protecting cells from apoptosis during osmotic stress. *Mol Cell Biol* **34**, 2450-2463
131. Goncalves, K. A., Silberstein, L., Li, S., Severe, N., Hu, M. G., Yang, H., Scadden, D. T., and Hu, G. F. (2016) Angiogenin promotes hematopoietic regeneration by dichotomously regulating quiescence of stem and progenitor cells. *Cell* **166**, 894-906
132. Olson, K. A., Verselis, S. J., and Fett, J. W. (1998) Angiogenin is regulated in vivo as an acute phase protein. *Biochem Biophys Res Commun* **242**, 480-483
133. Hooper, L. V., Stappenbeck, T. S., Hong, C. V., and Gordon, J. I. (2003) Angiogenins: a new class of microbicidal proteins involved in innate immunity. *Nat Immunol* **4**, 269-273
134. Lee, S. H., Kim, K. W., Min, K. M., Kim, K. W., Chang, S. I., and Kim, J. C. (2014) Angiogenin reduces immune inflammation via inhibition of TANK-binding kinase 1 expression in human corneal fibroblast cells. *Mediators Inflamm* **2014**, 861435
135. Hoang, T. T., Smith, T. P., and Raines, R. T. (2017) A boronic acid conjugate of angiogenin that shows ROS-responsive neuroprotective activity. *Angew Chem Int Ed Engl* **56**, 2619-2622
136. International Human Genome Sequencing, C. (2001) Initial sequencing and analysis of the human genome. *Nature* **409**, 860
137. Pizzo, E., Buonanno, P., Di Maro, A., Ponticelli, S., De Falco, S., Quarto, N., Cubellis, M. V., and D'Alessio, G. (2006) Ribonucleases and angiogenins from fish. *J Biol Chem* **281**, 27454-27460
138. Kazakou, K., Holloway, D. E., Prior, S. H., Subramanian, V., and Acharya, K. R. (2008) Ribonuclease A homologues of the zebrafish: polymorphism, crystal structures of two representatives and their evolutionary implications. *J Mol Biol* **380**, 206-222
139. Zhou, H.-M., and Strydom, D. J. (1993) The amino acid sequence of human ribonuclease 4, a highly conserved ribonuclease that cleaves specifically on the 3' side of uridine. *Eur J Biochem* **217**, 401-410
140. Strydom, D. J. (1998) The angiogenins. *Cell Mol Life Sci* **54**, 811-824
141. Green, S. A., Simoes-Costa, M., and Bronner, M. E. (2015) Evolution of vertebrates: a view from the crest. *Nature* **520**, 474-482
142. Anisimova, M., and Gascuel, O. (2006) Approximate likelihood-ratio test for branches: A fast, accurate, and powerful alternative. *Syst Biol* **55**, 539-552
143. Castresana, J. (2000) Selection of conserved blocks from multiple alignments for their use in phylogenetic analysis. *Mol Biol Evol* **17**, 540-552
144. Chevenet, F., Brun, C., Banuls, A. L., Jacq, B., and Christen, R. (2006) TreeDyn: towards dynamic graphics and annotations for analyses of trees. *BMC Bioinformatics* **7**, 439
145. Edgar, R. C. (2004) MUSCLE: multiple sequence alignment with high accuracy and high throughput. *Nucleic Acids Res* **32**, 1792-1797
146. Guindon, S., Dufayard, J. F., Lefort, V., Anisimova, M., Hordijk, W., and Gascuel, O. (2010) New algorithms and methods to estimate maximum-likelihood phylogenies: assessing the performance of PhyML 3.0. *Syst Biol* **59**, 307-321
147. Beintema, J. J., and Kleineidam, R. G. (1998) The ribonuclease A superfamily: general discussion. *Cell Mol Life Sci* **54**, 825-832
148. Irie, M., Nitta, K., and Nonaka, T. (1998) Biochemistry of frog ribonucleases. *Cell Mol Life Sci* **54**, 775-784
149. Pizzo, E., Varcamonti, M., Di Maro, A., Zanfardino, A., Giancola, C., and D'Alessio, G. (2008) Ribonucleases with angiogenic and bactericidal activities from the Atlantic salmon. *FEBS J* **275**, 1283-1295
150. Zhao, W., Beintema, J. J., and Hofsteenge, J. (1994) The amino acid sequence of iguana (*Iguana iguana*) pancreatic ribonuclease. *Eur J Biochem* **219**, 641-646

151. Doolittle, R. F. (2009) Step-by-step evolution of vertebrate blood coagulation. *Cold Spring Harb Symp Quant Biol* **74**, 35-40
152. Doolittle, R. F., and Surgenor, D. M. (1962) Blood coagulation in fish. *Am J Physiol* **203**, 964-970
153. Muñoz-Chápuli, R., Carmona, R., Guadix, J. A., Macías, D., and Pérez-Pomares, J. M. (2005) The origin of the endothelial cells: an evo-devo approach for the invertebrate/vertebrate transition of the circulatory system. *Evol Dev* **7**, 351-358
154. Jiang, Y., and Doolittle, R. F. (2003) The evolution of vertebrate blood coagulation as viewed from a comparison of puffer fish and sea squirt genomes. *Proc Natl Acad Sci* **100**, 7527-7532
155. Zendzian, E. N., and Barnard, E. A. (1967) Distributions of pancreatic ribonuclease, chymotrypsin, and trypsin in vertebrates. *Arch Biochem Biophys* **122**, 699-713
156. Beintema, J. J., Schuller, C., Irie, M., and Carsana, A. (1988) Molecular evolution of the ribonuclease superfamily. *Prog Biophys Mol Biol* **51**, 165-192
157. Chettri, J. K., Kuhn, J. A., Jaafar, R. M., Kania, P. W., Moller, O. S., and Buchmann, K. (2014) Epidermal response of rainbow trout to *Ichthyobodo necator*: immunohistochemical and gene expression studies indicate a Th1-/Th2-like switch. *J Fish Dis* **37**, 771-783
158. Cuchillo, C. M., Nogués, M. V., and Raines, R. T. (2011) Bovine pancreatic ribonuclease: Fifty years of the first enzymatic reaction mechanism. *Biochemistry* **50**, 7835-7841
159. D'Alessio, G., and Riordan, J. F. (1997) *Ribonucleases: structures and functions*, Academic Press
160. Marshall, G. R., Feng, J. A., and Kuster, D. J. (2008) Back to the future: ribonuclease A. *Biopolymers* **90**, 259-277
161. Glukhov, B. N., Jerusalimsky, A. P., Canter, V. M., and Salganik, R. I. (1976) Ribonuclease treatment of tick-borne encephalitis. *Arch Neurol* **33**, 598-603
162. Lee-Huang, S., Huang, P. L., Sun, Y., Kung, H. F., Blithe, D. L., and Chen, H. C. (1999) Lysozyme and RNases as anti-HIV components in beta-core preparations of human chorionic gonadotropin. *Proc Natl Acad Sci USA* **96**, 2678-2681
163. Rutkoski, T. J., Kink, J. A., Strong, L. E., and Raines, R. T. (2013) Human ribonuclease with a pendant poly(ethylene glycol) inhibits tumor growth in mice. *Transl Oncol* **6**, 392-397
164. Strong L. E., K. J. A., Mei B., Shahan M. N., Raines R. T. (2012) First in human past I clinical trial of QBI-139, a human ribonuclease variant, in solid tumors. *J Clin Oncol* **30**, TPS3113
165. Morita, T., Niwata, Y., Ohgi, K., Ogawa, M., and Irie, M. (1986) Distribution of two urinary ribonuclease-like enzymes in human organs and body fluids. *J Biochem* **99**, 17-25
166. Su, A. I., Wiltshire, T., Batalov, S., Lapp, H., Ching, K. A., Block, D., Zhang, J., Soden, R., Hayakawa, M., Kreiman, G., Cooke, M. P., Walker, J. R., and Hogenesch, J. B. (2004) A gene atlas of the mouse and human protein-encoding transcriptomes. *Proc Natl Acad Sci USA* **101**, 6062-6067
167. delCardayré, S. B., Ribó, M., Yokel, E. M., Quirk, D. J., Rutter, W. J., and Raines, R. T. (1995) Engineering ribonuclease A: Production, purification, and characterization of wild-type enzyme and mutants at Gln11. *Protein Eng.* **8**, 261-273
168. Gailani, D., Lasky, N. M., and Broze, G. J., Jr. (1997) A murine model of factor XI deficiency. *Blood Coagul Fibrinolysis* **8**, 134-144
169. Pauer, H.-U., Renné, T., Hemmerlein, B., Legler, T., Fritzlar, S., Adham, I., Muller-Esterl, W., Emons, G., Sancken, U., and Engel, W. (2004) Targeted deletion of murine coagulation factor XII gene—a model for contact phase activation *in vivo*. *Thromb. Haemost.* **92**, 503-508
170. Lin, H. F., Maeda, N., Smithies, O., Straight, D. L., and Stafford, D. W. (1997) A coagulation factor IX-deficient mouse model for human hemophilia B. *Blood* **90**, 3962-3966
171. Liu, P., Jenkins, N. A., and Copeland, N. G. (2003) A highly efficient recombineering-based method for generating conditional knockout mutations. *Genome Res* **13**, 476-484
172. Schmittgen, T. D., and Livak, K. J. (2008) Analyzing real-time PCR data by the comparative C(T) method. *Nat Protoc* **3**, 1101-1108

173. Schneider, C. A., Rasband, W. S., and Eliceiri, K. W. (2012) NIH Image to ImageJ: 25 years of image analysis. *Nat Methods* **9**, 671-675
174. Kelemen, B. R., Klink, T. A., Behlke, M. A., Eubanks, S. R., Leland, P. A., and Raines, R. T. (1999) Hypersensitive substrate for ribonucleases. *Nucleic Acids Res* **27**, 3696-3701
175. Lomax, J. E., Eller, C. H., and Raines, R. T. (2017) Comparative functional analysis of ribonuclease 1 homologs: molecular insights into evolving vertebrate physiology. *Biochem J* **474**, 2219-2233
176. Bravo, J., Fernandez, E., Ribo, M., de Llorens, R., and Cuchillo, C. M. (1994) A versatile negative-staining ribonuclease zymogram. *Anal Biochem* **219**, 82-86
177. Jagadeeswaran, P., Gregory, M., Johnson, S., and Thankavel, B. (2000) Haemostatic screening and identification of zebrafish mutants with coagulation pathway defects: an approach to identifying novel haemostatic genes in man. *Br J Haematol* **110**, 946-956
178. Cheng, Q., Tucker, E. I., Pine, M. S., Sisler, I., Matafonov, A., Sun, M. F., White-Adams, T. C., Smith, S. A., Hanson, S. R., McCarty, O. J., Renne, T., Gruber, A., and Gailani, D. (2010) A role for factor XIIa-mediated factor XI activation in thrombus formation in vivo. *Blood* **116**, 3981-3989
179. Merkulov, S., Zhang, W. M., Komar, A. A., Schmaier, A. H., Barnes, E., Zhou, Y., Lu, X., Iwaki, T., Castellino, F. J., Luo, G., and McCrae, K. R. (2008) Deletion of murine kininogen gene 1 (*mKng1*) causes loss of plasma kininogen and delays thrombosis. *Blood* **111**, 1274-1281
180. Sommeijer, D. W., van Oerle, R., Reitsma, P. H., Timmerman, J. J., Meijers, J. C., Spronk, H. M., and ten Cate, H. (2005) Analysis of blood coagulation in mice: pre-analytical conditions and evaluation of a home-made assay for thrombin-antithrombin complexes. *Thromb J* **3**, 12
181. Liu, Y., Jennings, N. L., Dart, A. M., and Du, X. J. (2012) Standardizing a simpler, more sensitive and accurate tail bleeding assay in mice. *World J Exp Med* **2**, 30-36
182. Buyue, Y., Whinna, H. C., and Sheehan, J. P. (2008) The heparin-binding exosite of factor IXa is a critical regulator of plasma thrombin generation and venous thrombosis. *Blood* **112**, 3234-3241
183. Beintema, J. J., Wietzes, P., Weickmann, J. L., and Glitz, D. G. (1984) The amino acid sequence of human pancreatic ribonuclease. *Anal Biochem* **136**, 48-64
184. Samad, F., and Ruf, W. (2013) Inflammation, obesity, and thrombosis. *Blood* **122**, 3415-3422
185. Ratnoff, O. D., and Colopy, J. E. (1955) A familial hemorrhagic trait associated with a deficiency of a clot-promoting fraction of plasma. *J Clin Invest* **34**, 602-613
186. Ratnoff, O. D., and Saito, H. (1982) The evolution of clot-promoting and amidolytic activities in mixtures of Hageman factor (factor XII) and ellagic acid. *J Lab Clin Med* **100**, 248-260
187. Renné, T., Pozgajová, M., Grüner, S., Schuh, K., Pauer, H.-U., Burfeind, P., Gailani, D., and Nieswandt, B. (2005) Defective thrombus formation in mice lacking coagulation factor XII. *J Exp Med* **202**, 271-281
188. Garcia, J. M., Garcia, V., Pena, C., Dominguez, G., Silva, J., Diaz, R., Espinosa, P., Citores, M. J., Collado, M., and Bonilla, F. (2008) Extracellular plasma RNA from colon cancer patients is confined in a vesicle-like structure and is mRNA-enriched. *RNA* **14**, 1424-1432
189. Leon, S. A., Shapiro, B., Sklaroff, D. M., and Yaros, M. J. (1977) Free DNA in the serum of cancer patients and the effect of therapy. *Cancer Res* **37**, 646-650
190. Cormier, S. A., Larson, K. A., Yuan, S., Mitchell, T. L., Lindenberger, K., Carrigan, P., Lee, N. A., and Lee, J. J. (2001) Mouse eosinophil-associated ribonucleases: a unique subfamily expressed during hematopoiesis. *Mamm Genome* **12**, 352-361
191. Dyer, K. D., and Rosenberg, H. F. (2005) The mouse RNase 4 and RNase 5/ang 1 locus utilizes dual promoters for tissue-specific expression. *Nucleic Acids Res* **33**, 1077-1086
192. Bleker, S. M., Coppens, M., and Middeldorp, S. (2014) Sex, thrombosis and inherited thrombophilia. *Blood Rev* **28**, 123-133
193. Artero, A., Tarin, J. J., and Cano, A. (2012) The adverse effects of estrogen and selective estrogen receptor modulators on hemostasis and thrombosis. *Semin Thromb Hemost* **38**, 797-807

194. Iwaki, T., and Castellino, F. J. (2006) Plasma levels of bradykinin are suppressed in factor XII-deficient mice. *Thromb Haemost* **95**, 1003-1010
195. Kaplan, A. P., and Joseph, K. (2014) Pathogenic mechanisms of bradykinin mediated diseases: dysregulation of an innate inflammatory pathway. *Adv Immunol* **121**, 41-89
196. Golias, C., Charalabopoulos, A., Stagikas, D., Charalabopoulos, K., and Batistatou, A. (2007) The kinin system - bradykinin: biological effects and clinical implications. Multiple role of the kinin system - bradykinin. *Hippokratia* **11**, 124-128
197. Falanga, A., Russo, L., and Milesi, V. (2014) The coagulopathy of cancer. *Curr Opin Hematol* **21**, 423-429
198. Falanga, A., Marchetti, M., and Russo, L. (2015) The mechanisms of cancer-associated thrombosis. *Thromb Res* **135 Suppl 1**, S8-s11
199. Mitrugno, A., Tormoen, G. W., Kuhn, P., and McCarty, O. J. (2016) The prothrombotic activity of cancer cells in the circulation. *Blood Rev* **30**, 11-19
200. Nickel, K. F., Labberton, L., Long, A. T., Langer, F., Fuchs, T. A., Stavrou, E. X., Butler, L. M., and Renné, T. (2016) The polyphosphate/factor XII pathway in cancer-associated thrombosis: novel perspectives for safe anticoagulation in patients with malignancies. *Thromb Res* **141**, S4-S7
201. Mami, I., Bouvier, N., El Karoui, K., Gallazzini, M., Rabant, M., Laurent-Puig, P., Li, S., Tharaux, P. L., Beaune, P., Thervet, E., Chevet, E., Hu, G. F., and Pallet, N. (2016) Angiogenin mediates cell-autonomous translational control under endoplasmic reticulum stress and attenuates kidney injury. *J Am Soc Nephrol* **27**, 863-876
202. Heyne, G. W., Plisch, E. H., Melberg, C. G., Sandgren, E. P., Peter, J. A., and Lipinski, R. J. (2015) A simple and reliable method for early pregnancy detection in inbred mice. *J Am Assoc Lab Anim Sci* **54**, 368-371
203. Theiler, K. (1989) *The house mouse: Atlas of embryonic development*, Springer Science+Business Media, LLC, New York, NY
204. Burton, G. J., and Fowden, A. L. (2015) The placenta: a multifaceted, transient organ. *Philos Trans R Soc Lond B Biol Sci* **370**
205. Garcia, M. D., and Larina, I. V. (2014) Vascular development and hemodynamic force in the mouse yolk sac. *Front Physiol* **5**, 308
206. Walls, J. R., Coultas, L., Rossant, J., and Henkelman, R. M. (2008) Three-dimensional analysis of vascular development in the mouse embryo. *PLoS One* **3**, e2853
207. Vasudevan, A., and Bhide, P. G. (2008) Angiogenesis in the embryonic CNS: A new twist on an old tale. *Cell Adh Migr* **2**, 167-169
208. Weiner, H., Weiner, L., and Swain, J. (1987) Tissue distribution and developmental expression of the messenger RNA encoding angiogenin. *Science* **237**, 280-282
209. Dilworth, M. R., and Sibley, C. P. (2013) Review: Transport across the placenta of mice and women. *Placenta* **34 Suppl**, S34-39
210. Rossant, J., and Cross, J. C. (2001) Placental development: Lessons from mouse mutants. *Nat Rev Genet* **2**, 538
211. Thornburg, K. L., Burry, K. J., Adams, A. K., Kirk, E. P., and Faber, J. J. (1988) Permeability of placenta to inulin. *Am J Obstet Gynecol* **158**, 1165-1169
212. Davisson, R. L., Hoffmann, D. S., Butz, G. M., Aldape, G., Schlager, G., Merrill, D. C., Sethi, S., Weiss, R. M., and Bates, J. N. (2002) Discovery of a spontaneous genetic mouse model of preeclampsia. *Hypertension (Dallas, Tex. : 1979)* **39**, 337-342
213. Wooding, P., and Burton, G. (2008) *Comparative placentation: structures, functions and evolution*, Springer Science & Business Media
214. Codoñer, F. M., Alfonso-Loeches, S., and Fares, M. A. (2010) Mutational dynamics of murine angiogenin duplicates. *BMC Evol Biol* **10**, 310
215. Jauniaux, E., Watson, A. L., Hempstock, J., Bao, Y.-P., Skepper, J. N., and Burton, G. J. (2000) Onset of maternal arterial blood flow and placental oxidative stress: a possible factor in human early pregnancy failure. *Am J Pathol* **157**, 2111-2122

216. Burton, G. J., Charnock-Jones, D. S., and Jauniaux, E. (2009) Regulation of vascular growth and function in the human placenta. *Reproduction* **138**, 895-902
217. Ko Ferrigno, P. (2016) Increasing experimental reproducibility, from antibodies to protein arrays. *Drug Discov Today* **21**, 1197-1199
218. Sinclair, N. R. (2004) B cell/antibody tolerance to our own antigens. *Front Biosci* **9**, 3019-3028
219. Andrievskaia, O., McRae, H., Elmgren, C., Huang, H., Balachandran, A., and Nielsen, K. (2006) Generation of antibodies against bovine recombinant prion protein in various strains of mice. *Clin Vaccine Immunol* **13**, 98-105
220. Zhou, H., Wang, Y., Wang, W., Jia, J., Li, Y., Wang, Q., Wu, Y., and Tang, J. (2009) Generation of monoclonal antibodies against highly conserved antigens. *PLoS One* **4**, e6087
221. Arevalo, J. H., Taussig, M. J., and Wilson, I. A. (1993) Molecular basis of crossreactivity and the limits of antibody-antigen complementarity. *Nature* **365**, 859-863
222. Landegren, U., Vänellid, J., Hammond, M., Nong, R. Y., Wu, D., Ullerås, E., and Kamali-Moghaddam, M. (2012) Opportunities for sensitive plasma proteome analysis. *Anal Chem* **84**, 1824-1830
223. Schwenk, J. M., Igel, U., Neiman, M., Langen, H., Becker, C., Bjartell, A., Ponten, F., Wiklund, F., Grönberg, H., Nilsson, P., and Uhlen, M. (2010) Toward next generation plasma profiling via heat-induced epitope retrieval and array-based assays. *Mol Cell Proteomics* **9**, 2497-2507
224. Smith, G. (1985) Filamentous fusion phage: novel expression vectors that display cloned antigens on the virion surface. *Science* **228**, 1315-1317
225. Yu, R., Wang, S., Yu, Y. Z., Du, W. S., Yang, F., Yu, W. Y., and Sun, Z. W. (2009) Neutralizing antibodies of botulinum neurotoxin serotype A screened from a fully synthetic human antibody phage display library. *J Biomol Screen* **14**, 991-998
226. Gao, J., Sidhu, S. S., and Wells, J. A. (2009) Two-state selection of conformation-specific antibodies. *Proc Natl Acad Sci* **106**, 3071-3076
227. Zhang, Y., and Skolnick, J. (2005) TM-align: a protein structure alignment algorithm based on the TM-score. *Nucleic Acids Res* **33**, 2302-2309
228. Xu, J., and Zhang, Y. (2010) How significant is a protein structure similarity with TM-score = 0.5? *Bioinformatics* **26**, 889-895
229. Sorrentino, S., Glitz, D. G., Hamann, K. J., Loegering, D. A., Checkel, J. L., and Gleich, G. J. (1992) Eosinophil-derived neurotoxin and human liver ribonuclease. Identity of structure and linkage of neurotoxicity to nuclease activity. *J Biol Chem* **267**, 14859-14865
230. Beckett, D., Kovaleva, E., and Schatz, P. J. (1999) A minimal peptide substrate in biotin holoenzyme synthetase-catalyzed biotinylation. *Protein Sci* **8**, 921-929
231. Ashkenazy, H., Abadi, S., Martz, E., Chay, O., Mayrose, I., Pupko, T., and Ben-Tal, N. (2016) ConSurf 2016: an improved methodology to estimate and visualize evolutionary conservation in macromolecules. *Nucleic Acids Res* **44**, W344-350
232. Ashkenazy, H., Erez, E., Martz, E., Pupko, T., and Ben-Tal, N. (2010) ConSurf 2010: calculating evolutionary conservation in sequence and structure of proteins and nucleic acids. *Nucleic Acids Res* **38**, W529-533
233. Celniker, G., Nimrod, G., Ashkenazy, H., Glaser, F., Martz, E., Mayrose, I., Pupko, T., and Ben-Tal, N. (2013) ConSurf: using evolutionary data to raise testable hypotheses about protein function. *Isr J Chem* **53**, 199-206
234. Glaser, F., Pupko, T., Paz, I., Bell, R. E., Bechor-Shental, D., Martz, E., and Ben-Tal, N. (2003) ConSurf: Identification of Functional Regions in Proteins by Surface-Mapping of Phylogenetic Information. *Bioinformatics* **19**, 163-164
235. Landau, M., Mayrose, I., Rosenberg, Y., Glaser, F., Martz, E., Pupko, T., and Ben-Tal, N. (2005) ConSurf 2005: the projection of evolutionary conservation scores of residues on protein structures. *Nucleic Acids Res* **33**, W299-W302
236. Schrodinger, L. (2015) The PyMOL molecular graphics system, version 1.8.

237. Holloway, D. E., Chavali, G. B., Hares, M. C., Subramanian, V., and Acharya, K. R. (2005) Structure of murine angiogenin: features of the substrate- and cell-binding regions and prospects for inhibitor-binding studies. *Acta Crystallogr D Biol Crystallogr* **61**, 1568-1578
238. Johnson, R. J., Lavis, L. D., and Raines, R. T. (2007) Intraspecies regulation of ribonucleolytic activity. *Biochemistry* **46**, 13131-13140
239. Leland, P. A., Staniszewski, K. E., Park, C., Kelemen, B. R., and Raines, R. T. (2002) The ribonucleolytic activity of angiogenin. *Biochemistry* **41**, 1343-1350
240. Gibson, D. G., Young, L., Chuang, R. Y., Venter, J. C., Hutchison, C. A., 3rd, and Smith, H. O. (2009) Enzymatic assembly of DNA molecules up to several hundred kilobases. *Nat Methods* **6**, 343-345
241. Rutkoski, T. J., Kurten, E. L., Mitchell, J. C., and Raines, R. T. (2005) Disruption of shape-complementarity markers to create cytotoxic variants of ribonuclease A. *J Mol Biol* **354**, 41-54
242. Fairhead, M., and Howarth, M. (2015) Site-specific biotinylation of purified proteins using BirA. *Methods Mol Biol* **1266**, 171-184
243. Li, Y., and Sousa, R. (2012) Expression and purification of E. coli BirA biotin ligase for in vitro biotinylation. *Protein Expr Purif* **82**, 162-167
244. Tokunaga, H., Tokunaga, M., and Nakae, T. (1981) Permeability properties of chemically modified porin trimers from Escherichia coli B. *J Biol Chem* **256**, 8024-8029
245. Goers, L., Freemont, P., and Polizzi, K. M. (2014) Co-culture systems and technologies: taking synthetic biology to the next level. *J Royal Soc Interface* **11**, 20140065
246. Thornton, C. R., Ryder, L. S., Le Cocq, K., and Soanes, D. M. (2015) Identifying the emerging human pathogen *Scedosporium prolificans* by using a species-specific monoclonal antibody that binds to the melanin biosynthetic enzyme tetrahydroxynaphthalene reductase. *Environ Microbiol* **17**, 1023-1038
247. Hornsby, M., Paduch, M., Miersch, S., Saaf, A., Matsuguchi, T., Lee, B., Wypisniak, K., Doak, A., King, D., Usatyuk, S., Perry, K., Lu, V., Thomas, W., Luke, J., Goodman, J., Hoey, R. J., Lai, D., Griffin, C., Li, Z., Vizeacoumar, F. J., Dong, D., Campbell, E., Anderson, S., Zhong, N., Graslund, S., Koide, S., Moffat, J., Sidhu, S., Kossiakoff, A., and Wells, J. (2015) A high through-put platform for recombinant antibodies to folded proteins. *Mol Cell Proteomics* **14**, 2833-2847
248. Riordan, J., and Vallee, B. (1972) [41] Acetylation. in *Methods in enzymology*, Elsevier. pp 494-499
249. Vanli, N., and Guo-Fu, H. U. (2015) Mechanism and function of angiogenin in prostate cancer. *Zhongguo sheng wu hua xue yu fen zi sheng wu xue bao* **31**, 1261-1266
250. Vert, A., Castro, J., Ribo, M., Benito, A., and Vilanova, M. (2016) A nuclear-directed human pancreatic ribonuclease (PE5) targets the metabolic phenotype of cancer cells. *Oncotarget* **7**, 18309-18324
251. van Gorp, E. C., Suharti, C., ten Cate, H., Dolmans, W. M., van der Meer, J. W., ten Cate, J. W., and Brandjes, D. P. (1999) Review: infectious diseases and coagulation disorders. *J Infect Dis* **180**, 176-186
252. Li, S., Hu, M. G., Sun, Y., Yoshioka, N., Ibaragi, S., Sheng, J., Sun, G., Kishimoto, K., and Hu, G. F. (2013) Angiogenin mediates androgen-stimulated prostate cancer growth and enables castration resistance. *Mol Cancer Res* **11**, 1203-1214
253. Lee, H. S., Lee, I. S., Kang, T. C., Jeong, G. B., and Chang, S. I. (1999) Angiogenin is involved in morphological changes and angiogenesis in the ovary. *Biochem Biophys Res Commun* **257**, 182-186
254. Cho, I., Yamanishi, S., Cox, L., Methe, B. A., Zavadil, J., Li, K., Gao, Z., Mahana, D., Raju, K., Teitler, I., Li, H., Alekseyenko, A. V., and Blaser, M. J. (2012) Antibiotics in early life alter the murine colonic microbiome and adiposity. *Nature* **488**, 621-626

255. Yan, J., Herzog, J. W., Tsang, K., Brennan, C. A., Bower, M. A., Garrett, W. S., Sartor, B. R., Aliprantis, A. O., and Charles, J. F. (2016) Gut microbiota induce IGF-1 and promote bone formation and growth. *Proc Natl Acad Sci USA* **113**, E7554-e7563
256. Yang, D., Chen, Q., Rosenberg, H. F., Rybak, S. M., Newton, D. L., Wang, Z. Y., Fu, Q., Tchernev, V. T., Wang, M., Schweitzer, B., Kingsmore, S. F., Patel, D. D., Oppenheim, J. J., and Howard, O. M. (2004) Human ribonuclease A superfamily members, eosinophil-derived neurotoxin and pancreatic ribonuclease, induce dendritic cell maturation and activation. *J Immunol* **173**, 6134-6142
257. Jahr, S., Hentze, H., Englisch, S., Hardt, D., Fackelmayer, F. O., Hesch, R.-D., and Knippers, R. (2001) DNA fragments in the blood plasma of cancer patients: quantitations and evidence for their origin from apoptotic and necrotic cells. *Cancer Res* **61**, 1659-1665
258. Cabrera-Fuentes, H. A., Lopez, M. L., McCurdy, S., Fischer, S., Meiler, S., Baumer, Y., Galuska, S. P., Preissner, K. T., and Boisvert, W. A. (2015) Regulation of monocyte/macrophage polarisation by extracellular RNA. *Thromb Haemost* **113**, 473-481
259. Martinez-Valle, F., Balada, E., Ordi-Ros, J., Bujan-Rivas, S., Sellas-Fernandez, A., and Vilardell-Tarres, M. (2009) DNase 1 activity in patients with systemic lupus erythematosus: relationship with epidemiological, clinical, immunological and therapeutical features. *Lupus* **18**, 418-423
260. Skaggs, B. J., Hahn, B. H., and McMahon, M. (2012) Accelerated atherosclerosis in patients with SLE--mechanisms and management. *Nat Rev Rheumatol* **8**, 214-223
261. Libby, P. (2002) Inflammation in atherosclerosis. *Nature* **420**, 868-874
262. Eller, C. H. (2014) *Interactions of Ribonuclease 1 with the Cell Surface*, University of Wisconsin-Madison, Madison, WI
263. Durr, U. H., Sudheendra, U. S., and Ramamoorthy, A. (2006) LL-37, the only human member of the cathelicidin family of antimicrobial peptides. *Biochim Biophys Acta* **1758**, 1408-1425
264. Yan, H., and Hancock, R. E. (2001) Synergistic interactions between mammalian antimicrobial defense peptides. *Antimicrob Agents Chemother* **45**, 1558-1560
265. Gallo, R. L., Kim, K. J., Bernfield, M., Kozak, C. A., Zanetti, M., Merluzzi, L., and Gennaro, R. (1997) Identification of CRAMP, a cathelin-related antimicrobial peptide expressed in the embryonic and adult mouse. *J Biol Chem* **272**, 13088-13093
266. Hofsteenge, J., Vicentini, A., and Zelenko, O. (1998) Ribonuclease 4, an evolutionarily highly conserved member of the superfamily. *Cell Mol Life Sci* **54**, 804-810
267. Baron, M. H., Isern, J., and Fraser, S. T. (2012) The embryonic origins of erythropoiesis in mammals. *Blood* **119**, 4828-4837
268. Nakata, D. (2014) Increased N-glycosylation of Asn(88) in serum pancreatic ribonuclease 1 is a novel diagnostic marker for pancreatic cancer. *Sci Rep* **4**, 6715
269. Snook, J. T. (1965) Dietary regulation of pancreatic enzyme synthesis, secretion and inactivation in the rat. *J Nutr* **87**, 297-305
270. Koczera, P., Martin, L., Marx, G., and Schuerholz, T. (2016) The ribonuclease A superfamily in humans: canonical RNases as the buttress of innate immunity. *Int J Mol Sci* **17**
271. Odegaard, J. I., and Chawla, A. (2011) Alternative macrophage activation and metabolism. *Annu Rev Pathol* **6**, 275-297
272. Kintscher, U., Hartge, M., Hess, K., Foryst-Ludwig, A., Clemenz, M., Wabitsch, M., Fischer-Posovszky, P., Barth, T. F., Dragun, D., Skurk, T., Hauner, H., Bluher, M., Unger, T., Wolf, A. M., Knippschild, U., Hombach, V., and Marx, N. (2008) T-lymphocyte infiltration in visceral adipose tissue: a primary event in adipose tissue inflammation and the development of obesity-mediated insulin resistance. *Arterioscler Thromb Vasc Biol* **28**, 1304-1310
273. Hotamisligil, G. S., Peraldi, P., Budavari, A., Ellis, R., White, M. F., and Spiegelman, B. M. (1996) IRS-1-mediated inhibition of insulin receptor tyrosine kinase activity in TNF- α - and obesity-induced insulin resistance. *Science* **271**, 665-670
274. Yang, D., Chen, Q., Rosenberg, H. F., Rybak, S. M., Newton, D. L., Wang, Z. Y., Fu, Q., Tchernev, V. T., Wang, M., Schweitzer, B., Kingsmore, S. F., Patel, D. D., Oppenheim, J. J., and

- Howard, O. M. Z. (2004) Human Ribonuclease A Superfamily Members, Eosinophil-Derived Neurotoxin and Pancreatic Ribonuclease, Induce Dendritic Cell Maturation and Activation. *The Journal of Immunology* **173**, 6134-6142
275. Tjørve, K. M. C., and Tjørve, E. (2017) The use of Gompertz models in growth analyses, and new Gompertz-model approach: An addition to the Unified-Richards family. *PLoS One* **12**, e0178691
276. Westman, S. (1968) Development of the obese-hyperglycaemic syndrome in mice. *Diabetologia* **4**, 141-149
277. Pulido, D., Moussaoui, M., Andreu, D., Nogues, M. V., Torrent, M., and Boix, E. (2012) Antimicrobial action and cell agglutination by the eosinophil cationic protein are modulated by the cell wall lipopolysaccharide structure. *Antimicrob Agents Chemother* **56**, 2378-2385
278. Pulido, D., Torrent, M., Andreu, D., Nogues, M. V., and Boix, E. (2013) Two human host defense ribonucleases against mycobacteria, the eosinophil cationic protein (RNase 3) and RNase 7. *Antimicrob Agents Chemother* **57**, 3797-3805
279. Salazar, V. A., Arranz-Trullen, J., Navarro, S., Blanco, J. A., Sanchez, D., Moussaoui, M., and Boix, E. (2016) Exploring the mechanisms of action of human secretory RNase 3 and RNase 7 against *Candida albicans*. *MicrobiologyOpen* **5**, 830-845
280. Turnbaugh, P. J., Ley, R. E., Mahowald, M. A., Magrini, V., Mardis, E. R., and Gordon, J. I. (2006) An obesity-associated gut microbiome with increased capacity for energy harvest. *Nature* **444**, 1027-1031
281. Ley, R. E., Backhed, F., Turnbaugh, P., Lozupone, C. A., Knight, R. D., and Gordon, J. I. (2005) Obesity alters gut microbial ecology. *Proc Natl Acad Sci USA* **102**, 11070-11075
282. Bastard, J. P., Maachi, M., Lagathu, C., Kim, M. J., Caron, M., Vidal, H., Capeau, J., and Feve, B. (2006) Recent advances in the relationship between obesity, inflammation, and insulin resistance. *Eur Cytokine Netw* **17**, 4-12